LIGHT EVOLUTION IN DISSIPATIVE WAVEGUIDE LATTICES

DISSERTATION

zur Erlangung des akademischen Grades

doctor rerum naturalium (Dr. rer. nat.)

vorgelegt

der Mathematisch-Naturwissenschaftlichen Fakultät

der Universität Rostock

von Toni Eichelkraut

geboren am 24. Oktober 1986 in Saalfeld

https://doi.org/10.18453/rosdok_id00002662

1. GUTACHTER: Prof. Dr. Alexander Szameit, Univ. Rostock, Institut für Physik

2. GUTACHTER: Prof. Dr. Holger Fehske, Univ. Greifswald, Institut für Physik

3. GUTACHTER: Prof. Dr. Stefan Rotter, TU Wien, Institut für Theoretische Physik

EINREICHUNG: Dezember 2018

TAG DER DISPUTATION: 26. April 2019

Dedicated to my family.

ABSTRACT

This thesis aims at laying the foundation for handling $\mathcal{PT}$ symmetric structures in fs-LASER-written waveguide arrays. This is done by presenting a thorough theoretical and experimental investigation of a new way to implement well defined losses in fs-LASER-written waveguides. Also it comprises the first experimental realization of a $\mathcal{PT}$ symmetric structure on this platform. In addition, a new coupled mode theory for dissipative waveguides is presented and experimentally verified.

The context of this thesis is structured as follows. After a short review of the current state of the art in chapter 2, in chapter 3 sinusoidally bent waveguides are presented as a novel way to introduce well controllable losses in waveguide lattices. The main question tackled in this chapter is whether bending losses may lead to an overall exponential decay of the waveguide's mode amplitude and how this behavior depends on the system parameters. Surprisingly, even though bending losses of waveguides have been studied intensively in areas such as optical fibers or integrated photonics, this investigation is the first to deal with periodically bent guides; hence evolution dynamics are found, which strongly deviate from those of isolated bends.

The findings of chapter 3 pave the way for the subsequent investigations presented in chapters 4 and 5, where dissipative systems are theoretically considered and sinusoidally bent waveguides are experimentally applied. Chapter 4 presents the first experimental investigation of $\mathcal{PT}$ symmetry in fs-LASER-written waveguides. A $\mathcal{PT}$ invariant structure is investigated in the so-called broken $\mathcal{PT}$ symmetric regime and a mobility transition from ballistic to diffusive transport is found. This finding is remarkable, as such dynamics are impossible in ordered, 1D hermitian systems.

Finally, chapter 5 revisits the well-known coupled mode theory governing the light evolution in discrete lattices. A new theory that covers the peculiarities of dissipative lattices is presented and investigated based on an experimental sample system.

ZUSAMMENFASSUNG

Diese Dissertation liefert die Basis für die Umsetzung $\mathcal{PT}$ symmetrischer Strukturen in fs-LASER geschriebenen Wellenleitergittern. Hierfür werden tiefgreifende theoretische und experimentelle Untersuchungen dargestellt, die sich mit einer neuen Art, wohldefinierte Verluste in Wellenleitergitter einzutragen, beschäftigen. Des weiteren beinhaltet diese Dissertation die erste experimentelle Realisierung $\mathcal{PT}$ symmetrischer Strukturen auf Basis von fs-LASER geschriebenen Wellenleitern. Darüber hinaus wird in dieser Arbeit eine neue Theorie gekoppelter Moden in dissipativen Wellenleitern präsentiert und experimentell verifiziert.

Der Inhalt dieser Arbeit ist wie folgt strukturiert. Nach einer kurzen Zusammenfassung des aktuellen Forschungsstandes in Kapitel 2, werden in Kapitel 3 sinus-förmig gekrümmte Wellenleiter diskutiert. Diese dienen als eine neuartige Methode, um kontrollierbare, optische Verluste in Wellenleitergitter einzutragen. Die zentrale Frage dieses Kapitels ist es, ob die eingetragenen Krümmungsverluste zu einem exponentiellen Abfall der Wellenleitermode führen und wie dieses Verhalten gegebenen Falls von den Systemparametern abhängt. Überraschender Weise ist diese Untersuchung die erste ihrer Art, die sich mit periodisch gekrümmten Wellenleitern beschäftigt; folglich werden neue Evolutionsregime gefunden, die sich stark von denen isolierter Krümmungen unterscheiden.

Die Ergebnisse aus Kapitel 3 ebnen den Weg für die Kapitel 4 und 5, in denen dissipative Systeme theoretisch untersucht werden und sinus-förmig gekrümmte Wellenleiter als experimentelles Werkzeug dienen. Hierbei wird in Kapitel 4 die erste experimentelle Umsetzung eines $\mathcal{PT}$ symmetrischen, fs-LASER geschriebenen Wellenleitergitters beschrieben. Eine $\mathcal{PT}$ invariante Struktur wird in der sogenannten gebrochenen $\mathcal{PT}$ Phase untersucht und ein Übergang vom ballistischen zum diffusiven Transportregime wird festgestellt. Diese Ergebnisse sind ebenso erstaunlich, wie beachtlich, da solch eine Propagationsdynamik in geordneten, eindimensionalen, hermitischen Systemen nicht vorkommen kann.

Abschließend greift Kapitel 5 noch einmal die altbekannte Theorie gekoppelter Moden auf, welche die Lichtausbreitung in diskreten Wellenleitergittern beschreibt. An ihre Stelle tritt hier eine neue Theorie, die die Besonderheiten eines dissipativen Gitters berücksichtigt. Experimentelle Beispiele verdeutlichen dabei die theoretischen Vorhersagen des Kapitels.

PUBLICATIONS

Due to priority reasons, some ideas and figures have appeared previously in the following publications.

JOURNAL PUBLICATIONS:

1. T. Eichelkraut, R. Heilmann, S. Weimann, S. Stützer, F. Dreisow, D. N. Christodoulides, S. Nolte, and A. Szameit. Mobility transition from ballistic to diffusive transport in non-Hermitian lattices. *Nature Communications*, 4:2533, Sep 2013.

2. T. Eichelkraut and A. Szameit. Photonics: Random sudoku light. *Nature*, 526(7575):643–644, Oct 2015. News & Views.

3. C. Vetter, T. Eichelkraut, M. Ornigotti, and A. Szameit. Generalized radially self-accelerating helicon beams. *Phys. Rev. Lett.*, 113:183901, Oct 2014.

4. C. Vetter, T. Eichelkraut, M. Ornigotti, and A. Szameit. Optimization and control of two-component radially self-accelerating beams. *Applied Physics Letters*, 107(21):211104, 2015.

5. T. Eichelkraut, C. Vetter, A. Perez-Leija, H. Moya-Cessa, D. N. Christodoulides, and A. Szameit. Coherent random walks in free space. *Optica*, 1(4):268–271, Oct 2014.

6. T. Eichelkraut, S. Weimann, S. Stützer, S. Nolte, A. Szameit. Radiation-loss management in modulated waveguides. *Opt. Lett.*, 39(24):6831–6834, Dec 2014.

7. S. Weimann, T. Eichelkraut, A. Szameit. Decay of bound states in oscillating potential wells. *Phys. Rev. A*, 97(5):053844, May 2018.

8. M. Golshani, S. Weimann, Kh. Jafari, M. Khazaei Nezhad, A. Langari, A. R. Bahrampour, T. Eichelkraut, S. M. Mahdavi, and A. Szameit. Impact of loss on the wave dynamics in photonic waveguide lattices. *Phys. Rev. Lett.*, 113:123903, Sep 2014.

9. T. Eichelkraut, G. A. Siviloglou, I. M. Besieris, and D. N. Christodoulides. Oblique Airy wave packets in bidispersive optical media. *Opt. Lett.*, 35(21):3655–3657, Nov 2010.

10. M. Gräfe, R. Heilmann, R. Keil, T. Eichelkraut, M. Heinrich, S. Nolte, and A. Szameit. Correlations of indistinguishable

particles in non-Hermitian lattices. *New Journal of Physics*, 15 (3):033008, 2013.

11. R. Filter, S. Mühlig, T. Eichelkraut, C. Rockstuhl, and F. Lederer. Controlling the dynamics of quantum mechanical systems sustaining dipole-forbidden transitions via optical nanoantennas. *Phys. Rev. B*, 86:035404, Jul 2012.

12. S. Fischer, F. Hallermann, T. Eichelkraut, G. von Plessen, K. W. Krämer, D. Biner, H. Steinkemper, M. Hermle, and J. C. Goldschmidt. Plasmon enhanced upconversion luminescence near gold nanoparticles–simulation and analysis of the interactions. *Opt. Express*, 20(1):271–282, Jan 2012.

13. S. Fischer, F. Hallermann, T. Eichelkraut, G. von Plessen, K. W. Krämer, D. Biner, H. Steinkemper, M. Hermle, and J. C. Goldschmidt. Plasmon enhanced upconversion luminescence near gold nanoparticles – simulation and analysis of the interactions: Errata. *Opt. Express*, 21(9):10606–10611, May 2013.

14. Z. Lin, H. Ramezani, T. Eichelkraut, T. Kottos, H. Cao, and D. N. Christodoulides. Unidirectional invisibility induced by PT-symmetric periodic structures. *Phys. Rev. Lett.*, 106:213901, May 2011.

15. I. Mingareev, R. Berlich, T. J. Eichelkraut, H. Herfurth, S. Heinemann, and M. C. Richardson. Diffractive optical elements utilized for efficiency enhancement of photovoltaic modules. *Opt. Express*, 19(12):11397–11404, Jun 2011.

CONFERENCE PROCEEDINGS:

15. T. Eichelkraut, R. Heilmann, S. Stützer, S. Nolte, and A. Szameit. Sharp transition between ballistic and diffusive transport in PT -symmetric media. In *2013 Conference on Lasers and Electro-Optics - International Quantum Electronics Conference*, page CD.8.4. Optical Society of America, 2013.

16. T. Eichelkraut, C. Vetter, A. Perez-Leija, D. N. Christodoulides, and A. Szameit. Quantum random walks in free space. In *CLEO: 2014*, page FF1D.1. Optical Society of America, 2014.

17. T. Eichelkraut, S. Weimann, and A. Szameit. Managing radiation loss in photonic waveguides for applications in PT-symmetric systems. In *Conference on Lasers and Electro-Optics*, page SF1P.6. Optical Society of America, 2016.

18. T. J. Eichelkraut, G. A. Siviloglou, D. N. Christodoulides, and I. M. Besieris. Oblique Airy wavepackets in bidispersive optical

media. In *Conference on Lasers and Electro-Optics 2010*, page QWA3. Optical Society of America, 2010.

19. M. Gräfe, R. Heilmann, R. Keil, T. Eichelkraut, M. Heinrich, S. Nolte, and A. Szameit. Indistinguishable particles in non-hermitian lattices and their correlations. In *2013 Conference on Lasers and Electro-Optics - International Quantum Electronics Conference*, page IA.P.24. Optical Society of America, 2013.

20. T. Kottos, H. Ramezani, Z. Lin, T. Eichelkraut, H. Cao, and D. Christodoulides. Unidirectional invisibility of photonic periodic structures induced by PT-symmetric arrangements. In *Frontiers in Optics 2011/Laser Science XXVII*, page FWM3. Optical Society of America, 2011.

21. M. Ornigotti, T. Eichelkraut, and A. Szameit. Quasi-PT symmetry in waveguide optical directional couplers. In *CLEO: 2014*, page FM4C.4. Optical Society of America, 2014.

22. H. Ramezani, Z. Lin, T. Eichelkraut, T. Kottos, H. Cao, and D. Christodoulides. Broad band unidirectional invisibility using PT-symmetry. In *CLEO:2011 - Laser Applications to Photonic Applications*, page QMA3. Optical Society of America, 2011.

23. C. Vetter, T. Eichelkraut, and A. Szameit. An archimedean screw made of light. In *2013 Conference on Lasers and Electro-Optics - International Quantum Electronics Conference*, page CH.7.5. Optical Society of America, 2013.

24. C. Vetter, T. Eichelkraut, M. Ornigotti, and A. Szameit. Radially self-accelerating beams. In *CLEO: 2014*, page FM4D.3. Optical Society of America, 2014.

25. C. Vetter, A. Dudley, T. Eichelkraut, C. Schulze, M. Ornigotti, M. Duparré, A. Forbes, and A. Szameit. New manifestations of self-accelerating light: radial & angular self-acceleration. In *2015 European Conference on Lasers and Electro-Optics - European Quantum Electronics Conference*, page CH.2.4. Optical Society of America, 2015.

CONTENTS

ACRONYMS

1D	one-dimensional
2D	two-dimensional
3D	three-dimensional
CMT	coupled mode theory
FLDW	fs-LASER direct writing
PML	perfectly matched layers
PHE	Paraxial Helmholtz Equation
QM	quantum mechanics
SE	Schrödinger Equation

1

INTRODUCTION

The introduction of $\mathcal{PT}$ symmetry in quantum mechanics (QM) in 1998 initiated a paradigm change in physics [7]. Before the seminal work of Bender and Boettcher was published, hermitian operators were heralded as the only physically relevant entities. This notion is based on the assumption that the result of a physical measurement is given by an Eigen-value of the corresponding (observable) operator. Since the measurement always yields a real value, all Eigen-values of such observables must be real as well. This leads to the natural choice of hermitian operators, which have an entirely real Eigen-value spectrum. However, as Bender and Boettcher pointed out, the condition of an operator being hermitian is overly restrictive and a consistent quantum theory can be build on other classes of operators that still posses an entirely real Eigen-value spectrum. For instance, so-called $\mathcal{PT}$ symmetric QM can be formulated by replacing the mathematical condition of hermiticity by the additional physical assumption that the evolution of a quantum system looks the same after flipping space and time.

In 2007, the concept of $\mathcal{PT}$ symmetry was adopted in optics [30] and it substantially influenced the way scientists viewed the evolution and manipulation of light [79]. Before, loss was typically considered undesirable and minimized or avoided in every optical system, whenever possible. However, with the arrival of $\mathcal{PT}$ symmetry, physicists began to realize that certain well balanced gain-loss modulations can lead to peculiar propagation dynamics, which were thought to be physically impossible before. Hence, it was understood that loss - well placed and well controlled - can play a vital and most of all beneficial role in the propagation dynamics of optical systems. This notion was carried even further, when it was realized that $\mathcal{PT}$ symmetric evolution dynamics are even possible in entirely passive structures, where no gain is present at all [37].

In order to make the unique properties of $\mathcal{PT}$ symmetry experimentally accessible, it seems apparent that it is necessary to locally imprint and control the amount of loss. In turn, this addresses the need for a versatile platform, which allows these kinds of manipulations on an experimental basis. Evanescently coupled waveguides

produced by fs-LASER direct writing (FLDW) are a suitable candidate which fulfills exactly these essential requirements.

The door towards fs-LASER-written waveguides and waveguide arrays was pushed wide open in 1996 by the discovery of permanent glass modifications induced by visible femtosecond LASER irradiation [21]. Indeed, it took only a couple of years until in 2004 the first experimental demonstration of such a fs-LASER-written waveguide system was presented [75]. It is definitely no exaggeration to claim that this demonstration marked the hour of the birth of one of the most interesting research platforms of today, which draws its strength and superiority from the degree of freedom and accessibility of physical phenomena which were so far experimentally entirely inaccessible.

The theoretical grounds of evanescently coupled waveguides were already laid in 1965 within the context of the coupling of optical fibers [45]; and in 1973, the first experiment was conducted utilizing channel waveguides, which were fabricated in GaAs by proton implantation [89]. Surprisingly, the research area of evanescently coupled waveguides remained scarcely investigated until 1988, when interest in the non-linear dynamics of such systems began to rise [16]. From today's perspective, one can only speculate that the lack of interest in these systems in the late '70s and early '80s was due to the obvious experimental limitations and difficulties posed by the specific semiconductor platform, which also entail a rather slow prototyping. Maybe it was for these reasons that with the advent of the FLDW technique [44], the research interest in evanescently coupled waveguide arrays was newly sparked. Since then, the platform has proven to be a versatile tool in many aspects.

What makes fs-LASER-written waveguide arrays such a powerful tool is the fact that the discrete evolution dynamics of light within an array is analogous to the Schrödinger Equation (SE) in QM. In this respect, waveguide arrays are since used to emulate and study quantum-mechanical effects, such as Bloch Oscillations, Zener Tunneling, Anderson Localization, or Landau Levels in Graphene [78, 65, 92, 93, 56], just to name a few. In addition, fs-LASER-written waveguides constitute a unique physical system of their own and hence stimulate a lot of research both in the linear as well as the non-linear regime [17, 55, 29, 103, 66]. On top of this fundamental research interest, the ability to fabricate arbitrary three-dimensional (3D) structures has promoted waveguide arrays in fused silica as a prime candidate for quantum computing or microfluidic devices. In total, all these properties and possible applications render fs-LASER-written waveguide arrays as a very promising research platform for future applications.

It is in exactly this sense that this thesis presents a versatile path towards $\mathcal{PT}$ symmetry in fs-LASER-written waveguide lattices. This

work contains a thorough theoretical and experimental investigation of a way to implement well defined losses in fs-LASER-written waveguides. Also it comprises the first experimental realization of a $\mathcal{PT}$ symmetric structure on this platform. In addition, a new coupled mode theory for dissipative waveguides is presented and experimentally verified.

This context is structured as follows. After a short review of the current state of the art in chapter 2, in chapter 3 sinusoidally bent waveguides are presented as a novel way to introduce well controllable losses in waveguide lattices. The main question tackled in this chapter is whether bending losses may lead to an overall exponential decay of the waveguide's mode amplitude and how this behavior depends on the system parameters. Surprisingly, even though bending losses of waveguides have been studied intensively in areas such as optical fibers or integrated photonics, this investigation is the first to deal with periodically bent guides; hence evolution dynamics are found which strongly deviate from those of isolated bends.

The findings of chapter 3 pave the way for the subsequent investigations presented in chapters 4 and 5, where dissipative systems are theoretically considered and sinusoidally bent waveguides are experimentally applied. Chapter 4 presents the first experimental investigation of $\mathcal{PT}$ symmetry in fs-LASER-written waveguides. A $\mathcal{PT}$ invariant structure is investigated in the so-called broken $\mathcal{PT}$ symmetric regime and a mobility transition from ballistic to diffusive transport is found. This finding is remarkable, as such dynamics are impossible in ordered, one-dimensional (1D) hermitian systems.

Finally, chapter 5 revisits the well-known coupled mode theory governing the light evolution in discrete lattices. A new theory that covers the peculiarities of dissipative lattices is presented and investigated based on an experimental sample system.

All in all, with its three main parts, this thesis aims at laying the theoretical and experimental foundation for handling $\mathcal{PT}$ symmetric or, more generally, dissipative structures in fs-LASER-written waveguide arrays.

2

FUNDAMENTALS & STATE OF THE ART

2.1 THEORY OF OPTICAL WAVEGUIDING

In this section the foundation of optical waveguiding will be laid. The summary of the most important equations, concepts and notions will start from the fundamental equations of Electrodynamics, namely Maxwell's Equations. This early entry point is important, as it is essential for this thesis to understand which assumptions and approximations are usually made and how things differ if one considers dissipative systems instead of their usually lossless counterparts. Along these lines, within this section, certain terms, such as waveguide or Eigen-mode, will be defined for usage throughout the entire thesis. This is necessary, as for a number of terms one can usually find deviating notions within the literature. It is important to state, that it is not the intention of this section to rate any deviating definition; this section is merely supposed to serve as a basis for a common vocabulary.

2.1.1 *From Maxwell's Equations to the Paraxial Helmholtz Equation*

The dynamics of optical waveguides as well as all electromagnetic phenomena are governed by Maxwell's Equations. In the absence of free electric charges and free currents, the medium assisted equations can be expressed as

$$\begin{aligned} \vec{\nabla}\vec{\mathcal{D}}\left(\vec{r},\omega\right) &= 0 \\ \vec{\nabla}\vec{\mathcal{B}}\left(\vec{r},\omega\right) &= 0 \\ \vec{\nabla}\times\vec{\mathcal{E}}\left(\vec{r},\omega\right) &= i\omega\vec{\mathcal{B}}\left(\vec{r},\omega\right) \\ \vec{\nabla}\times\vec{\mathcal{H}}\left(\vec{r},\omega\right) &= -i\omega\vec{\mathcal{D}}\left(\vec{r},\omega\right) \end{aligned}$$

in the frequency domain. Within the context of this thesis only systems with a linear, isotropic optical response are considered, hence the field components can be connected in the following way

$$\begin{aligned} \vec{\mathcal{D}}\left(\vec{r},\omega\right) &= \epsilon_0\varepsilon\left(\vec{r},\omega\right)\vec{\mathcal{E}}\left(\vec{r},\omega\right) \\ \vec{\mathcal{B}}\left(\vec{r},\omega\right) &= \mu_0\vec{\mathcal{H}}\left(\vec{r},\omega\right). \end{aligned}$$

Moreover, within the physical system under consideration the electric permittivity is assumed to be slowly varying, which means that $\vec{\nabla}\vec{\mathcal{D}} = \epsilon_0\varepsilon\vec{\nabla}\vec{\mathcal{E}} + \epsilon_0\vec{\mathcal{E}}\vec{\nabla}\varepsilon \approx \epsilon_0\varepsilon\vec{\nabla}\vec{\mathcal{E}}$ and hence also the electric field is divergence free, i.e. $\vec{\nabla}\vec{\mathcal{E}} = 0$. As an immediate consequence one can derive the Helmholtz Equation for the electric field components, that is

$$\vec{\nabla}^2\vec{\mathcal{E}} + \tfrac{\omega^2}{c^2}\varepsilon\vec{\mathcal{E}} = 0 \ ,$$

whereas between free space permittivity, free space permeability and the speed of light the relation $\epsilon_0\mu_0 c^2 = 1$ holds. Up to this point the set of Maxwell's Equations was simplified to the Helmholtz Equation only by making assumptions about the underlying dielectric medium. In order to derive the Paraxial Helmholtz Equation (PHE) assumptions about the electric field have to be made as well. The first assumption is that in Cartesian coordinates the three electric field components are decoupled and it is sufficient to consider only one component, for instance subsequently it will be assumed that the electric field is linearly polarized, i.e. $\vec{\mathcal{E}}(\vec{r},\omega) = \mathcal{E}(\vec{r},\omega)\,\vec{e}_y$. From that it follows that one can move from a vectorial to a scalar Helmholtz Equation for the field component $\mathcal{E}(\vec{r},\omega)$, keeping in mind that the field components still have to obey the divergence condition $\vec{\nabla}\vec{\mathcal{E}} = 0$, hence they are coupled. The last step towards the PHE is the assumption that the field component is comprised of a quickly oscillating term e^{ikz} and an envelope $\mathcal{A}(\vec{r},\omega)$ which is slowly varying with respect to the z-direction, such that $\mathcal{E}(\vec{r},\omega) = \mathcal{A}(\vec{r},\omega)\,e^{ikz}$ whereas $\partial_z^2\mathcal{A} \approx 0$. With that one arrives at the PHE for the slowly varying amplitude $\mathcal{A}$, which reads

$$i2k\partial_z\mathcal{A} \quad = \quad -\left(\partial_x^2 + \partial_y^2\right)\mathcal{A} + \left(k^2 - \tfrac{\omega^2}{c^2}\varepsilon\right)\mathcal{A} \ . \tag{2.1}$$

Additionally, one can define $k := k_0 n_0$ with $k_0^2 := \omega^2/c^2$ and $n(\vec{r},\omega) = n_0 + \delta n(\vec{r},\omega) := \sqrt{\varepsilon(\vec{r},\omega)}$, where it is assumed that the refractive index n is only slightly varying around the position-independent bulk index n_0, hence it is assumed that $\delta n^2 \approx 0$. For mathematical convenience, one can introduce normalized coordinates with $x = x_0\xi$, $y = x_0\eta$, and $z = z_0\zeta$ with $z_0 = 1/k_0$ and $x_0 = 1/k_0\sqrt{2n_0}$. Then the PHE can be written as

$$i\partial_\zeta\mathcal{A} \quad = \quad -\left(\partial_\xi^2 + \partial_\eta^2\right)\mathcal{A} - \delta n\mathcal{A} \ . \tag{2.2}$$

The PHE (2.2) is mathematically equivalent to the SE in QM. While the SE describes the temporal evolution of the probability amplitude of a quantum-mechanical state, eq. (2.2) describes the spatial propagation of the field envelope $\mathcal{A}$ along the ζ-direction and inside a weak refractive index landscape given by δn. The direction along the ζ-coordinate is called propagation direction or longitudinal direction, whereas the coordinate plane of $\zeta = const.$ is called the transverse plane. In subsequent sections, all considerations will be confined to

only one transverse dimension, i.e. it will be assumed that $\mathcal{A}$ is independent of the transverse coordinate η.

2.1.2 *Free Space Propagation*

In the absence of a refractive index profile, that is $\delta n = 0$, the propagation dynamics of certain fields can be expressed analytically. A special class of solutions to eq. (2.2) is the class of plane waves; the Ansatz $\mathcal{A} = e^{i(\alpha\xi - \beta\zeta)}$ yields the dispersion relation for these paraxial plane waves

$$\beta = \alpha^2.$$

Note that this dispersion relation can also be derived by inserting the plane wave Ansatz into the non-paraxial Helmholtz Equation and expressing the resulting dispersion relation as a taylor expansion, i.e. $\beta = \sqrt{k^2 - \alpha^2} \approx k - 1/2k\alpha^2 + \mathcal{O}\left(\alpha^4\right)$. This derivation provides an intuitive picture of paraxiality.

Plane waves are so-called Eigen-modes of free space, meaning their spatial profile does not change during propagation. Another special class of solutions to eq. (2.2) are so-called Gaussian Beams, whose transverse profile is characterized by the Gaussian Shape

$$\mathcal{A}_0(\xi) = \mathcal{A}(\xi, \zeta = 0) = e^{-\frac{\xi^2}{w_0^2}} e^{i\alpha_0 \xi}$$

and their propagation dynamics can be expressed as

$$\mathcal{A}(\xi, \zeta) = \frac{1}{\sqrt{1 + i\frac{\zeta}{\zeta_0}}} e^{-\frac{\omega_0^2}{4}\frac{\alpha_0^2}{\left(1 - i\frac{\zeta_0}{\zeta}\right)}} e^{-\frac{\xi^2}{\omega_0^2\left(1 + i\frac{\zeta}{\zeta_0}\right)}} e^{i\frac{\alpha_0}{1 + i\frac{\zeta}{\zeta_0}}\xi} \tag{2.3}$$

where $\zeta_0 = w_0^2/4$. In contrast to plane waves, Gaussian Beams are not Eigen-modes of eq. (2.2) as their beam profile changes during propagation. To be precise, the shape of Gaussian Beams remains Gaussian, whereas their width increases with increasing propagation distance. An example of a propagating Gaussian Beam is shown in fig. 2.1.

2.1.3 *One-Dimensional Waveguide*

Due to the analogy between SE and PHE, it is convenient to borrow concepts from QM, where for instance the evolution dynamics of a wave packet within a simple box potential are well known. Adopting this knowledge, one can consider a refractive index profile of

$$\delta n = \begin{cases} \delta n_{max} & ;\ |\xi| < w \\ 0 & ;\ else \end{cases} \tag{2.4}$$

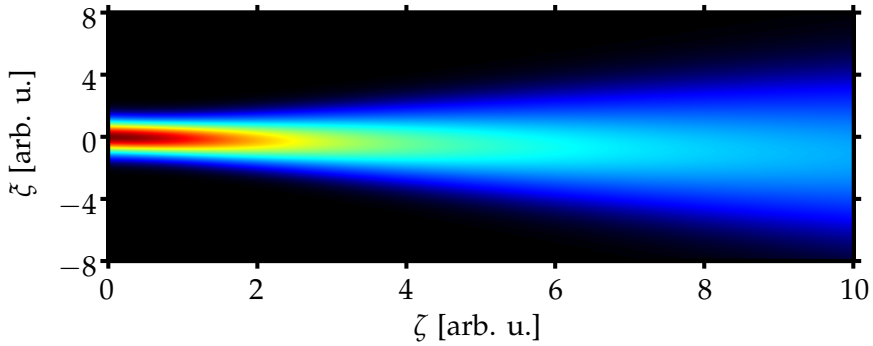

Figure 2.1: Intensity $|\mathcal{A}|^2$ of a propagating Gaussian Beam with $w_0 = 3$ and $\alpha_0 = 0.5$.

which shows a box profile with respect to the ξ-direction, but is invariant with respect to the ζ-direction. For this type of potential one can easily find a solution to eq. (2.2) in the form of

$$\mathcal{A} = \Phi(\xi)\, e^{-i\beta\zeta} \tag{2.5}$$

with a transverse profile given by

$$\Phi(\xi) = \begin{cases} \cos(\kappa_1 w)\, e^{\kappa_2(\xi+w)} & ;\ \xi < -w \\ \cos(\kappa_1 \xi) & ;\ |\xi| < w \\ \cos(\kappa_1 w)\, e^{-\kappa_2(\xi-w)} & ;\ \xi > w \end{cases} \tag{2.6}$$

where $\kappa_1 = \sqrt{\delta n_{max} + \beta}$, $\kappa_2 = \sqrt{-\beta}$ and the dispersion relation reads

$$\kappa_1 \sin(\kappa_1 w) = \kappa_2 \cos(\kappa_1 w). \tag{2.7}$$

In contrast to the dispersion relation of plane waves, which yields a continuous set of modes, this condition determines a discrete set of values for the propagation constant β. Equivalent to plane waves, eq. (2.5) resembles an Eigen-mode of the given potential, as the transverse beam profile does not change during propagation. In addition to being an Eigen-mode eq. (2.5) is a bound mode, which means that its transverse profile is square-integrable and confined to a region around the potential. Figure 2.2 shows an example of a refractive index profile δn and the corresponding transverse mode profile $\Phi(\xi)$. Subsequently, a refractive index profile which supports bound modes will be referred to as a waveguide. Moreover, only waveguides supporting a single bound mode will be considered.

2.2 COUPLED MODE THEORY OF HERMITIAN SYSTEMS

2.2.1 *Coupled Mode Equations*

Consider a refractive index landscape δn which consists of a collection of well-separated waveguides δn_j, each supporting a single

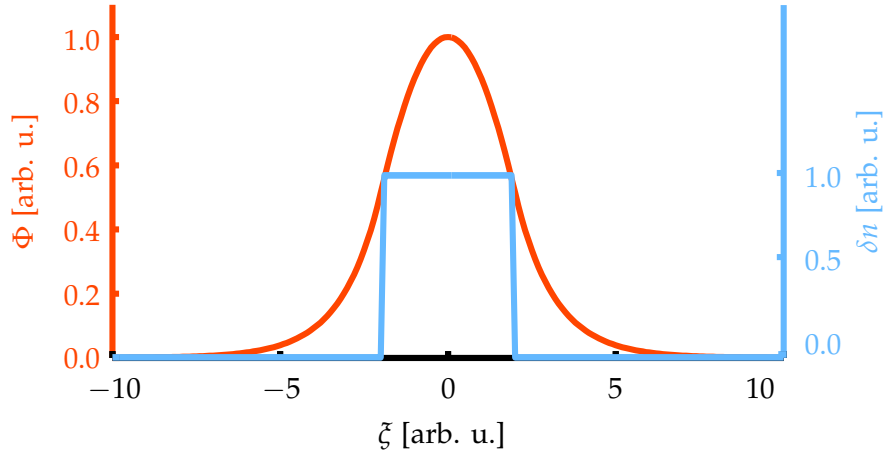

Figure 2.2: Transverse mode and refractive index profile for $\delta n_{max} = 1$ and $w = 2$.

bound mode with a transverse profile Φ_j and a propagation constant β_j. Assuming that the total field of such a structure is given by the superposition of these modes with ζ-dependent amplitudes $\tilde{a}_j$, i.e.

$$\mathcal{A} = \sum_j \tilde{a}_j(\zeta)\,\Phi_j(\xi)\,e^{-i\beta_j\zeta},$$

from eq. (2.2) one can derive the following set of coupled equations

$$i\sum_j \dot{\tilde{a}}_j \langle \Phi_l|\Phi_j\rangle e^{-i\beta_{jl}\zeta} = \sum_{j,m\neq j} \tilde{a}_j \langle \Phi_l|\delta n_m|\Phi_j\rangle e^{-i\beta_{jl}\zeta},$$

where $\langle \Phi_j|\Phi_l\rangle = \int \Phi_j^*\Phi_l d\xi$, $\langle \Phi_j|\delta n_l|\Phi_m\rangle = \int \Phi_j^*\delta n_l \Phi_m d\xi$, and $\beta_{jl} = \beta_j - \beta_l$. In a first order approximation, one can assume that $\langle \Phi_j|\Phi_l\rangle = \delta_{jl}$ and $\langle \Phi_j|\delta n_l|\Phi_m\rangle = \delta_{jl}\left(C_{j+}\delta_{m(j+1)} + C_{j-}\delta_{m(j-1)}\right)$, which reflects the fact that the modes are assumed to be orthogonal and that only modes of neighboring waveguides couple with each other. This assumption is valid if the waveguides are far enough apart, such that only a small portion of the evanescent part of the mode field reaches the region of the neighboring waveguide. The resulting evolution equation for the amplitudes reads

$$i\dot{\tilde{a}}_j = C_{j+}\tilde{a}_{j+1}e^{-i\beta_{(j+1)j}\zeta} + C_{j-}\tilde{a}_{j-1}e^{-i\beta_{(j-1)j}\zeta},$$

which is almost the desired coupled mode equation except for the occurring exponential terms. Fortunately, these can be eliminated by setting $a_j = \tilde{a}_j e^{-i\gamma_j\zeta}$ and $\gamma_j = \gamma_{j-1} + \beta_{(j-1)j}$. Moreover, from energy conservation, i.e. $\sum_j \partial_\zeta |a_j|^2 = 0$, it follows that the coupling constants C_{j+} and C_{j-} are not independent of each other, but rather fulfill the symmetry relation $C_{j+} = C_{(j+1)-} =: C_j \in \mathbb{R}$. This leads to the coupled mode equation

$$i\dot{a}_j = \gamma_j a_j + C_j a_{j+1} + C_{j-1}a_{j-1}. \tag{2.8}$$

Note that eq. (2.8) represents the simplest case of a coupled mode equation; more elaborate versions can be obtained by taking into account coupling between arbitrary guides $\left[\left\langle \Phi_j \left| \delta n_{j+l} \right| \Phi_{j+l} \right\rangle \neq 0\right]$, self-coupling $\left[\left\langle \Phi_j \left| \delta n_{j+l} \right| \Phi_j \right\rangle \neq 0\right]$, or non-orthogonality of the modes $\left[\left\langle \Phi_j | \Phi_{j+l} \right\rangle \neq 0\right]$.

2.2.2 *Directional Coupler*

In order to have an intuitive understanding of the evolution dynamics described by eq. (2.8) a system of just two waveguides shall be considered. This setup is also often referred to as directional coupler. The two evolution equations of a none-detuned directional coupler, for which $\beta_{12} = 0$, are

$$\begin{aligned} i\dot{a}_1 &= C_1 a_2 \\ i\dot{a}_2 &= C_1 a_1 \end{aligned}$$

with the solution

$$\begin{aligned} a_1 &= \cos\left(C_1 \zeta\right) \\ a_2 &= i \sin\left(C_1 \zeta\right) \end{aligned}$$

for the specific initial conditions $a_1\left(0\right) = 1$ and $a_2\left(0\right) = 0$. The evolu-

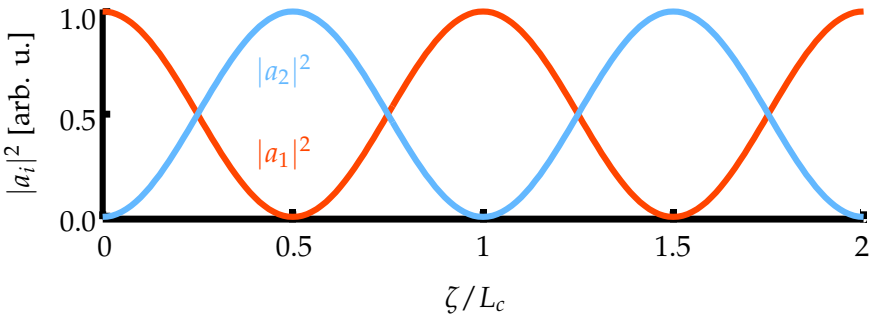

Figure 2.3: Intensities $|a_1|^2$ and $|a_2|^2$ of a symmetric directional coupler.

tion of the mode amplitudes is graphically depicted in fig. 2.3, where one can see that the net intensity periodically oscillates between both waveguides. The period of one oscillation is called coupling length L_c and is related to the coupling constant via $C_1 L_c = 2\pi$. Due to this relation, simple directional couplers are used experimentally to retrieve C_1 from measurements of L_c.

2.2.3 *Homogeneous Lattice*

Another important example is the infinite homogeneous lattice with its evolution equations

$$i\dot{a}_j = C\left(a_{j+1} + a_{j-1}\right). \tag{2.9}$$

If one assumes that initially only the zeroth waveguide is excited, that is $a_j(0) = \delta_{0j}$, and the lattice extends to infinity in both directions, one can easily solve for the ζ-dependent amplitudes. From eq. (2.9) it follows that the evolution pattern is symmetric, hence $a_j = a_{-j}$ and specifically $i\dot{a}_0 = 2Ca_1$. If one compares this to well known relations for Bessel Functions, i.e. $J_l(\xi) = (-1)^l J_{-l}(\xi)$ and $2\partial_\xi J_l(\xi) = J_{l-1}(\xi) - J_l(\xi)$, one finds

$$a_j(\zeta) = i^j J_j(2C\zeta), \tag{2.10}$$

which shows that the evolution dynamics of a homogeneous waveguide lattice can be explicitly expressed in terms of Bessel Functions. Figure 2.4 shows the characteristic propagation pattern for such a single site excitation and $C = 1$.

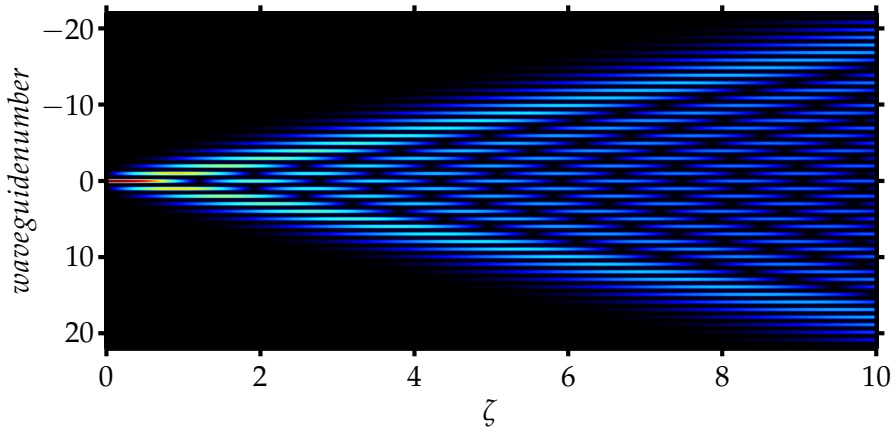

Figure 2.4: Evolution of a single site excitation of a homogeneous lattice with $C = 1$.

Another important relation concerns the variance of the wave packet, generally defined by $\sigma(\zeta) = \int \mathcal{A}^*(\xi,\zeta)\,\xi^2\mathcal{A}(\xi,\zeta)\,d\xi$. In a discrete waveguide array this reduces to $\sigma(\zeta) = \sum_j j^2 |a_j|^2$ and in the case of a homogeneous lattice it can even be expressed analytically, i.e.

$$\sigma(\zeta) = 2C^2\zeta^2,$$

where the relation $\sum_{l=1} l^2 J_l^2(\xi) = \xi^2/4$, which follows from [35] p.941 WA 47(1) for $n = 1$, was used. This is a very important finding, as it shows that the propagation dynamics of this specific lattice are ballistic, whereas the definition of ballistic propagation states that the variance of the wave packet grows quadratically with ζ. In the literature three main types of propagation dynamics or transport regimes are known, namely localization, for which the variance of the wave packet is constant with respect to ζ, diffusive transport, where the variance grows linearly with ζ, and the aforementioned ballistic transport [4, 65, 67, 92, 94, 93]. For a 1D hermitian waveguide array one can even make the following general statement.

For any ordered lattice the propagation regime is ballistic.

That is, if there is no disorder in the system, for instance a random distribution of C_j or γ_j, the transport regime will be of ballistic nature. It is important to note, that the transport regime is a fundamental property of the underlying lattice itself and is completely independent of the specific excitation.

Before closing the discussion about the homogeneous lattice, one should take a look at its Eigen-states and the dispersion relation. From Fourier theory, one finds that any arbitrary initial distribution $a_j(0)$ can be expressed through its spectrum $f_0(\varphi)$ in the form of $a_j(0) = \frac{1}{2\pi} \int_{-\pi}^{\pi} f_0(\varphi) e^{-ij\varphi} d\varphi$. Further, it follows that eq. (2.9) can be transfered to Fourier-space reading $i\partial_\zeta f(\varphi,\zeta) = 2C\cos(\varphi) f(\varphi,\zeta)$. Consequentially, the evolution of the spectral components $f(\varphi,\zeta)$ is given by an exponential dependence, i.e. $f(\varphi,\zeta) = f_0(\varphi) e^{-i2C\cos(\varphi)\zeta}$. As a conclusion, one can easily see that these spectral components represent Eigen-modes in the form of

$$a_j(\varphi,\zeta) = e^{-i(j\varphi+\beta\zeta)}$$

with the dispersion relation

$$\beta = 2C\cos(\varphi).$$

It can be noted that these modes are not localized as they are a discrete version of plane waves. Moreover, the set of modes is continuous as $-\pi \leq \varphi \leq \pi$.

2.3 NUMERICAL AND EXPERIMENTAL METHODS

2.3.1 *Numerical Methods - Perfectly Matched Layers*

In practically all fields of physics numerics are used to support either analytical calculations or experimental work. This is also true for waveguides produced by FLDW. Usually and especially in the case of 1D lattices the numerical effort is quite low compared to other field such as numerical relativistics and numerical tasks can well be accomplished using standard desktop machines. In the simplest case one can take eq. (2.8) as a basis of numerical investigation. In this situation one does not even have to take care of a spatial discretization scheme as the equation is already discrete in space. Moreover, if interested in a finite array, as found in every experiment, also numerical boundary conditions are of no concern. Under more evolved circumstances, for instance when probing the validity of eq. (2.8), one usually takes eq. (2.2) as a starting point of numerical investigation. While one does have to take care of the spatial discretization one can still disregard boundary conditions in most standard use cases. This

is true because if one ensures that one or more waveguides are excited with their respective Eigen-modes and the array is sufficiently far away from the numerical boundary, then the amount of light radiated away from the array is negligibly small and can mostly be neglected. When investigating lattices where waveguides are bent or segmented the light radiated away from the guides can usually not be neglected. In this case, the standard approach is to insert an additional absorbing medium, i.e. an imaginary potential, at the numerical boundaries in order to absorb light that hits the boundaries and prevent it from being reflected back into the waveguide region. In fig. 2.5 (a), an additional imaginary potential that grows quadratically outside the waveguide region is depicted. Even though the potential is only gradually increasing, the drawback of this type of boundary modification is that it is not entirely reflectionless. In fact, there is no complex potential which is reflectionless for arbitrary angles of incidence. Usually in most applications this is no obstacle as one is interested in systems where most of the light remains within the waveguide lattice. In this thesis, however, the situation is different. The system under consideration is designed such that after a certain propagation distance most of the light which is initially localized inside the waveguide is radiated away and the light intensity inside the waveguide region should tend to zero. As a consequence any reflections from numerical boundaries are crucial to the accuracy and validity of simulations. One way to minimize reflections from numerical boundaries is to utilize perfectly matched layers (PML). The idea behind this type of boundary modification is not to introduce an additional potential, but rather to extend the coordinate space into the complex domain. This Ansatz is possible since a solution to the PHE is an analytic function of its coordinates. Hence a solution for real coordinates is also valid for contours within the complex plane. If one considers, for instance, a plane wave $\mathcal{A} = e^{i(\alpha\xi' - \beta\zeta)}$ along a contour $\xi' = \xi + i\Theta(\xi)$ as shown in fig. 2.5 (b) where the complex coordinate ξ' is given in terms of the real variable ξ, one finds

$$\mathcal{A} = e^{i\alpha\xi - \alpha\Theta(\xi) - \beta\zeta} \tag{2.11}$$

in terms of the real coordinate ξ. For positive α and an increasing function $\Theta(\xi)$ this solution is decaying as ξ increases. That means, the solution behaves like the solution in an absorbing medium. However, the important difference is that in the region where $\Theta(\xi) = 0$ the solution coincides with a plane wave as found for real coordinates, which means there is no back reflection from the absorbing region. As a matter of fact, the complex contour results in a reflectionless absorbing medium. As stated above the analytically continued solution obeys the PHE. In order to avoid solving the PHE along a complex contour it seems more convenient to find a transformed equation in

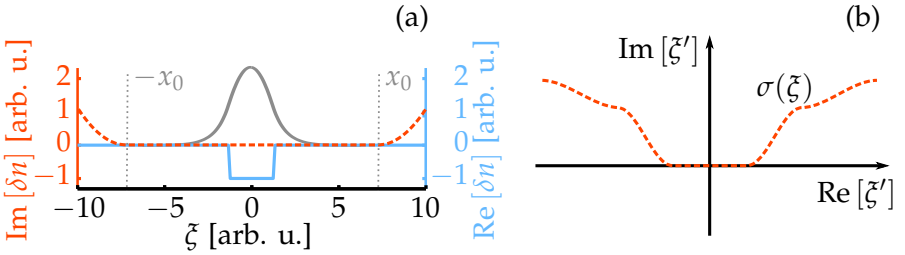

Figure 2.5: (a) Illustration of absorbing boundary conditions. An additional imaginary part is added to the potential at the edge of the computational cell. (b) In contrast to absorbing boundary conditions, PML rely on an analytic continuation of the field along a suitable trajectory in the complex plane. Along the contour the complex coordinate ξ' is given in terms of a real variable as $\xi' = \xi + i\Theta(\xi)$.

terms of the real coordinates. This is easily done by replacing the derivatives according to

$$\partial_{\xi'} = \frac{1}{1 + i\Theta_\xi}\partial_\xi,$$

where $\Theta_\xi = \frac{\partial\Theta}{\partial\xi}$. As a consequence, with additional PML the 1D PHE can be written as

$$i\partial_\zeta \mathcal{A} \;=\; -\left(v v_\xi \partial_\xi + v^2\partial_\xi^2\right)\mathcal{A} - \delta n\mathcal{A}\ , \tag{2.12}$$

where $v = \left(1 + i\Theta_\xi\right)^{-1}$ and $v_\xi = \frac{\partial v}{\partial\xi}$.

Unfortunately, PML are only perfectly reflectionless for the exact PHE. As soon as the equation is being discretized, numerical reflections occur. Nontheless, numerical reflections are usually very small and can be made arbitrarily small by the right choice of parameters. In fact, this is also true for non-PML absorbers. However, the advantage of PML is that a much smaller layer thickness is needed, which in turn might save a lot of computational power. In some cases a PML thickness of half a wavelength or thinner might be sufficient. As it turns out, this is not the case in this investigation. One can already see from eq. (2.11) that the absorption within the PML depends on the angle of incidence, i.e. α in eq. (2.11), and since the light that is being radiated away from the waveguide hits numerical boundaries under very small angles quite thick PML are needed within the context of this thesis.

In order to verify the effectiveness of the PML, the numerical scheme is being tested with the known solution of Gaussian Beams, i.e. eq. (2.3), and the numerical reflection of these beams launched under different angles of incidence is measured. Figure (2.6) shows two cases where a Gaussian Beam is being launched within the computational cell. The top graph in both subfigures is equal to the absolute difference between the numerical and analytical value at $\xi = 0$, i.e.

$\Delta = |\mathcal{A}_{\text{num}}(\xi = 0, \zeta) - \mathcal{A}_{\text{ana}}(\xi = 0, \zeta)|$. For illustration purposes the coordinate line $\xi = 0$ is drawn as a gray dashed line on top of the amplitude of the Gaussian Beam. The analysis suggests that the PML

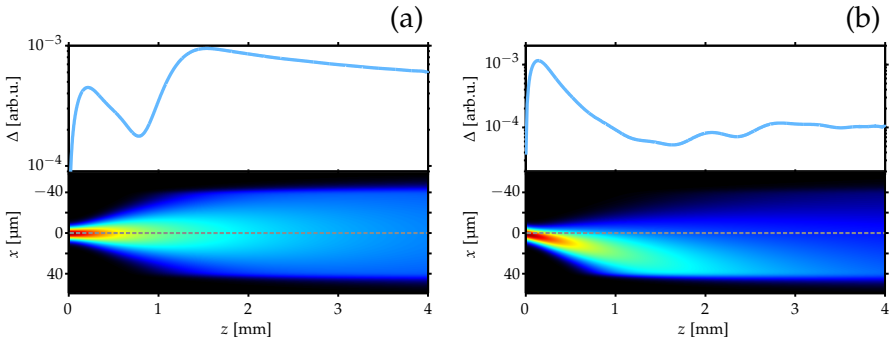

Figure 2.6: (a) Bottom: Simulated light evolution of a Gaussian Beam with an initial width of $w_0 = 6\,\mu\text{m}$ and a tilt angle of $\alpha_0 = 0$. Top: Deviation between simulated amplitude of Gaussian Beam at $\xi = 0$ and analytical solution as given by eq. (2.3). (b) Equivalent to (a) the evolution of a Gaussian Beam with $\alpha_0 = 0.015$ is depicted and compared to the analytical formula.

yield a good reflectionless absorption of the incident light. Yet, it shall be stated that in contrast to statements found in the literature the PML thickness is about 32 wavelengths. This is necessary because of the large aspect ratio of the system under investigation and the fact that light hits the boundaries under very small grazing angles. As it follows from eq. (2.11) for decreasing α the absorption within the PML decreases as well. Accordingly light that enters the PML under small angles reenters the computational cell after a certain propagation distance if the PML are not sufficiently thick. In turn, for a given PML thickness, this fact yields an upper bound for the longitudinal dimension of the computational cell.

2.3.2 *Fabrication of Optical Waveguides*

Within the recent past, arrays of evanescently coupled waveguides have attracted a lot of research interest. As a consequence a number of platforms to implement evanescently coupled waveguides have been established; these include AlGaAs heterostructures, LiNb wafers, or optical fibers, to name just a few [90, 102, 32, 104, 74]. Throughout this thesis optical waveguides will be generated in the bulk of fused silica using the technique of FLDW[44]. Since its discovery in 1996 [21], this technique's potential of creating an arbitrary 3D index profile has been harnessed in a large number of complex photonic systems in fused silica [95]. The technique itself relies on nonlinear processes inside the glass medium which cause a permanent restructuring and an increase of the refractive index[44]. In contrast to other nano-structuring techniques, FLDW is not limited to fused

silica [70], but its applicability extends over a large variety of glasses [84, 28, 105], crystalline materials such as silicon [68] and lithium niobate [13, 101, 39] as well as polymers [46].

The experimental structures investigated in this thesis were generated using a commercially available Amplitude fiber LASER system. For the inscription, the LASER pulses at a wavelength of 532 nm, a pulse length of 300 fs (full width at half maximum), a repetition rate of 200 kHz, and an energy of approximately 250 nJ are tightly focused into fused silica (Corning HPFS 7980) using a 20× microscope objective (NA= 0.35). As the focal spot has a diameter of a few µm light intensities are very high and field ionization as well as multiphoton absorption processes occur. Together with onsetting avalanche ionization, recombination, and restructuring processes, this leads to a permanent modification of the material [14, 15]. In order to fabricate optical waveguides the silica wafer is moved with respect to the focal spot using a Computer controlled positioning system (Aerotech). The velocity of the wafer movement, also termed writing velocity, is used to tune the propagation constants of the modes of the individual waveguides. This can be achieved since the writing velocity determines the amount of energy deposited in the glass and consequentially the refractive index increase. The larger the writing velocity is the less energy gets deposited; hence the smaller the refractive index increase of the modified region. A typical writing velocity is 100 mm/min which results in a refractive index increase on the order of $\delta n = 5 \times 10^{-4}$.

Figure 2.7 (b) displays that the cross section of the resulting waveguides is oval with dimensions of approximately $10 \times 4\,\mathrm{mm}^2$. This profile was calculated by numerical inversion of the Helmholtz Equation from the mode profile shown in fig. 2.7 (c) [59]. As a consequence of the oval cross section, the waveguides are not polarization degenerate but rather support two linearly polarized Eigen-modes. Within the further analysis of this thesis, the coupling of these polarization modes in arrays of waveguides can be neglected as it is usually very small. For that reason subsequently the waveguides will still be referred to as single mode. However, it is interesting to note that there exist techniques to induce a significant coupling between both polarizations. This is used for example when waveguide arrays are utilized as quantum gates.

2.3.3 *Measurement Technique - Fluorescence Measurements*

Experiments were conducted utilizing a fluorescence measurement technique [96, 97, 40, 65]. This techniques builds on the fact that non-bridging oxygen hole color centers are created inside the waveguide region during the FLDW process. For this to occur fused silica with a high content of hydroxide is necessarry. Illuminating the waveguides

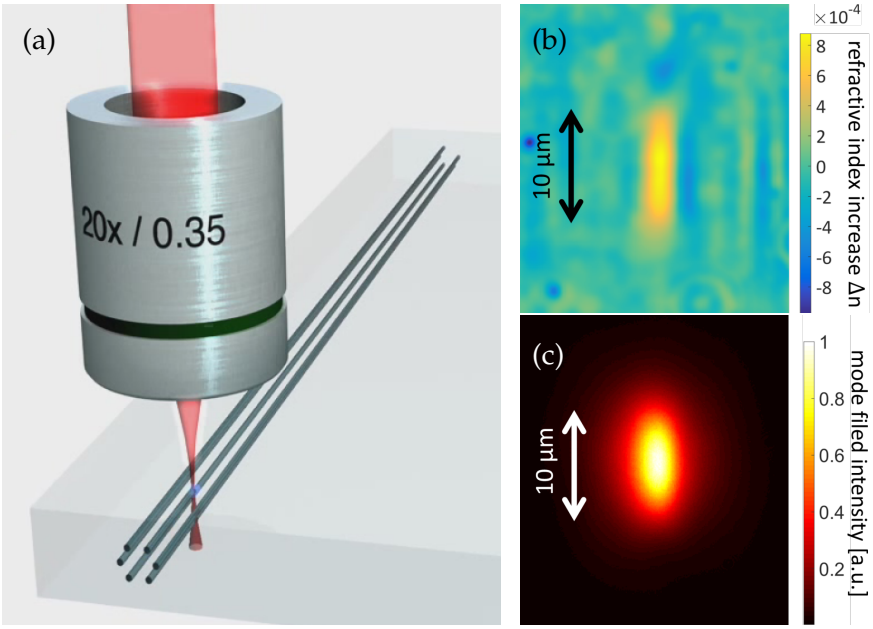

Figure 2.7: (a) Scheme of the FLDW process. The LASER is focused inside the glass sample which is continuously moved in order to fabricate elongated waveguides. (b) Transverse cross-section of a fs-LASER-written waveguide. (c) Transverse cross-section of the mode supported by the waveguide shown in (b).

with a HeNe-LASER at a wavelength of 633 nm results in an excitation of these color centers and fluorescence at a wavelength of 650 nm. While the excitation light is being guided along the waveguides the fluorescence is being emited isotropically and can be observed with a CCD-camera from above the glass sample, as depicted in fig. 2.8 (a). Figure 2.8 (b) contains a fluorescence image as observed with a CCD-camera exemplarily given for a homogeneous lattice governed by eq. 2.9 and a single excited waveguide.

The fluorescence measurement technique provides an image of the light evolution inside a waveguide array. In particular, these images also contain transverse information, i.e. the transverse mode profile of the waveguides. However, throughout this thesis only the longitudinally resolved amplitude of the waveguide modes is of interest. In this regard, a technique to extract the waveguide amplitudes and focus on small signal to noise ratios in the underlying fluorescence images is discussed in the next section.

2.3.4 *Post Processing of Fluorescence Images*

In order to extract data from fluorescence images, all measured images are post processed numerically. In the following, the post processing algorithm to extract amplitude data from the measurements is being explained exemplarily.

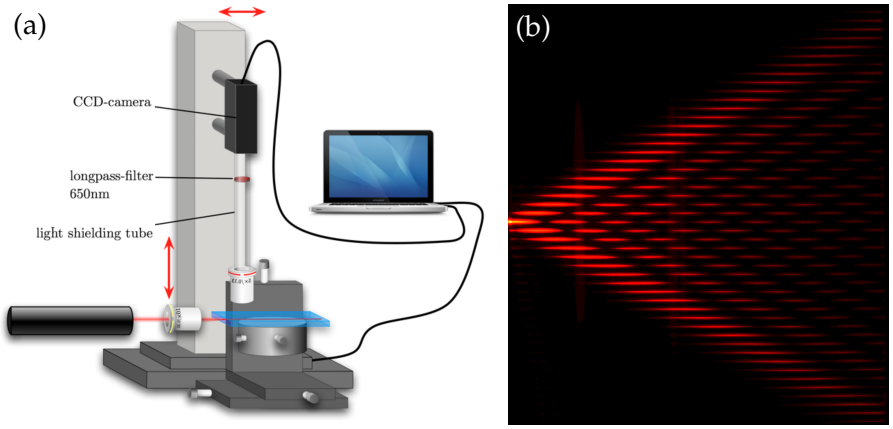

Figure 2.8: (a) Fluorescence measurement setup. Glass chip with waveguides is being illuminated with a HeNe-LASER and a 10×microscope objective. The CCD-camera mounted on a translation stage scans along the sample. The single images are stitched together at the PC after the scanning process. (b) Fluorescence image of a ballistic array for a single waveguide excitation.

Figure 2.9 (a) shows the raw fluorescence image. The image contains two main sources of errors, which can be minimized. The first error is due to misalignment of the sample, especially rotation. For this reason, the first operation which is performed is a rotation of the raw data. The best rotation angle is found by finding

$$\max_{\alpha}\left[\max_{j}\sum_{l} I_{jl}\left(\alpha\right)\right]$$

where I_{jl} is the intensity at row j and column l and α is the rotation angle. Figure 2.9 (b) shows the maxium column sum of (a) as a function of α. Here, the maximum is found at $\alpha_0 = -0.104$, showing that the raw data was rotated by a slight angle. Figure 2.9 (c) depicts the re-rotated data.

The second major error source is noise. In order to reduce the noise, the image is being filtered, both transverse as well as longitudinally. As a transverse filter the shape of the transverse mode is being used. To approximate this shape, the aligned image is averaged over all columns. From this, the normalized mode profile can be retrieved, as shown in fig. 2.9 (d). Moreover, the averaging procedure yields the central position of the waveguide as well - corresponding to row j_0 in (c). Figure 2.9 (e) shows the filtered image, where fig. 2.9 (d) was used as a transverse filter. The mode amplitude, shown in fig. 2.9 (f), is finally retrieved from (e) by extracting the row j_0 from (e). To estimate the noise level in (e), the average signal outside of the waveguide region is calculated. This value is finally subtracted from (f).

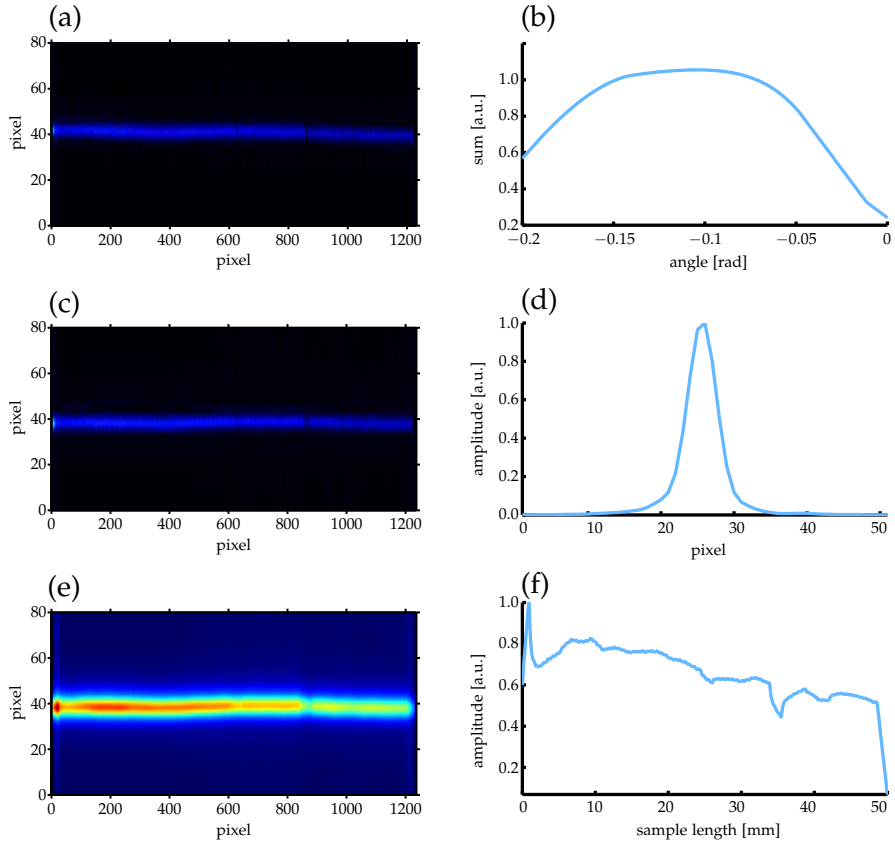

Figure 2.9: (a) Raw fluorescence image. (b) Maximum row sum as a function of rotation angle. (c) Rotated image, where the rotation angle is obtained from (b). (d) approximated mode profile. Obtained by summing over the rows of (c). (e) Filtered image, where fig. (c) was horizontally averaged and vertically filtered using the normalized profile given by fig. (d). (f) Mode amplitude extracted from (e).

2.4 $\mathcal{PT}$ SYMMETRY

2.4.1 *$\mathcal{PT}$ Symmetric Quantum Mechanics*

One of the axioms of standard QM states that the evolution of a quantum system is described by a hermitian Hamiltonian [18]. In contrast to other assumptions about QM, like causality, conservation of probability, or real energy values, the assumption of hermiticity seems purely mathematical and less physically motivated. It is true that the choice of hermitian operators in QM yields a lot of nice properties like real Eigen-values or a unitary evolution; from an axiomatic point of view however one has to acknowledge that hermiticity is not a physical requirement but rather a mathematical convenience. In 1998, with their seminal work Bender and colleagues reignited the discussion about $\mathcal{PT}$ symmetry in physics [7]. In this context, they argued that the condition of a Hamiltonian being hermitian is overly restrictive

and that a consistent quantum theory can be build on other classes of operators. For instance, so-called $\mathcal{PT}$ symmetric QM can be formulated by replacing the mathematical condition of hermiticity by the additional physical assumption that the evolution of a quantum system looks the same after flipping space and time. Mathematically, this leads to the condition that a system's Hamiltonian H commutes with the parity-time-reversal operator ($\mathcal{PT}$), i.e.

$$[H, \mathcal{PT}] = 0. \tag{2.13}$$

In order to lay the ground work for $\mathcal{PT}$ symmetric optics, subsequently, the fundamental properties of $\mathcal{PT}$ symmetric QM will be summarized. It will be discussed how $\mathcal{PT}$ symmetric QM compares to standard QM; as a quantum theory can only be considered a valid theory if it ensures at least real Eigen-values of observables and a unitary evolution of the quantum system.

To investigate these specific requirements some basic properties of the $\mathcal{PT}$ operator are needed. As the $\mathcal{PT}$ operator is a product of the parity operator $\mathcal{P}$ and the time-reversal operator $\mathcal{T}$, one plausible physical property is that $(\mathcal{PT})^2 = \mathbb{1}$. This simply means that flipping space and time twice in a row reproduces the initial situation. From the structure of the SE it is apparent that a proper definition of the time-reversal operator is given by the complex conjugation, i.e. $\mathcal{T}A\mathcal{T} = A^*$ and $\mathcal{T}|\Psi\rangle = |\Psi^*\rangle$ [10]. The parity operator $\mathcal{P}$ can simply be defined in position space as $P|x\rangle = |-x\rangle$ [9].

These basic properties lead to the statement that if the $\mathcal{PT}$ operator and the Hamiltonian H share a common set of Eigen-vectors, the Eigen-values E of the Hamiltonian are real [8]. This is can simply be shown by applying $\mathcal{PT}$ to the Eigen-value equation $H|\Psi\rangle = E|\Psi\rangle$ and using eq. (2.13) on the left hand side. One finds $E = E^*$ stating that the energy Eigen-values must be real. Before continuing the discussion about the unitary evolution, the nomenclature used throughout this thesis needs to be commented. Note that eq. (2.13) is not a sufficient condition for the system to be $\mathcal{PT}$ symmetric, it is merely the condition for the Hamiltonian to be $\mathcal{PT}$ invariant. The system is said to be $\mathcal{PT}$ symmetric if and only if H and $\mathcal{PT}$ share a common set of Eigen-vectors [22]. From linear algebra it is known that the commutation of two linear operators is equivalent to them sharing a common set of Eigen-vectors. However, from its definition it follows that $\mathcal{T}$ and also $\mathcal{PT}$ are anti-linear and hence the aforementioned equivalence is not valid. That means that one has to check the symmetry of the Eigen-vectors in order to make a statement about the symmetry of the system. Throughout this thesis, a Hamiltonian is said to be $\mathcal{PT}$ *invariant* if eq. (2.13) is satisfied and the System is said to be $\mathcal{PT}$ *symmetric* if H and $\mathcal{PT}$ share a common set of Eigen-vectors. As stated above, it follows that the Hamiltonian of a $\mathcal{PT}$ symmetric system has real Eigen-values.

Regarding the unitary evolution of the quantum system, it is evident that $\partial_t \langle\Psi|\Psi\rangle \neq 0$ for non-hermitian Hamiltonians[1] which means that the evolution is not unitary [83]. However, it turns out that the unitary evolution can be restored by introducing a new inner product. Already by using the so-called $\mathcal{PT}$ inner product, which is defined as $\langle\Psi|\Phi\rangle_{\mathcal{P}} = \int \Psi^*(-x)\,\Phi(x)\,\mathrm{d}x$, one finds $\partial_t \langle\Psi|\Psi\rangle_{\mathcal{P}} = 0$ [9]. Yet this inner product yields states with negative norm and hence the Hilbert space metric associated with this particular inner product is indefinite [63]. One could try to formulate a quantum theory by insisting that physical states must have positive norm, however this would lead to QM on a nonlinear state space and would still leave many open interpretational questions [9]. The resolution, accepted throughout the literature, is the introduction of the $\mathcal{CPT}$ inner product which ensures a unitary evolution and a positive norm [9, 62]. The $\mathcal{CPT}$ inner product makes use of the linear operator $\mathcal{C}$ which is the observable that represents the measurement of the signature of the norm within the $\mathcal{PT}$ inner product of a state, as such it is also dependent on the Hamiltonian itself. As a consequence in $\mathcal{PT}$ symmetric QM the interesting situation arises that each Hamiltonian comes with its own inner product.

When $\mathcal{PT}$ symmetry was first introduced in quest of a physical alternative to the mathematical axiom of hermiticity, it was quickly realized that it allows for a different class of Hamiltonians [10]. The first Hamiltonian which was considered in the original paper by Bender and colleagues, namely

$$H = p^2 - x^2\,(ix)^m\,, \tag{2.14}$$

extended[2] the harmonic oscillator into the complex plane [7]. It was conjectured and later proven in ref. [24] that this class of systems is $\mathcal{PT}$ symmetric for all $m \geq 0$. At a value of $m = 0$ the $\mathcal{PT}$ symmetry of these systems breaks spontaneously and for $m < 0$ the Eigenvalues of H are complex. In this regime the Hamiltonian is still $\mathcal{PT}$ invariant whereas H and $\mathcal{PT}$ do not share a common set of Eigenvectors anymore.

Even though many complex systems exhibiting an imaginary external potential can be observed in science, including Hamiltonians describing delocalization transitions in condensed matter systems [38] or even models stemming from population biology [69], from a fundamental point of view it seems unfeasible to study the fundamental

1 If H is not hermitian, then $H \neq H^\dagger$ and hence $\partial_t \langle\Psi|\Psi\rangle = \langle\Psi|\,(\partial_t\,|\Psi\rangle) + (\partial_t \langle\Psi|)\,|\Psi\rangle = -\langle\Psi|\,iH\,|\Psi\rangle + \langle\Psi|\,iH^\dagger\,|\Psi\rangle = -i\,\langle\Psi|\,(H - H^\dagger)\,|\Psi\rangle \neq 0$.

2 Even though $\mathcal{PT}$ symmetric QM allows for accessing Hamiltonians, which are prohibited in hermitian QM, it cannot be called a generalization of standard QM. During the scientific discussion inspired by $\mathcal{PT}$ symmetry a generalization of hermitian QM was formulated [63]. Within this general pseudo-hermitian QM, both hermitian and $\mathcal{PT}$ symmetric QM are specific realizations. Within this context, a $\mathcal{PT}$ symmetric system could be considered (pseudo)-hermitian regarding the $\mathcal{CPT}$ inner product.

properties and behavior of systems such as the one in eq. (2.14) on an experimental basis in the context of QM. As will be discussed in the next section, the field of optics yields the perfect playground for such investigations as arbitrary complex potentials are experimentally accessible at a much smaller expense.

2.4.2 $\mathcal{PT}$ Symmetric Optics

As stated in section 2.1.1, the PHE (2.2) is mathematically equivalent to the SE. From this it follows that the concept of $\mathcal{PT}$ symmetry can be carried over to paraxial optics in a straight forward fashion. In 2007, this was first realized by El-Ganainy et al. in ref. [30] where they developed a formalism suitable for describing coupled optical $\mathcal{PT}$ symmetric systems and thus laid the theoretical ground work for $\mathcal{PT}$ symmetric optics. The authors stated that as a direct consequence of the symmetry, the optical potential δn in eq. (2.2) must satisfy

$$\delta n\left(\xi\right) = \delta n^{*}\left(-\xi\right),$$

that is it must be comprised of a symmetric index profile and an antisymmetric gain/loss profile. The first experimental realizations of simple $\mathcal{PT}$ systems were reported in Refs. [37, 82] where the authors considered simple $\mathcal{PT}$ dimer structures and investigated the beam dynamics. Already these kinds of synthetic $\mathcal{PT}$ materials were shown to exhibit unique characteristics such as power oscillations, loss induced optical transparency, etc. Regarding the fact that even such simple $\mathcal{PT}$ cells can exhibit unconventional features, the natural follow-up question was what novel and interesting properties can be expected from more complex structures, like $\mathcal{PT}$ symmetric lattices. This question was first addressed in ref. [58] and even extended to the non-linear regime in ref. [64]. Originating from these works, many unique characteristics of $\mathcal{PT}$ symmetric optical systems have been theoretically predicted as well as experimentally observed [56, 57, 11, 98, 26, 79, 1]. All these findings have only been possible because $\mathcal{PT}$ optics differs in one particular and important aspect from $\mathcal{PT}$ symmetric QM. Considering this, one could even argue that it is in this sense where $\mathcal{PT}$ symmetric optics is even more interesting than $\mathcal{PT}$ symmetric QM. The property concerned is that $\mathcal{PT}$ symmetric QM comes with a Hamiltonian-dependent inner product, whereas in $\mathcal{PT}$ symmetric optics this is not the case. While in QM the measurement process itself and hence the inner product cannot be "observed" experimentally the situation is different in optics. In optics one measures the intensity I, which corresponds to the absolute square of the slowly varying envelope $\mathcal{A}$, i.e. $I\left(x\right) \sim \left|\mathcal{A}\left(x\right)\right|^{2} = \mathcal{A}^{*}\left(x\right)\mathcal{A}\left(x\right)$. From that, one can readily conclude that the only meaningful inner product in optics is given by the standard inner product, i.e. $\langle\mathcal{A}|\mathcal{A}'\rangle = \int \mathcal{A}^{*}\left(x\right)\mathcal{A}'\left(x\right)\mathrm{d}x$, hence

one cannot simply chose the appropriate inner product corresponding to $\mathcal{PT}$ symmetry. As an immediate consequence one finds that Eigen-vectors of $\mathcal{PT}$ symmetric Hamiltonians are not orthogonal. In the same fashion, other properties that distinguish $\mathcal{PT}$ symmetric optical systems from corresponding $\mathcal{PT}$ symmetric QM systems follow from the presence of a predefined inner product in optics. And it is in this sense where $\mathcal{PT}$ symmetric optics might be more interesting than its QM counterpart, as one is indeed able to observe seemingly non-unitary "quantum" evolutions, non-orthogonal Eigen-states and other usually forbidden characteristics of quantum systems.

2.4.3 *Passive $\mathcal{PT}$ Symmetry*

The first experimental observations of $\mathcal{PT}$ symmetric optics were based on platforms where one was able to introduce well-defined gain and loss in order to account for an appropriate complex optical potential. As researchers aspired to access more and more complex structures, the well-defined introduction of gain turned out to be the bottle neck of possible implementations. It was then argued that propagation dynamics equivalent to those of $\mathcal{PT}$ symmetric structures could also be achieved in entirely passive structures, where one exhibits no gain, but only loss. This is true as long as the structure is "quasi" $\mathcal{PT}$ symmetric around the mean loss of the structure. In case of a simple directional coupler this was rigorously shown in ref. [71] and shall be briefly recapitulated here for clarity.

In order to do so the example of a simple directional coupler presented in section 2.2.2 shall be extended to the $\mathcal{PT}$ symmetric regime. This can be achieved by "inserting" gain of strength Γ into the first waveguide and loss of equal strength $(-\Gamma)$ in the second waveguide. In this specific case the coupled mode equation reads

$$i\partial_\zeta \begin{pmatrix} a_1 \\ a_2 \end{pmatrix} = \begin{pmatrix} i\Gamma & C_1 \\ C_1 & -i\Gamma \end{pmatrix} \begin{pmatrix} a_1 \\ a_2 \end{pmatrix} . \tag{2.15}$$

From which one can easily calculate the Eigen-values as well as Eigen-vectors, which are

$$\begin{pmatrix} a_1 \\ a_2 \end{pmatrix}_\pm = \begin{pmatrix} 1 \\ \frac{i\Gamma + E_\pm}{C} \end{pmatrix}, \qquad E_\pm = \pm\sqrt{C^2 - \Gamma^2} .$$

It is interesting to note that the structure of the Eigen-values reveals a breaking of the $\mathcal{PT}$ symmetry for $C = \Gamma$, that is the system is $\mathcal{PT}$ symmetric for $C > \Gamma$. In this regime the system shows those power oscillations typical for $\mathcal{PT}$ symmetric systems. An illustrative example is presented in fig. (2.10) (a), here $C_1 = 1$ and $\Gamma = 0.2$. In

the same fashion, one can verify that Eigen-values and Eigen-vectors of a system described by

$$i\partial_\zeta \begin{pmatrix} a_1 \\ a_2 \end{pmatrix} = \begin{pmatrix} 0 & C_1 \\ C_1 & -2i\Gamma \end{pmatrix} \begin{pmatrix} a_1 \\ a_2 \end{pmatrix} \tag{2.16}$$

are given by

$$\begin{pmatrix} a_1 \\ a_2 \end{pmatrix}_\pm = \begin{pmatrix} 1 \\ \frac{E_\pm}{C} \end{pmatrix}, \qquad E_\pm = i\Gamma \pm \sqrt{C^2 - \Gamma^2} \ .$$

This latter case describes a directional coupler, which is not $\mathcal{PT}$ symmetric, since both diagonal terms are not complex conjugates of each other. In fact, in this specific case the first waveguide contains neither gain nor loss and the second waveguide contains twice the loss compared to the aforementioned $\mathcal{PT}$ coupler. However, as the structure of the Eigen-values suggests, even in this entirely passive case the propagation dynamics are equivalent to the $\mathcal{PT}$ symmetric case up to a global the damping factor $e^{-\Gamma\zeta}$. Figure (2.10) (b) shows a graphical representation of this fact. In accordance with (a) $C_1 = 1$ and $\Gamma = 0.2$. It is well visible that the dynamics underneath the exponential envelope are the same as those of (a). In fact, mathematically it is easy to see that both cases can be transformed into each other via $(a_1,\ a_2)^\top \to e^{-\Gamma\zeta}\,(a_1,\ a_2)^\top$.

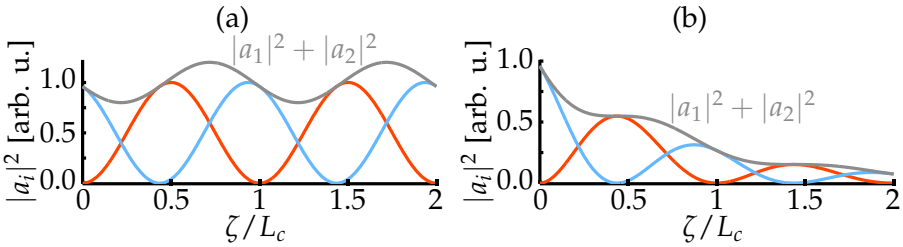

Figure 2.10: (a) Amplitudes $|a_1|^2$ and $|a_2|^2$ as well as total power $|a_1|^2 + |a_2|^2$of a $\mathcal{PT}$ symmetric directional coupler. (b) Amplitudes $|a_1|^2$ and $|a_2|^2$ as well as total power $|a_1|^2 + |a_2|^2$of a passive $\mathcal{PT}$ symmetric coupler. Both graphs follow equations (2.15) and (2.16) respectively, whereas $C_1 = 1$ and $\Gamma = 0.2$ in both cases.

The arguments applied to this simple case of a directional coupler can be applied to any general $\mathcal{PT}$ symmetric lattice, i.e. one can always use a transformation $a_n \to e^{-\Gamma\zeta} a_n$ with an appropriate global damping factor Γ and turn a truly $\mathcal{PT}$ symmetric system into a passive $\mathcal{PT}$ system. In this process, regardless of the specific realization the underlying $\mathcal{PT}$ propagation dynamics will be preserved in the passive case. As mentioned before this is highly important for experimental realizations, as the task of implementing gain and loss in a well defined fashion reduces to the insertion of loss only.

3

REALIZING LOSS IN MODULATED WAVEGUIDES

Since $\mathcal{PT}$ symmetric systems entered optics [7, 30], it became evident that loss is not only an unwanted side effect of an optical system but can introduce a variety of new and exciting physical phenomena such as unusual beam dynamics [58, 109], $\mathcal{PT}$ symmetric solitons [64, 23], Bloch Oscillations and dynamic localization in complex crystals [56, 57], and even optical tachyons [98]—as long as the loss can be introduced in a controlled manner. As the most natural way of implementing $\mathcal{PT}$ symmetry is using systems of evanescently coupled waveguides, the loss management in the individual waveguides is the crucial step in the fabrication process. Currently, there are three different techniques available. First, when implementing waveguides in an AlGaAs heterostructure (the most popular fabrication technique of waveguides these days), additional losses can be introduced by adding a thin chromium layer on top of the particular waveguides [37]. Second, waveguides obtained by Titan-indiffusion into LiNb wafers can exhibit additional loss due to the optical excitation of electrons from Fe^{2+} color centers to the conduction band [82]. Recently, a ground-breaking third technology was introduced: $\mathcal{PT}$ synthetic lattices with time as the "transverse" coordinate, where losses are obtained by acousto-optical modulation [79]. The downside of the first two approaches is that they are inherently planar, with no possibility of involving a second transverse dimension. Also, it seems that the third approach is limited to 1D systems due to practical reasons, and additionally the evolution equations in these systems do not perfectly match the set of coupled Schrödinger-like equations as required in the original proposal of optical $\mathcal{PT}$ symmetry.

In this chapter a new technique for achieving a controllable amount of loss in waveguides will be discussed. The platform of choice will be waveguides created by FLDW, as discussed in section 2.3. Throughout the work of this thesis several approaches to introduce well defined losses in waveguides have been pursued. These are not discussed in the main body of this thesis but are briefly compared and evaluated in appendix A.1. As a result it is argued, that radiation loss due to a sinusoidal bending of waveguides is more advantages than other approaches. In section 3.1 the nature of this type of loss mechanism is discussed in detail on a numerical basis. As this nu-

merical investigation reveals a seemingly counter-intuitive behavior the loss mechanism due to periodically bending the waveguides is investigated analytically in more depth in section 3.2. In order to grasp the essence of the underlying mechanisms a 1D SE with a sinusoidally oscillating box-potential is assumed as a model system. Most importantly, section 3.2 shows that the loss mechanism under investigation leads to an exponential decay of the intensity along the propagation direction inside the waveguide. The resulting exponential decay rate is given in closed form as a function of all relevant system parameters. Finally, in section 3.3 experimental results for sinusoidally bent waveguides are discussed. It is found that numerical results, analytical description as well as experimental observations are in very good agreement.

3.1 NUMERICAL INVESTIGATION OF MODULATED WAVEGUIDES

3.1.1 *Light Propagation in Sinusoidally Bent Waveguides*

For analyzing the light propagation in sinusoidally bent waveguides, the following parameters are chosen. The wavelength $\lambda = 0.633\,\mu m$ and the background refractive index $n_0 = 1.45$. For numerical reasons, the refractive index increase is not modeled as a rect-function but rather a super-Gaussian of power 16, i.e.

$$\delta n = \delta n_{max} \exp\left[-\left(\frac{\xi - \xi_0}{w_{wg}}\right)^{16}\right], \tag{3.1}$$

with $\delta n_{max} = 6 \cdot 10^{-4}$ and $w_{wg} = 3/x_0\,\mu m$. Note that, following section 2.1.1, $w_{wg} = 50.71$ in dimensionless units as $x_0 = 0.0592\,\mu m$ for this set of parameters. Moreover the center of the waveguide oscillates sinusoidally with

$$\xi_0 = d\left[1 - \cos\left(\frac{2\pi}{p}\zeta\right)\right]. \tag{3.2}$$

In fig. 3.1 (a) the simulated transverse mode profile as well as the associated potential of a straight waveguide is shown, correspondingly the evolution of the bound mode's phase is depicted in subfigure (b). From this graph one can extract a period length of 1.98 mm or equivalently a propagation constant of $3.17\,mm^{-1}$. As will be shown subsequently, the bound mode's propagation constant is an important parameter for the behavior of sinusoidally modulated system.

If a sinusoidal modulation is introduced to the center of the waveguide, radiation losses occur due to the bending of the waveguide. In fig. 3.2 (a) the light evolution for a sinusoidally bent waveguide is shown for an oscillation period of 1 mm. The top subfigure of fig. 3.2 (a) represents the amplitude at the center of the waveguide as a function of the propagation distance. The logarithmic plot suggests

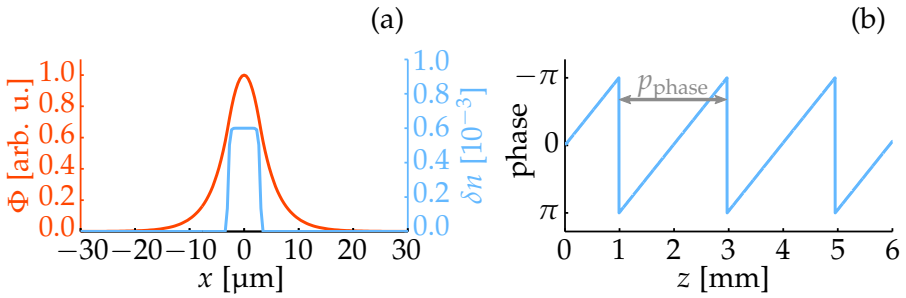

Figure 3.1: (a) Transverse mode profile (red) and corresponding waveguide profile (blue) as described by eq. (3.1). (b) Phase evolution of the mode shown in (a) along a straight waveguide. The period length $p_{\text{phase}} = 1.98\,\text{mm}$.

that the mean dependence can well be described by an exponential decay as indicated by the dashed line. On the other hand, locally one can observe local maxima and minima while the amplitude oscillates with a period of 500 µm, which corresponds to twice the bending frequency. Since the loss in this system is caused by the bending of

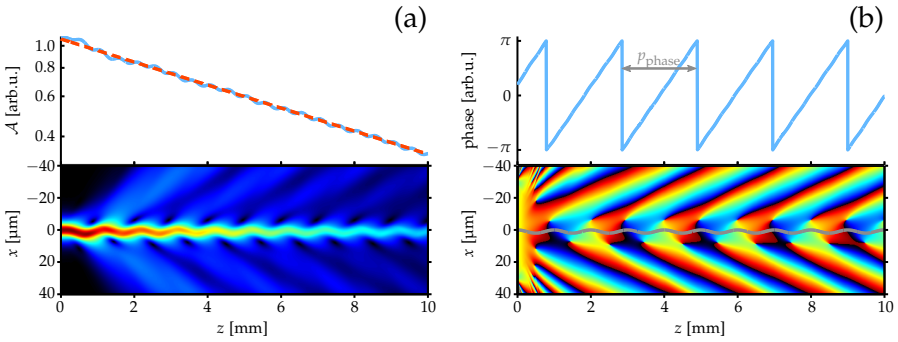

Figure 3.2: (a) Bottom: Light evolution (amplitude) for sinusoidally bent waveguide with an oscillation period of 1 mm. Top: Amplitde of the light field at the center of the waveguide as a function of propagation distance (blue solid line). The red dashed line corresponds to an exponential decay with a decay rate of $1.16 \cdot 10^{-1}\,\text{mm}^{-1}$. (b) Bottom: Phase evolution corresponding to (a). Top: Phase at the center of the waveguide. The period length $p_{\text{phase}} = 2.05\,\text{mm}$.

the waveguide one could expect the loss to grow monotonically with increasing bending frequency (or equivalently with decreasing bending period). That this naive assumption cannot be true is already clear when considering the light evolution for very high frequencies. It is intuitively clear that in this case, i.e. when the bending frequency approaches infinity, the loss of the bound mode should be zero. In this situation, the bound mode is too inert to follow the quick oscillations of the waveguide and as a consequence experiences an effective lossless potential. One can expect this effective potential to be equal to the temporal average of the true potential. This lossless limiting

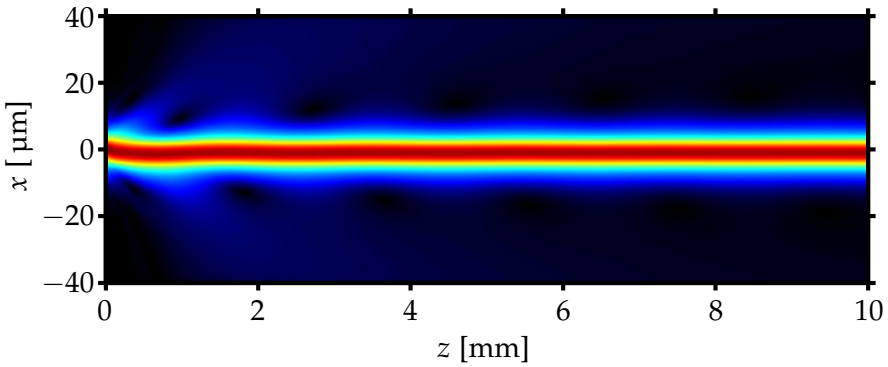

Figure 3.3: Light evolution (amplitude) for sinusoidally bent waveguide with an oscillation period of 5 µm.

case is depicted in fig. 3.3. Here the light evolution for a sinusoidally bent waveguide with an oscillation period of 5 µm is shown. After an initial decay, the Eigen-mode of the effective potential is quickly established and the transverse mode profile becomes $z-$independent. The initial decay is due to the fact that the waveguide is excited by the Eigen-mode of the straight waveguide.

3.1.2 *Decay vs. Oscillation Period*

From the previous paragraph it follows that for both zero and infinite bending the decay of the bound mode is zero and for intermediate bending there is a measurable loss due to the curvature of the guide. Moreover, the loss can well be approximated as an exponential decay. Ultimately, in order to controllably manufacture lossy waveguides the question is, how the decay behaves as a function of the bending period. In order to approach the answer to this, fig. 3.4 contains the extracted decay rates for various oscillation periods. As illustrated in this graph, the loss's dependence on the oscillation period can be divided into four regions. It will be discussed subsequently, that on one hand these four regions differ quantitatively regarding the mere value of the loss but on the other hand in these regions the behavior of the loss also strongly differs qualitatively.

Starting the discussion in region four of fig. 3.4, one can see, that the decay rate in the waveguide is negligibly small, hence the guide can be approximated as being straight. As an example, fig. 3.5 shows the evolution dynamics of a waveguide with an oscillation period of 2.5 mm. From subfigure (a) it is apparent that the intensity inside the waveguide almost does not drop during evolution. The initially stronger oscillations (up to a propagation distance of approx. 7.5 mm) also decay during propagation.

The most curious property of the evolution dynamics is the behavior of the phase. First of all, the period of the phase oscillation

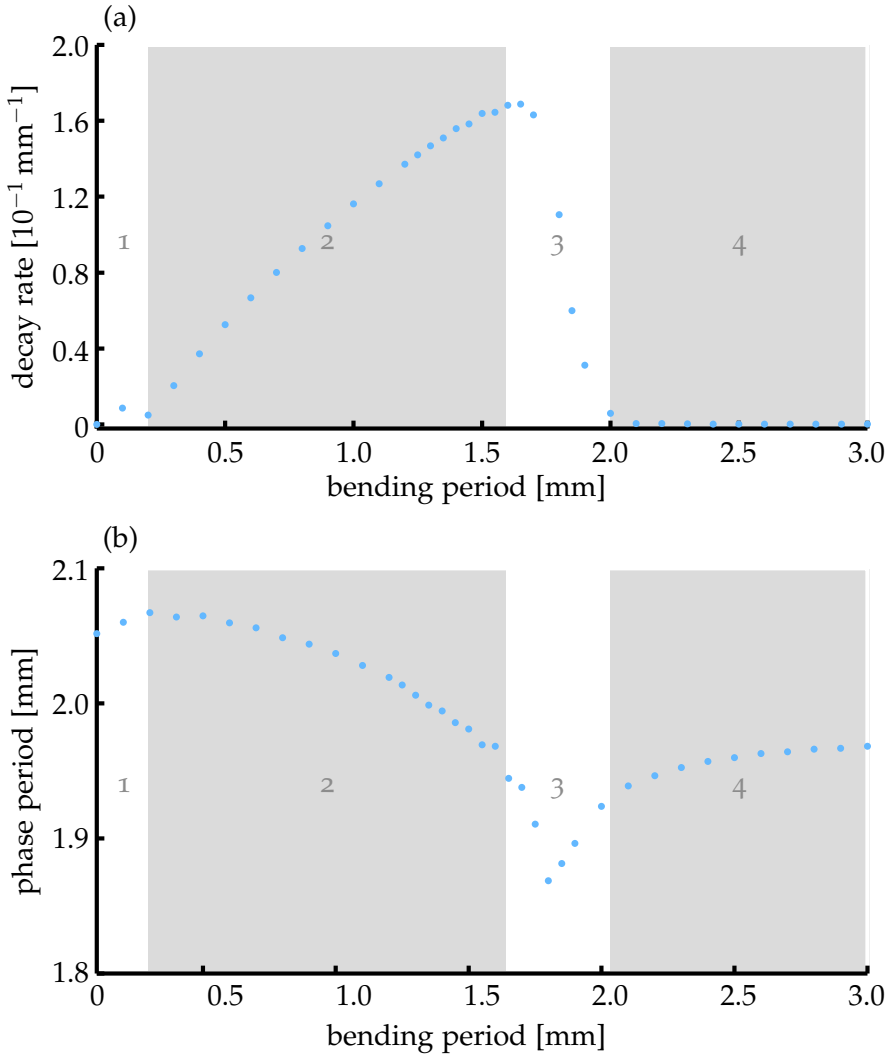

Figure 3.4: (a) Decay rate as a function of bending period of the oscillating waveguide. (b) Phase oscillation period of light inside of the waveguide as a function of bending period.

along the waveguide amounts to 1.95 mm, which is almost identical to the period within the straight waveguide (1.98 mm). It is very interesting to find that this period length is almost constant throughout region four (fig. 3.4), even at small periods where the bending approaches the straight waveguide's phase oscillation period. In this respect, maybe the most important finding is that the boundary between region four and region three in fig. 3.4 coincides with the phase oscillation period of the straight waveguide's bound mode.

In addition, it is instructive to study the presence and location of the phase singularities shown in the bottom graph of fig. 3.5 (b). The plot shows that the waveguide is seemingly arched around the phase singularities. This property links all realizations in region four (fig. 3.4). What distinguishes the locations for different oscillation periods

is the distance to the waveguide. It can be found that for larger oscillation periods the location of the phase singularities is further away from the waveguide, while for smaller period lengths the phase singularities are located closer to the waveguide. This behavior can well be explained using the following intuition.

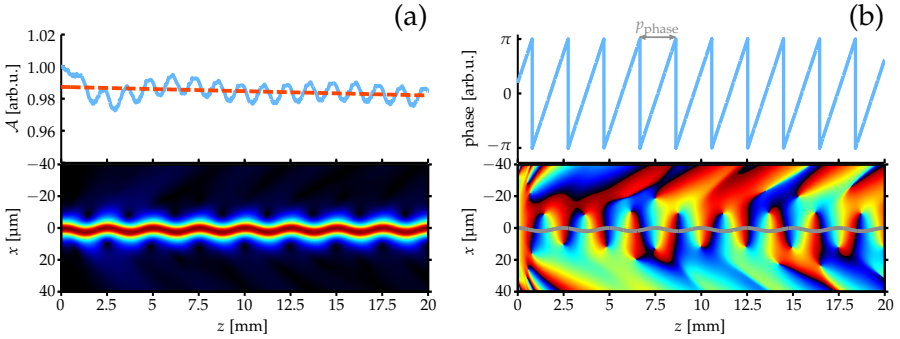

Figure 3.5: (a) Bottom: Light evolution (amplitude) for sinusoidally bent waveguide with an oscillation period of 2.5 mm. Top: Amplitde of the light field at the center of the waveguide as a function of propagation distance (blue solid line). The red dashed line corresponds to an exponential decay with a decay rate of $2.7 \cdot 10^{-4}\,\text{mm}^{-1}$. (b) Bottom: Phase evolution corresponding to (a). Top: Phase at the center of the waveguide. The period length $p_{\text{phase}} = 1.95\,\text{mm}$.

If one considers a straight waveguide, there are no phase singularities, as the surfaces of equal phase are parallel (transverse) planes [fig. 3.6 (a)]. If a section of the waveguide is bent along an arc the formerly parallel phase planes overlap in the center of the circle [fig. 3.6 (b)]. Consequentially, a phase singularity appears in the center of the circle. It is obvious that the smaller the radius of curvature is, the closer the singularity is to the guide. Regarding the influence of

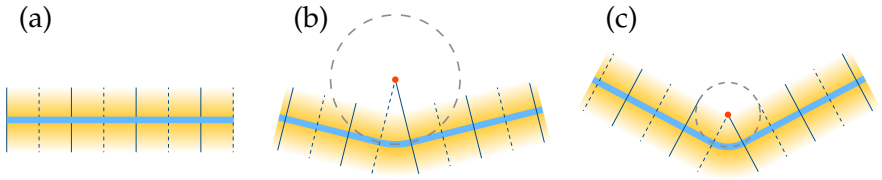

Figure 3.6: Scheme of three waveguides (light blue lines) with different bending radii. The transverse phase planes are denoted by dark blue lines and the mode volume is shaded orange. At the center of the circle (red dot), where the phase planes overlap, occurs a phase singularity.

the location of the singularities on the propagation dynamics of the waveguide mode, one can suspect that the singularity has no effect, if it is well outside of the mode volume [fig. 3.6 (b)]. Only when the singularity is inside of the mode volume [fig. 3.6 (c)], it affects

the propagation dynamics, since the field amplitude has to be zero at the location of the singularity. Due to this effect, if the singularity is close enough to the waveguide, the mode gets "squeezed" out of the waveguide region and bending losses occur.

Even though for a sinusoidally bent waveguide the situation is a little bit more involved, the principle behavior is equivalent. If the phase singularities are sufficiently close to the guide (inside of the mode volume), bending losses start to occur. Interestingly, this transition seems to take place when the modulation frequency coincides with the bound mode's propagation constant.

In region three the exponential decay rate increases when increasing the oscillation frequency. Figure 3.7 illustrates the propagation dynamics for an exemplary oscillation period of 1.85 mm. Most notably in this region the decay differs more strongly from the average exponential decay. The deviation is illustrated by the dotted gray line in fig. 3.7 (a). From this, one can see that in addition to the small scale oscillations with a period equal to the modulation frequency of the waveguide there is another large scale oscillation. In this specific case it has a period of approximately 15 mm.

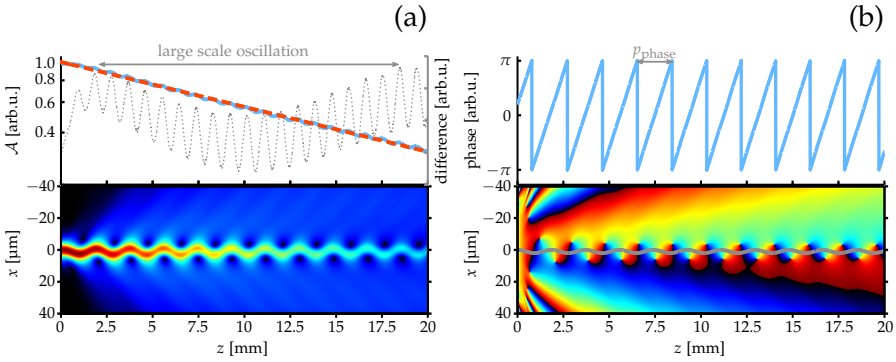

Figure 3.7: (a) Bottom: Light evolution (amplitude) for sinusoidally bent waveguide with an oscillation period of 1.85 mm. Top: Amplitde of the light field at the center of the waveguide as a function of propagation distance (blue solid line). The red dashed line corresponds to an exponential decay with a decay rate of $5.9 \cdot 10^{-2}\,\text{mm}^{-1}$. The dotted gray line (ordinate on the right hand side) corresponds to the difference between the two logarithms of amplitude and the mean exponential decay respectively. (b) Bottom: Phase evolution corresponding to (a). Top: Phase at the center of the waveguide. The period length $p_{\text{phase}} = 1.87\,\text{mm}$.

Compared to region four (fig. 3.4) in region three the phase singularities are closer to the waveguide as well as slightly shifted to larger propagation distances. A difference that can be observed comparing fig. 3.5 (b) and fig. 3.7 (b). This indicates a qualitatively different propagation behavior. While in region four almost no light is radiated away from the waveguide, the situation is different in region three. There the curvature is large enough to cause a substantial

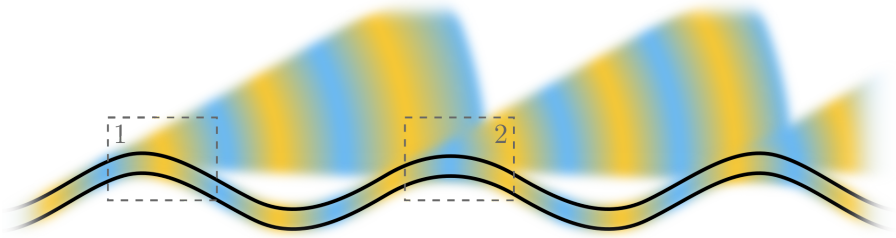

Figure 3.8: Schematic illustration of light being radiated away from sinusoidally bent waveguides. In regions 1 and 2 (dashed boxes) light is emitted and reabsorbed. Light cones from subsequent emission regions overlap and interfere.

amount of radiation. In fig. 3.8 this process is schematically illustrated. Light leaves the waveguide where the curvature is strongest [areas 1 and 2 in fig. 3.8]. However, the angle under which light is radiated away from the guide is very small, so that first of all part of the light radiated away in area 1 re-enters the waveguide in area 2 and second of all the two emerging light cones strongly overlap. Due to this strong overlap the light can interfere. Depending on the relative phase difference the net power, which is radiated away from the waveguide, is either amplified or suppressed respectively. This effect is best illustrated in fig. 3.2 (a), where the light cones at every second bend are suppressed. The finding is also supported by the phase evolution shown in fig. 3.2 (b), where one can see that the phase difference between two consecutive bends is in the order of π, causing destructive interference of the radiated light.

In conclusion, the existence of a maximum exponential decay rate and the decline of decay when increasing the oscillation frequency of the guides (as observed in region two of fig. 3.4) can be explained by the interference between light that is radiated away from consecutive bends. It should also be emphasized that region two in fig. 3.4, where the decay rate decreases for increasing oscillation frequencies, is well above the regime where the waveguide can be approximated as an effective medium. To support that statement fig. 3.9 shows the light

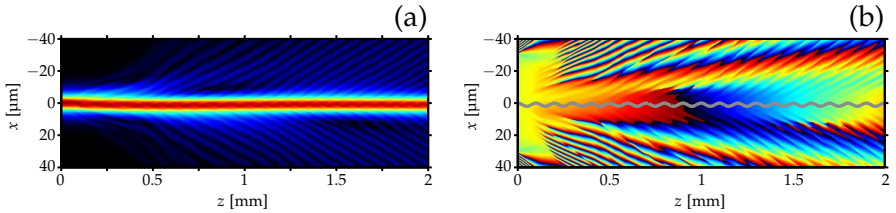

Figure 3.9: (a) Light evolution (amplitude) for sinusoidally bent waveguide with an oscillation period of 0.1 mm. (b) Phase evolution corresponding to (a).

evolution for an oscillation period of 100 µm (region one in fig. 3.4). It is well visible that in contrast to fig. 3.3 the light mainly follows

the oscillation of the waveguide. Moreover, the light cones that are radiated away from the bends are visible in fig. 3.9 (a) while (b) shows that the phase evolution is by no means similar to that of a stationary mode.

3.1.3 *Concluding the Numerical Investigation*

In summary, the light evolution inside sinusoidally oscillating waveguides was studied numerically. It was found that the overall decay inside the guides can well be approximated as being exponential. Moreover the simulations verified the intuition that the decay vanishes for straight waveguides as well as for quickly oscillating ones, that can be approximated as an effective medium. For medium oscillation frequencies the decay rate shows a single distinct maximum. The investigation suggests that the behavior of the decay as a function of the oscillation period is well connected to the interference of light that is radiated away from distinct bends of the waveguide. An important quantitative finding is that the decay is negligibly small as long as the oscillation frequency of the guide is smaller than the phase oscillation period of the bound mode of the straight waveguide. At this specific frequency the exponential decay suddenly starts to increase.

3.2 ANALYTICAL DESCRIPTION OF AN OSCILLATING POTENTIAL

Even though the numerical study yields an insight into the underlying physics of the system, it lacks the ability to make more quantitative statements such as the magnitude and location of the maximum decay rate as a function of the system parameters. The goal of this section is to answer this need and to give an analytical expression for the exponential decay rate. In order to do so, the system under consideration will be eq. (3.10) equipped with the oscillating box potential

$$\delta n = \begin{cases} \delta n_{max} & ;\ |\xi - \xi_0| < w \\ 0 & ;\ else \end{cases} \tag{3.3}$$

where the center of the potential is given by eq. (3.2). Note that the box potential differs slightly from the super-Gaussian Potential [eq. (3.1)] used in the numerical study. However, this does not pose a limitation to the validity, since, as it will be pointed out at the end of this section, the findings of this section can well be generalized to an arbitrary potential.

3.2.1 *Straight Waveguide Revisited*

The first step in the analysis is to revisit the straight waveguide case and to make some more statements about it which will turn out to be necessary for solving the oscillating case. In section 2.1.3 it was stated that the transverse mode profile of the Eigen-mode of a box potential is given by eq. (5.3) and the mode's Eigen-frequency is determined by the dispersion relation eq. (2.7). As a matter of fact, this is only half of the story, since the box potential (3.3) also supports a continuous, infinite set of so-called radiation modes. A basis (complete set of Eigen-modes) then consists of all radiation modes as well as the single bound mode.

In elementary QM these radiation modes are usually discussed in terms of a scattering problem, where a radiation mode is formed by the incident, reflected, and transmitted plane wave as well as the forward and backwards propagating waves inside of the box. A complete set of radiation modes is formed by taking into account incident fields both from the left and the right side of the potential for all positive propagation constants as defined in eq. (2.5).

Since these types of radiation modes do not possess a nice symmetry, i.e. they are neither symmetric nor antisymmetric, it is advantageous for further calculations to symmetrize them. This can easily be done by calculating the symmetric and antisymmetric superposition of left and right incident modes with the same propagation constant, respectively. This way, the spatial structure of the modes is given by

$$\Phi_s(\xi,\beta) = \begin{cases} \mathrm{Re}\left[A_s e^{-ik_2(\xi+w)}\right] & ;\ \xi < -w \\ \cos(k_1\xi) & ;\ |\xi| < w \\ \mathrm{Re}\left[A_s e^{ik_2(\xi-w)}\right] & ;\ \xi > w \end{cases} \tag{3.4}$$

for the symmetric modes and

$$\Phi_a(\xi,\beta) = \begin{cases} -\mathrm{Re}\left[A_a e^{-ik_2(\xi+w)}\right] & ;\ \xi < -w \\ \sin(k_1\xi) & ;\ |\xi| < w \\ \mathrm{Re}\left[A_a e^{ik_2(\xi-w)}\right] & ;\ \xi > w \end{cases} \tag{3.5}$$

for the antisymmetric modes. Moreover

$$\begin{aligned} A_s &= \cos(k_1 w) + i\tfrac{k_1}{k_2}\sin(k_1 w) \\ A_a &= \sin(k_1 w) - i\tfrac{k_1}{k_2}\cos(k_1 w) \\ k_1 &= \sqrt{\beta + \delta n_{max}} \\ k_2 &= \sqrt{\beta} \end{aligned} \tag{3.6}$$

where $\beta \geq 0$. The normalization of these modes is given by

$$\langle \Phi_{a/s}(\beta) | \Phi_{a/s}(\beta') \rangle = 2\pi k_2 |A_{a/s}|^2 \delta(\beta - \beta') \tag{3.7}$$

for the radiation modes and

$$\langle \Phi_b | \Phi_b \rangle = \frac{\delta n_{max}}{\kappa_2^3} \sin^2(\kappa_1 w) + w \tag{3.8}$$

for the bound mode. A more detailed mathematical calculation of eq. (3.7) can be found in app. A.2 and A.3.

3.2.2 *Oscillating Potential*

Having exhaustively investigated the properties of the straight waveguide one can turn to the oscillating case. The first step in the analysis will be to consider a moving frame of reference in which the potential is stationary. In this specific case, the transformation reads

$$\begin{aligned} \xi' &= \xi - \xi_0(\zeta) \\ \zeta' &= \zeta \end{aligned} \tag{3.9}$$

where ξ_0 is given by eq. (3.2) and in the new frame of reference the 1D PHE reads

$$i\partial_\zeta \mathcal{A} = -\partial_{\xi'}^2 \mathcal{A} - \delta n(\xi') \mathcal{A} + i\nu d \sin(\nu\zeta) \partial_{\xi'} \mathcal{A} \ . \tag{3.10}$$

Equation (3.10) represents a 1D PHE equipped with a stationary potential δn and an additional external oscillating term containing the derivative of the field. It is interesting to note that eq. (2.2) or equivalently eq. (3.10) can be transformed to a similar form where the term $i\nu d \sin(\nu\zeta) \partial_{\xi'}$ is replaced by $\nu^2 d \cos(\nu\zeta) \xi'$. Applying this so-called Kramers-Henneberger Transformation, the equation is well known in many fields of physics, as it represents the dynamics of an electronic wave function under the influence of an external electric field. This system is of central interest in the field of attosecond physics, where the equation is studied in great detail [20, 52, 54]. Unfortunately, the literature of attosecond science does not provide knowledge which is particularly relevant for the present investigation. Therefor there are mainly two reasons. One reason being that the quantities of interest in attosecond pulse generation differ from those of this thesis. While in attosecond physics researchers are interested in the ionization process and the resulting properties of the free electron, in the underlying waveguide system the analysis is focused on the bound state. Another reason is tied to the fact that the atomic system, which is considered in attosecond physics, is much more complex than the underlying waveguide system, which leads to the fact that a detailed analytical investigation is impractical and many studies are carried out numerically.

Considering the structure of eq. (3.10) - with its static potential and ζ-dependent perturbation - one might wish two apply Fermi's Golden Rule[31, 18] in order to retrieve the exponential decay rate that was predicted by the simulations. However, therein lie several

inadequacies. The first shortcoming is that Fermi's Golden Rule is rigorously derived for time-independent perturbations. Even though generalizations of Fermi's Golden Rule for time-dependent perturbations have been derived [88], they might lack the practicability of Fermi's original statement. Moreover, a hasty application of Fermi's Golden Rule to eq. (3.10) will lead to errors. Secondly, by just applying Fermi's Rule, one would simply postulate an exponential decay of the waveguide amplitude. While on one hand, this might seem acceptable, as the numerics clearly show this kind of behavior, on the other hand, this procedure could not serve as a rigorous proof of the average exponential decay, which in turn is the goal of this chapter. Moreover, the application of Fermi's Rule does not yield the higher order corrections to the average behavior. As a matter of fact, throughout the literature, a number of authors [33, 2, 19, 73, 99, 108, 25] have criticized the mathematical grounds of Fermi's derivation, presented generalizations, and even showed the invalidity in certain scenarios. In this sense, subsequently the cautious route of avoiding Fermi's Golden Rule and presenting a careful fundamental derivation is taken.

3.2.3 *Coupled Mode Theory and First Order Perturbation*

The reason for performing transformation (3.9) and continuing the analysis with eq. (3.10) is the fact that eq. (3.10) can more easily be handled in terms of perturbation theory. Regarding the amplitude d as a small perturbation, it is quite convenient that the perturbation term is linear in d. In fact, if $d = 0$ eq. (3.10) reduces to the well known static case. In this sense, the general solution strategy is to expand the field $\mathcal{A}$ in terms of the modes of the static potential and to perform a first order perturbation approximation afterwards. With this, the field can be written as

$$\begin{aligned} \mathcal{A}(\xi', \zeta) &= c_b(\zeta)\,\Phi_b(\xi')\,e^{-i\beta_b\zeta} \\ &+ \int_0^\infty \left[c_s(\zeta,\beta)\,\Phi_s(\xi') + c_a(\zeta,\beta)\,\Phi_a(\xi')\right] e^{-i\beta\zeta}\mathrm{d}\beta \end{aligned} \tag{3.11}$$

denoting the superposition of a single bound and a continuum of radiation mode, whereas for each propagation constant $\beta > 0$ there is one symmetric and one antisymmetric mode. The coefficients c represent yet unknown mode amplitudes which vary with propagation distance ζ. At this point, the goal of the analysis is to find the ζ-dependence of the coefficient c_b, which represents the amplitude of the bound mode. It will be shown that to first order c_b is given by an exponential decay, i.e. $c_b \sim e^{-\Gamma\zeta}$.

Inserting eq. (3.11) into eq. (3.10) and projecting it onto each of the Eigen-modes of the straight guide one obtains the system of coupled equations

$$\begin{aligned}
\partial_\zeta c_b &= \nu d \sin(\nu\zeta) \int_0^\infty c_a I_{ba} e^{i\beta_{ba}\zeta} \mathrm{d}\beta_a \\
\partial_\zeta c_s &= \nu d \sin(\nu\zeta) \int_0^\infty c_a I_{sa} e^{i\beta_{sa}\zeta} \mathrm{d}\beta_a \\
\partial_\zeta c_a &= \nu d \sin(\nu\zeta) \left\{ c_b I_{ab} e^{i\beta_{ab}\zeta} + \int_0^\infty c_s I_{as} e^{i\beta_{as}\zeta} \mathrm{d}\beta_s \right\}
\end{aligned} \tag{3.12}$$

which links the ζ-dependent coefficients c_i. In this system of equations the dependence on the transverse coordinate is eliminated and implicitly expressed in the overlap integrals $I_{jl} = \langle \Phi_j | \partial_{\tilde{\zeta}} | \Phi_l \rangle / \|\Phi_j\|^2$; also $\beta_{jl} = \beta_j - \beta_l$ where $j, l \in \{a, b, s\}$.

At this point, it might be advantageous to make use of the specific choice of initial conditions which is of interest for this analysis. In accordance with both the simulations as well as subsequent experiments only the case of

$$\begin{aligned}
c_a(\zeta = 0) = c_s(\zeta = 0) &= 0 \\
c_b(\zeta = 0) &= 1
\end{aligned}$$

will be considered. These conditions represent the fact that initially all light is confined within the bound mode. With these specific initial conditions the formal integration of the equations for c_a and c_s yields

$$\begin{aligned}
c_s(\zeta) &= \nu d \int_0^\zeta \sin(\nu\tau) \int_0^\infty c_a(\tau) I_{sa} e^{i\beta_{sa}\tau} \mathrm{d}\beta_a \mathrm{d}\tau \\
c_a(\zeta) &= \nu d \int_0^\zeta \sin(\nu\tau) \left\{ c_b(\tau) I_{ab} e^{i\beta_{ab}\tau} + \int_0^\infty c_s(\tau) I_{as} e^{i\beta_{as}\tau} \mathrm{d}\beta_s \right\} \mathrm{d}\tau.
\end{aligned}$$

Since the goal of this analysis is to find the longitudinal behavior of the amplitude of the bound mode, i.e. $c_b(\zeta)$, the next step consists of iteratively inserting the newly found equations for c_a and c_s into the first equation of the system (3.12) in order to remove the dependence on c_a and c_s and to obtain an integro-differential equation for the coefficient c_b. In the spirit of first order perturbation theory subsequently only the term quadratic in νd will be considered and all higher order terms will be neglected. This approximation is valid if

$$\nu d \ll 1 \tag{3.13}$$

and poses a joined condition on the oscillation frequency and amplitude. With this condition the equation for c_b reduces to

$$\partial_\zeta c_b = \nu^2 d^2 \sin(\nu\zeta) \int_0^\infty \int_0^\zeta \sin(\nu\tau)\, c_b(\tau)\, I_{ab} I_{ba} e^{i\beta_{ab}\tau} e^{i\beta_{ba}\zeta} \mathrm{d}\tau \mathrm{d}\beta_a \ . \tag{3.14}$$

It must be noted that due to the approximation above eq. (3.14) is only valid in a regime where both oscillation frequency and amplitude are

small. However, this condition is well met within the experiments under consideration.

It is instructive to reflect on the physical meaning of the approximation (3.13). To this end, fig. 3.10 illustrates the mode coupling as given by eq. (3.12). It is shown that the bound mode only couples directly to the antisymmetric modes. Whereas the antisymmetric radiation modes also couple to the symmetric radiation modes. In this sense, the above approximation implies that the coupling to the symmetric radiation modes is entirely disregarded and these modes play no role in the radiation process.

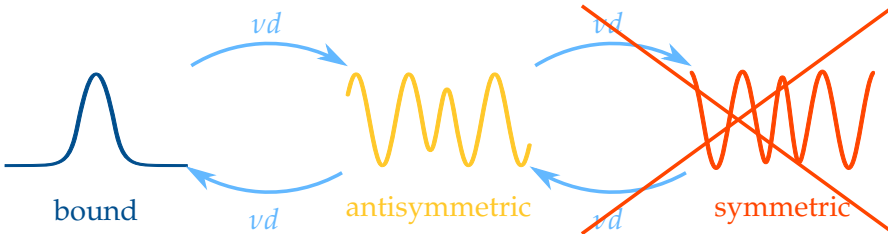

Figure 3.10: Schematic illustration of the mode coupling in accordance with eq. (3.12). The applied approximation is equivalent to neglecting the coupling to the symmetric modes.

3.2.4 *Markovian Approximation*

Considering eq. (3.14) it is interesting to mention that up to this point neither the explicit shape of the modes nor the structure of the perturbation operator have been used. Hence eq. (3.14) can be considered as a general expression for any sinusoidally oscillating potential. In order to further simplify and even solve eq. (3.14) the kernel of the integral needs to be evaluated. It is

$$\begin{aligned} I_{ab}I_{ba} &= -\frac{\langle\Phi_b|\partial_{\tilde{\zeta}}|\Phi_a\rangle^2}{\|\Phi_b\|^2\|\Phi_a\|^2} \\ &= -\alpha\frac{k_2\sin^2(k_1 w)}{\beta_a+\delta n_{max}\cos^2(k_1 w)}\frac{1}{(\beta_a-\beta_b)^2} \\ &=: -\alpha S(\beta_a) \end{aligned} \tag{3.15}$$

with

$$\alpha = \frac{2\delta n_{max}^2(\beta_b+\delta n_{max})\kappa_2\cos^2(\kappa_1 w)}{\pi\{\delta n_{max}\cos^2(\kappa_1 w)+(\beta_b+\delta n_{max})\kappa_2 w\}} \ .$$

Note that α is a constant factor regarding the integration in eq. (3.14) as it only depends on parameters of the straight waveguide. Furthermore, it is assumed that in eq. (3.15) $k_{1/2} = k_{1/2}(\beta_a)$.

With this result at hand, one can test the validity of eq. (3.14). In order to do so, both eq. (3.12) as well as eq. (3.14) were numerically integrated using the parameters from the previous section. Figure 3.11 shows the results of an example simulation for an oscillation period of 1 mm. The solid blue line corresponds to the amplitude of

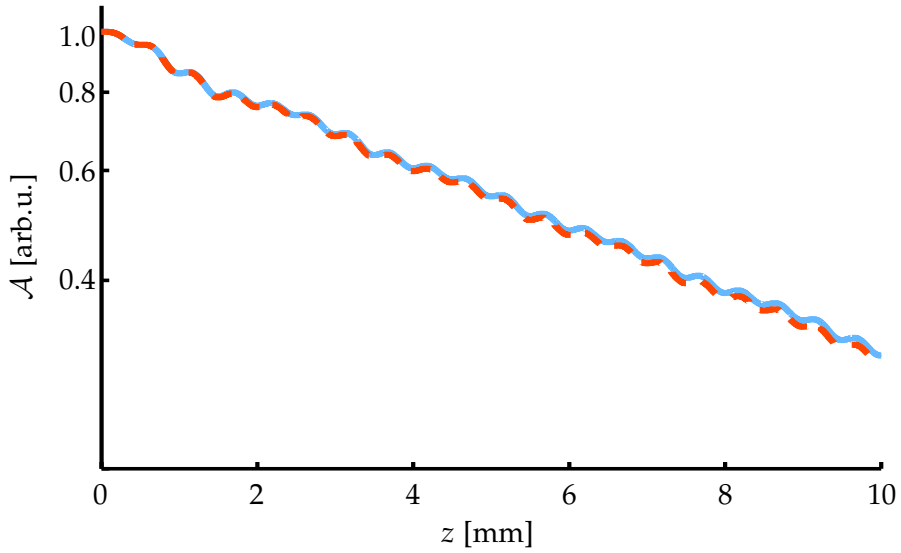

Figure 3.11: Amplitude of the bound mode for a sample simulation with a period of 1 mm. The solid blue line corresponds to the amplitude of the bound mode calculated from the complete system of equations (3.12). The dashed red line shows the evolution of the bound mode's amplitude calculated using eq. (3.14).

the bound mode calculated from the complete system of equations (3.12). Its result is identical to the values presented in fig. 3.2. The dashed red line shows the evolution of the bound mode's amplitude calculated using eq. (3.14). It is evident that it only deviates slightly from the rigorous calculation. This shows that the approximation (3.14) holds and proves the fact that the involvement of the symmetric modes in the radiation process can readily be neglected.

Continuing the analysis of eq. (3.14) it is advantageous to reverse the order of integration and rewrite it as

$$\partial_\zeta c_b = -\alpha\nu^2 d^2 \sin(\nu\zeta) \int_0^\zeta \sin(\nu(\zeta-\tau))\, c_b(\zeta-\tau) \int_0^\infty S(\beta_a)\, e^{i\beta_{ba}\tau} \mathrm{d}\beta_a \mathrm{d}\tau \tag{3.16}$$

where eq. (3.15) as well as the substitution $\tau' = \zeta - \tau$ was used. Investigating the temporal behavior of the kernel $\int_0^\infty S(\beta_a)\, e^{-i\beta_a\tau} \mathrm{d}\beta_a$ numerically, it was found that it is only significantly different from zero in a very small interval $\tau < \tau_c$. Moreover, in this interval c_b is only slowly varying and can hence be regarded as constant around $\tau \approx 0$, i.e.

$$c_b(\zeta-\tau) \approx c_b(\zeta)\,. \tag{3.17}$$

With the same argument it follows that the upper limit of the temporal integration in eq. (3.16) does not have a significance any more and can hence very well be extended to infinity. The term $\sin(\nu(\zeta-\tau))$ however is not slowly varying within the interval $0 < \tau < \tau_c$ and has

to be considered fully. With this Markovian Approximation eq. (3.16) reduces to the ordinary first order differential equation

$$\partial_\zeta c_b = -\alpha\nu^2 d^2 \sin(\nu\zeta)\, c_b \int_0^\infty \sin(\nu(\zeta-\tau)) \int_0^\infty S(\beta_a)\, e^{i\beta_{ba}\tau} \mathrm{d}\beta_a \mathrm{d}\tau \ . \tag{3.18}$$

Using eq. (A.7), the integration in eq. (3.18) can be carried out and

$$\partial_\zeta c_b = -\alpha\nu^2 d^2 c_b \left[\sin^2(\nu\zeta)\, T(\beta_b,\nu) + \tfrac{\sin(2\nu\zeta)}{2} U(\beta_b,\nu)\right] \tag{3.19}$$

is obtained, where the two ζ-independent terms $T(\beta_b,\nu)$ and $U(\beta_b,\nu)$ are given by

$$\begin{aligned} T(\beta_b,\nu) &= \tfrac{\pi\tilde{S}(\beta_b+\nu)}{2} - iPV\int_0^\infty \tfrac{(\beta_a-\beta_b)S(\beta_a)}{(\beta_a-\beta_b)^2-\nu^2}\mathrm{d}\beta_a \\ U(\beta_b,\nu) &= PV\int_0^\infty \tfrac{\nu S(\beta_a)}{(\beta_a-\beta_b)^2-\nu^2}\mathrm{d}\beta_a + i\tfrac{\pi\tilde{S}(\beta_b+\nu)}{2}. \end{aligned} \tag{3.20}$$

Note that here $\tilde{S}(\beta_b+\nu)$ was used instead of $S(\beta_b+\nu)$. This short hand notation is supposed to represent

$$\tilde{S}(\beta_b+\nu) = \begin{cases} S(\beta_b+\nu) & \nu \geq |\beta_b| \\ 0 & \nu < |\beta_b| \end{cases}$$

following the fact that the term $\delta(\beta_b-\beta_a+\nu)$ in eq. (A.7) is only different from zero if $\nu > |\beta_b|$. Also note that both $T(\beta_b,\nu)$ and $U(\beta_b,\nu)$ are split into real and imaginary part which is ensured since both $\tilde{S}$ and the integrals are purely real.

One last integration of eq. (3.19) yields the final expression for the amplitude of the bound mode within an oscillating waveguide, it reads

$$\begin{aligned} c_b(\zeta) &= \exp\left[-\tfrac{\alpha\nu^2 d^2}{2} T(\beta_b,\nu)\,(\zeta-\sin(2\nu\zeta))\right] \\ &\times \exp\left[-\tfrac{\alpha\nu d^2}{4} U(\beta_b,\nu)\,(1-\cos(2\nu\zeta))\right]. \end{aligned} \tag{3.21}$$

Analyzing the structure of eq. (3.21) one can identify several terms which are qualitatively different. Starting with the second exponential, one finds that it only contributes to a periodic oscillation, whereas the real part of U is responsible for an amplitude oscillation and its imaginary part is responsible for a corresponding phase oscillation; also the first exponential in eq. (3.21) contains an oscillating part. All oscillating terms in eq. (3.21) have the same frequency, which corresponds to twice the oscillation frequency of the waveguide. This observation was already made in connection with the simulations and hence is in perfect agreement. Moreover, the numerical investigation revealed that these oscillations are only small and can be neglected for long term evolution [compare figs. 3.2, 3.5, 3.7, and 3.11].

The only term in eq. (3.21) which contributes to a long term modulation is $c_b \sim \exp\left[-\frac{\alpha\nu^2 d^2}{2} T\left(\beta_b, \nu\right)\zeta\right]$. Since T consists of both a real and an imaginary part, it follows that only one term, namely

$$c_b \sim \exp\left[-\frac{\pi\alpha\nu^2 d^2}{4}\tilde{S}\left(\beta_b+\nu\right)\zeta\right], \tag{3.22}$$

contributes to an exponential decay, while the imaginary part of T is responsible for an additional linear phase. Inserting the argument $\beta_b + \nu$ into the definition of S in eq. (3.15) one finds that the exponential decay rate can be written as

$$\Gamma = \begin{cases} \frac{\pi\alpha d^2}{4}\frac{k_2 \sin^2(k_1 w)}{\beta_b+\nu+\delta n_{max}\cos^2(k_1 w)} & \nu \geq |\beta_b| \\ 0 & \nu < |\beta_b| \end{cases} \tag{3.23}$$

where $k_1 = \sqrt{\beta_b + \nu + \delta n_{max}}$, $k_2 = \sqrt{\beta_b + \nu}$ and $c_b \sim \exp\left[-\Gamma\zeta\right]$. Note that eq. (3.22) might be misleading, as it suggests that the decay rate is proportional to ν^2, however since $\tilde{S}\left(\beta_b+\nu\right) \sim \nu^{-2}$ the direct ν-dependence cancels. This fact is much clearer represented in eq. (3.23).

3.2.5 *Discussion*

Equation (3.23) presents the desired exponential decay rate for sinusoidally oscillating waveguides. As it was presumed from the results of the simulations in the previous section, the light evolution inside a sinusoidally oscillating waveguide can well be approximated as an overall exponential decay. The theoretical considerations suggest that this exponential decay is accompanied by minor amplitude and phase oscillations, with a frequency of twice the modulation frequency of the bent guide. As it is of minor interest in this thesis, the amplitude of these small oscillations is not given in closed form but can be found in terms of Chauchy Principal Values in eq. (3.20).

The exponential decay rate given by eq. (3.23) is in very good agreement with rigorous simulations. Figure 3.12 presents a comparison of both results. A very peculiar feature that can be found in both graphs and is most pronounced in the analytic curve is the fact that the decay is zero for modulation frequencies smaller than β_b. While this peculiarity was difficult to interpret with the simulations, it becomes even more obvious with the analytic considerations. As the analytical calculations are based on a mode-picture, it might be helpful to adopt a quantum-mechanical picture, where the propagation constant corresponds to the energy of a state. In this picture, one can argue that it takes at least a perturbation energy ν larger than $|\beta_b|$ in order to transfer energy from the bound state with a negative energy of β_b to the continuum of free modes with positive energy. Vice versa,

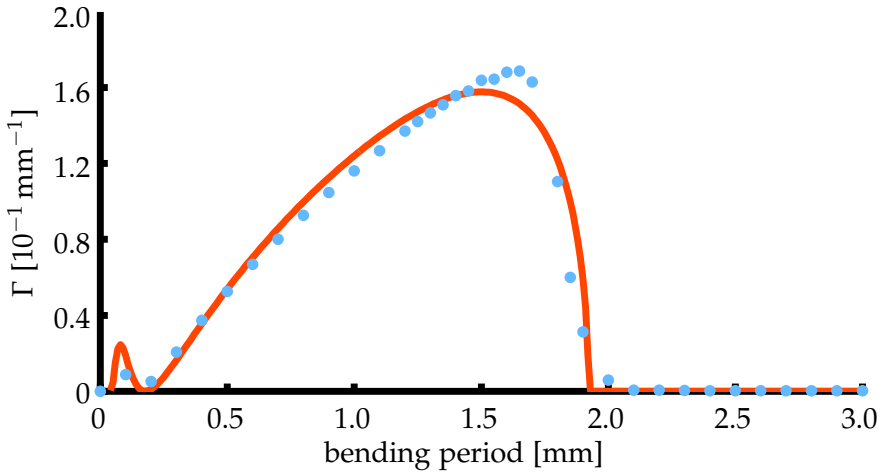

Figure 3.12: Exponential decay rate as a function of oscillation period

for a perturbation with an energy $\nu \leq |\beta_b|$ the bound mode just does not couple to the continuum, hence it does not decay.

From an experimental point of view, the question might arise: How to implement a certain loss for a given waveguide geometry, i.e. for w and δn_{max} being fixed? To answer this question, it is necessary to determine the maximum achievable loss and the corresponding modulation frequency for this specific configuration. Answering this question would formally involve finding the maximum of eq. (3.23). Unfortunately, the common procedure of calculating $\frac{\mathrm{d}\Gamma}{\mathrm{d}\nu} = 0$ and then solving for ν does not yield a closed form expression for the frequency ν. To overcome this dilemma, one can guess a rough estimate of the maximum by setting

$$k_1 w = \frac{\pi}{2}$$

in eq. (3.23), which corresponds to the maximum of the sine in the numerator and the minimum of the cosine in the denominator. With the definition of k_1 one can solve for the modulation frequency and obtains

$$\nu_{\mathrm{max,est}} = \frac{\pi^2}{4w^2} - \delta n_{max} - \beta_b. \tag{3.24}$$

Figure 3.12 shows that for the given set of parameters such an estimation yields a modulation period of $p_{\mathrm{max,est}} = 919\,\mu\mathrm{m}$ and the true maximum can be found at larger modulation periods. Even though $\nu_{\mathrm{max,est}}$ does not yield the exact maximum, at least it yields a lower bound and might be helpful in experimental parameter studies.

Interpreting the behavior of the decay rate, it is important to fill eq. (3.23) with a physical understanding. Recollecting that $S(\beta_a)$ originates form the overlap integral between antisymmetric radiation mode and the perturbed bound mode [eq. (3.15)], it merely represents the coupling strength between bound and antisymmetric modes.

Moreover, eq. (3.22) states that for the exponential decay only one of the antisymmetric modes, namely the mode with $\beta_a = \beta_b + \nu$, is relevant. This represents the physical fact that only for a single radiation mode a certain phase matching condition is met. Even though the bound mode couples to the entire spectrum of antisymmetric radiation modes, there is only one propagation constant $\beta_a = \beta_b + \nu$ for which the light, which is scattered into this mode, accumulates constructively during a series of oscillation cycles $2\pi n/\nu$. Again, one can refer to the discussion carried out in section 3.1 and centered around fig. 3.8. Already in this discussion, it was argued that the light radiated away from the waveguide leaves only in particular direction. This argument is supported mathematically in this section, in addition the analytical derivation yields the exact value of this radiation direction which is given by $\sqrt{\beta_b+\nu}/k$.

Investigating the decay rate as a function of the system parameters δn_{max} and w, one might jump to the hasty conclusion that the dependence might be trivial. As a variation of δn_{max} or w leads to the bound mode being either tighter or looser bound, one might think that the tighter the mode is bound the smaller the exponential decay and that β_b is the only relevant parameter. However, this premature assumption is misleading. Even though it is true for a quite large parameter range, there is yet another range where the assumption fails. Taking a look at eq. (3.24) one finds the rather interesting case of

$$\frac{\pi^2}{4w^2} = \delta n_{max}. \tag{3.25}$$

For this specific parameter set, eq. (3.23) yields an infinite decay rate Γ as the modulation frequency ν approaches β_b. However, a strongly decaying c_b violates eq. (3.17) which states that c_b is only slowly varying in a sufficiently small interval. In turn eq. (3.23) cannot hold in the resonance region determined by eq. (3.25). Indeed fig. 3.13 shows

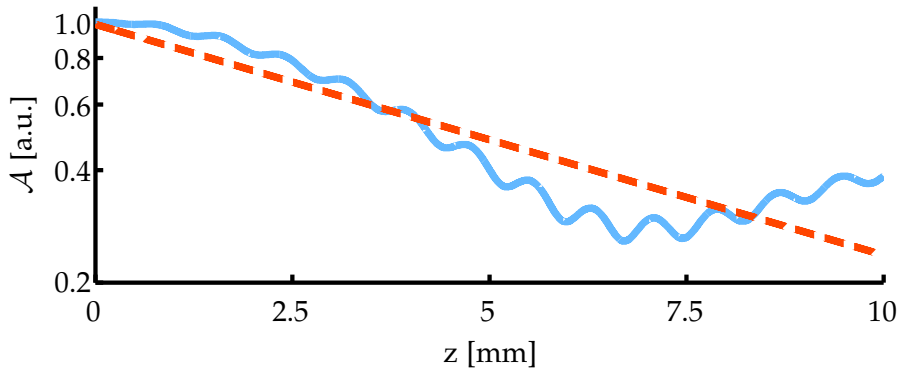

Figure 3.13: Amplitude of the light field (solid blue line) at the center of a waveguide with $\delta n_{max} = 6 \cdot 10^{-4}$, $w = 3.78\,\mu m$ and $p = 1.6\,mm$. The red line corresponds to an exponential decay.

that for $\delta n_{max} = 6 \cdot 10^{-4}$, $w = 3.78\,\mu m$ and $p = 1.6\,mm$ the amplitude

of the bound mode does not follow an exponential decay at all. As a consequence, even though at first glance it seems that eq. (3.25) provides a misleading resonance and uncovers a flaw in the derivation, the opposite is the case. Equation (3.25) provides an experimentally valuable finding in the sense that if one is interested in implementing an exponential decay utilizing sinusoidally bent waveguides, one needs to avoid the parameter range defined by eq. (3.25).

3.2.6 *High Frequency Regime*

The previous findings are limited to small frequencies, as stated by eq. (3.13). On the other hand it was found in section 3.1 that the loss of a sinusoidally modulated waveguide vanishes for very high frequencies. This section serves as a rigorous prove of the numerical findings in this specific high frequency limit. The starting point of the subsequent analysis shall be eq. (2.2) together with the sinusoidally oscillating potential. In general, the field can be decomposed into its Fourier-components as

$$\mathcal{A}(\zeta) = \int_{-\infty}^{\infty} \tilde{\mathcal{A}}(\beta)\, e^{i\beta\zeta} \mathrm{d}\beta.$$

If it can be assumed that the spectral width of $\mathcal{A}(\zeta)$ is limited and there exists a frequency $\beta_{\max}$ for which holds that if $|\beta| > |\beta_{\max}|$ then $A(\beta) \approx 0$, then one can find a small longitudinal interval Z with $Z \ll 2/\beta_{\max}$ so that

$$\langle \mathcal{A}(\zeta) \rangle_\zeta = \frac{1}{Z} \int_{\zeta-\frac{Z}{2}}^{\zeta+\frac{Z}{2}} \mathcal{A}(\zeta')\, \mathrm{d}\zeta' = \mathcal{A}(\zeta).$$

This is true, because one can exchange the Fourier integral and the temporal averaging and then for each Fourier component

$$\frac{1}{Z} \int_{\zeta-\frac{Z}{2}}^{\zeta+\frac{Z}{2}} \tilde{\mathcal{A}}(\beta)\, e^{i\beta\zeta'} \mathrm{d}\zeta' = \begin{cases} \tilde{\mathcal{A}}(\beta)\, e^{i\beta\zeta} & ;\ |\beta| \leq |\beta_{\max}| \\ 0 & ;\ |\beta| > |\beta_{\max}| \end{cases}.$$

Applying this moving average to the PHE one finds

$$i\partial_\zeta \mathcal{A}(\xi,\zeta) = -\partial_\xi^2 \mathcal{A}(\xi,\zeta) + \langle \delta n \rangle_\zeta(\xi)\, \mathcal{A}(\xi,\zeta)$$

where it was used that $\langle \partial_\zeta \mathcal{A} \rangle_\zeta = \partial_\zeta \langle \mathcal{A} \rangle_\zeta$ as well as $\langle \delta n \mathcal{A} \rangle_\zeta = \langle \delta n \rangle_\zeta \mathcal{A}$, utilizing the same argument as above. If the frequency ν with which the potential δn is oscillating is much larger than $2\pi/Z$ then the mean potential $\langle \delta n \rangle_\zeta$ is constant along the longitudinal axis. As a consequence, in this high frequency limit the field amplitude $\mathcal{A}$ only feels a constant potential along the ζ-direction. In general, the shape of

the potential changes due to the averaging procedure and it should be stated that $\langle \delta n \rangle_\zeta \neq \delta n \left(\xi - \langle \xi_0 \rangle_\zeta \right)$. Instead, for a box potential with the specific parameters $d = 1\,\mu\text{m}$ and $w = 3\,\mu\text{m}$ the potential is depicted in fig. 3.14. In general, due to the average potential being different from the original potential also the shape of the bound mode changes. However, for the specific parameters under consideration, both profiles are almost identical.

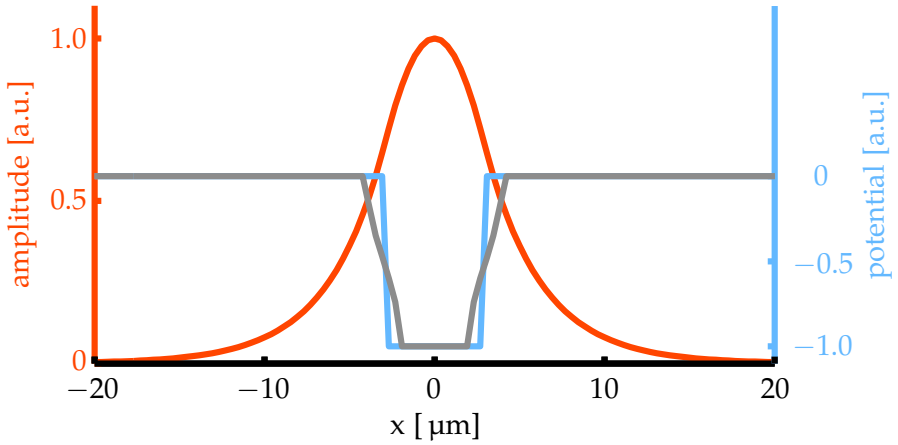

Figure 3.14: Comparison between straight waveguide and average potential for high oscillation frequencies with $d = 1\,\mu\text{m}$ and $w = 3\,\mu\text{m}$. The blue line represents the straight box potential, whereas the gray line shows the oscillating average potential. For the parameters under consideration the Eigen-mode profile of both potentials (red line) is almost identical.

If such an averaged potential is excited with its own bound mode then - in the high frequency limit - the evolution is stationary and $\mathcal{A}(\xi, \zeta) = \Phi(\xi) \exp[i\beta_b \zeta]$. In this case $\beta_{\max}$ can simply be identified with β_b and one finds the condition

$$\beta_b \ll \frac{2}{Z} < \frac{2\pi}{Z} \ll \nu$$

which relates the modulation frequency of the potential with the propagation constant of the bound mode. This condition determines the validity of the high frequency approximation above, for which the loss of the bound mode is identical to zero.

3.3 EXPERIMENTAL REALIZATION OF WELL-CONTROLLABLE LOSS

Sinusoidally bent waveguides were fabricated in order to experimentally verify the theoretical predictions. The main experimental interest lies in confirming the average exponential decay as well as the frequency dependence as proposed in fig. 3.12. To this end, several samples with period lengths ranging from 100 µm to 50 mm were written.

All samples share a common length of 50 mm as well as a sine amplitude of 1.45 µm. Figure 3.15 (a) exemplarily shows the fluorescence image of a sinusoidally bent waveguide with an oscillation period of 3.9 mm. This image, where the oscillation takes place within the focal plane, was taken solely for illustration purposes. For the true measurement images, from which the light amplitude is extracted, the waveguide oscillates orthogonal with respect to the focal plane of the imaging objective. From such an image the extracted light amplitude is shown in fig. 3.15 (b), where the period is 3.9 mm as well. Figure 3.15 (b), where the intensity-axis is scaled logarithmically, shows the typical characteristics of a fluorescence measurement. After a propagation distance of 12 mm the graph clearly shows a linear slope, indicating the exponential decay of the light intensity. In this particular example the slope is $-0.42\,\mathrm{cm}^{-1}$. Initially, for propagation distances smaller than 12 mm, the behavior strongly deviates from the subsequent exponential behavior. This effect can be attributed to coupling the free-space LASER-beam into the glass chip using a microscope objective. As a consequence, in all samples this coupling-region was neglected, when evaluating the light evolution.

After post-processing the raw images, all samples show the aforementioned exponential decay. Hence, the experiments confirm the theoretical predictions. Theory and simulation also predict slight deviations from this exponential decay, specifically periodic amplitude oscillations. As the measurements show, these oscillations are in the same order of magnitude as the noise level.

Figure 3.16 contains the extracted decay rates for all realizations with different period lengths. For large period lengths, e.g. 50 mm, the decay rate [$0.08\,\mathrm{cm}^{-1}$] differs only minimally from the intrinsic decay of straight waveguides. This behavior continues for period lengths down to 10 mm, for which the decay only increases by 20%. As the graph in fig. 3.16 shows, a pronounced frequency dependence of the bending induced decay can be observed for period lengths between 200 µm and 10 mm, spanning roughly two orders of magnitude. The maximum loss is achieved at a period length of 1.2 mm. Here, the decay, exhibiting a value of $1.0\,\mathrm{cm}^{-1}$, exceeds the intrinsic loss by over an order of magnitude.

Comparing the experimentally measured decay rates [fig. 3.16] with the theoretically predicted ones [fig. 3.4] a good agreement is asserted. Clearly, both graphs show negligible decay for small and large periods respectively and exhibit a single pronounced maximum in the range of a few *mm* of period length. The experimental results differ in the fact that the sudden drop, which is theoretically predicted, cannot be confirmed by the measurements. In fact, this difference between theory and experiment can be attributed to the dimensionality, since the experimental waveguides exhibit a two-dimensional (2D) cross

section, whereas the theoretical model is based on a single transverse dimension.

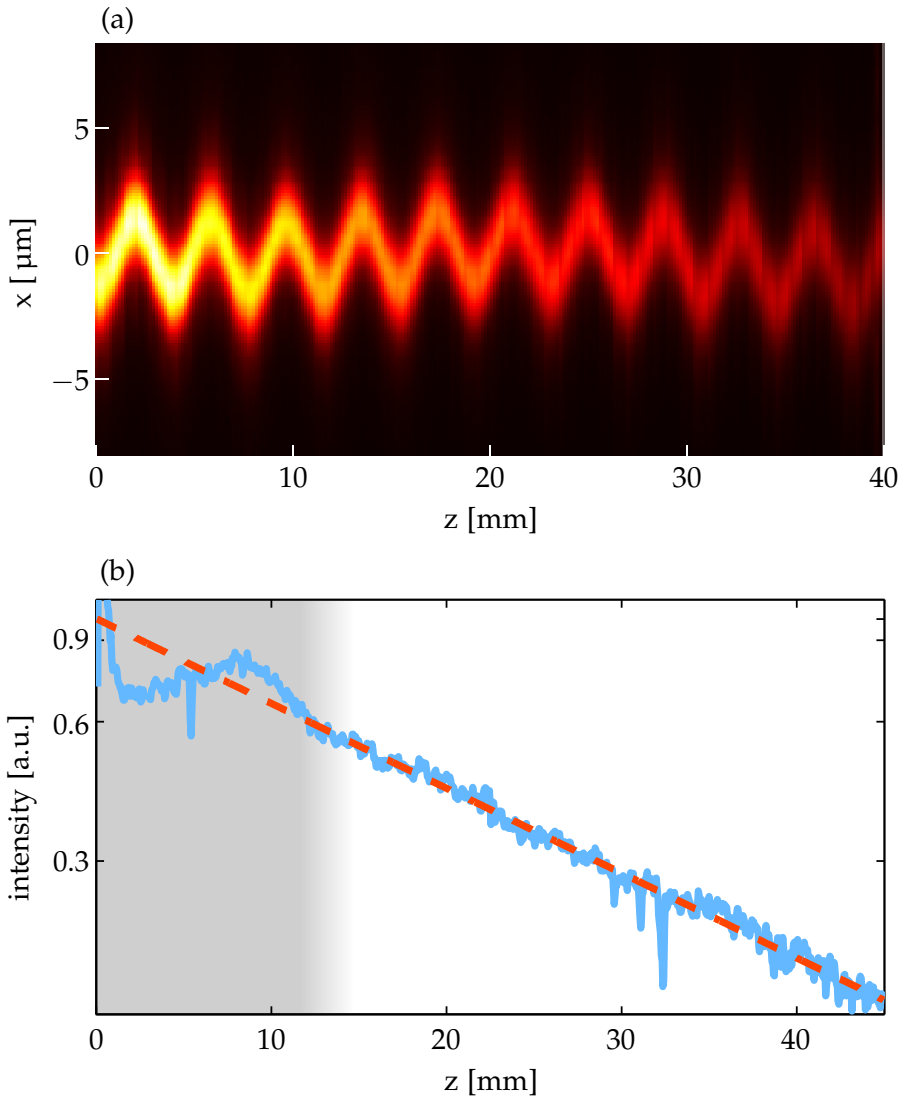

Figure 3.15: (a) Fluorescence image of a sinusoidally bent waveguide with an oscillation period of 3.9 mm. (b) Light intensity extracted from a sinusoidally bent waveguide with a period of 3.9 mm. This intensity data is not extracted from (a), but rather an equivalent guide, where the oscillation amplitude is orthogonal to the focal plane of the imaging system.

To this end, fig. 3.16 also contains the decay rates extracted from 2D simulations. This data shows the same gradual drop as the experimental data. The gradual decrease can be explained by the behavior of the phase matching condition discussed on page 45. There it was argued that only a single radiation mode takes part in the scattering process. In 2D this condition is weakened, as phase matching can be fulfilled by a collection of radiation modes with different transverse momenta.

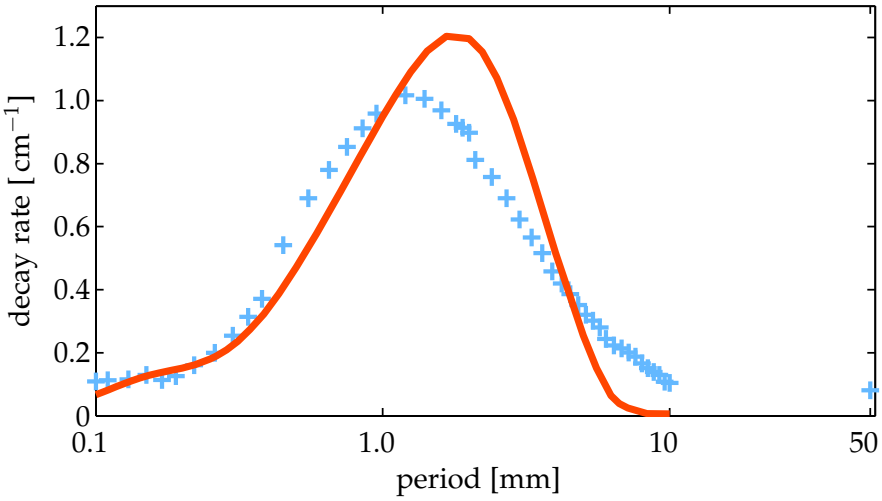

Figure 3.16: Experimentally measured intensity decay rate (blue crosses) and decay rate extracted from 2D simulations (red line).

3.4 CHAPTER SUMMARY

In this chapter, a versatile way to introduce well-controllable optical loss in fs-LASER-written waveguides was introduced and discussed on both a theoretical and experimental basis. Here, the basic idea was to periodically bend the guides transverse to the propagation direction of light in order to repeatedly cause fractions of the guided light to be radiated away. While in principle, the elementary loss is due to the curvature of the guides, the analysis revealed that interference effects play an immense role and that loss cannot be increased arbitrarily by merely increasing the curvature of the waveguides.

The main achievement of this chapter was the theoretical and experimental verification that loss, which is introduced in the aforementioned way, leads to an overall exponential decay of the amplitude of the bound waveguide mode. In order to ensure this behavior, the sinusoidally bent waveguides are designed such that the modulation amplitude is kept relatively small and in turn the modulation frequency is used as a tuning parameter to control the amount of loss.

The investigation of the frequency dependence of the exponential decay revealed that there is virtually no loss for small and high modulation frequencies, respectively. For intermediate modulation frequencies, the decay rate increases and a single pronounced maximum can be observed. The analytical expression for the decay rate, which is derived in this chapter, is accompanied by an intuitive understanding, that relates the propagation dynamics of sinusoidally bent waveguides to the interference effects of radiated light.

The results presented in this chapter form the basis of the subsequent investigations, since they prove that sinusoidally bent waveguides can be experimentally applied to mimic lossy media. The ad-

vantage of the presented technique is that it can be incorporated into the well-established FLDW process without the need of an additional pre- or post-processing step. With this, it enables the implementation and study of $\mathcal{PT}$ symmetric and other dissipative structures on the platform of fs-LASER-written waveguide arrays.

4

TRANSPORT IN NON-HERMITIAN SYSTEMS

The deceleration of wave transport in a lattice due to disorder was introduced in physics about 100 years ago with the famous Drude model. Paul Drude explained the conductance of metals by free electrons that are scattered by the atomic lattice, which in turn results in a diffusive transport [27]. The diffusion process is ubiquitous. It governs the effects of electric and thermal conductivity in solids [27, 50], particle mixing in fluids [72] and spin diffusion effects [91], just to name a few. In this context, it is generally agreed that all systems that exhibit sub-ballistic transport are inherently disordered. Today, disorder is explored in many disciplines, such as optics [86], solid-state physics [80], acoustics [42] and matter waves [12, 81]. In particular, optical systems attracted much interest, and so far numerous sub-ballistic transport phenomena based on disorder have been observed; these include Anderson Localization [86, 4, 53], quantum decoherence [3], Levy Flights [5] and anomalous diffusion [60]. The understanding of diffusive (and in general sub-ballistic) transport naturally assumes hermiticity of the Hamiltonian, as this ensures the reality of the eigenvalue spectrum and, therefore, energy conservation. However, dissipative (that is, lossy) systems that interact with their environment are by far the most common. With the damped pendulum as the simplest example, dissipation is the basis for phenomena like the Carnot Process or negative temperature coefficient thermistors. In the nonlinear regime, dissipative structures are encountered even in the everyday world, for instance, in the form of heat convection of a candle light, cyclons, the famous Belousov–Zhabotinsky Reaction [34] and, above all, in living organisms. As discussed in section 2.4.1, $\mathcal{PT}$ symmetric systems have recently received considerable attention [7]. Moreover, as explained in section 2.4.2, optical structures provide an exceptional platform for the implementation of $\mathcal{PT}$ symmetric physics, where the (symmetric) refractive index distribution represents the real part of the complex potential, whereas the (antisymmetric) gain-loss profile has the role of its imaginary part [30]. In optical $\mathcal{PT}$ symmetrical systems, the short-term evolution of (optical) wave packets exhibits peculiar features and is highly non-intuitive [58, 64, 56, 37, 82, 79]. In this context, perhaps, it is natural to ask how periodic but dissipative structures affect the long-term

wave transport - a question of fundamental importance in numerous physical systems.

In this chapter, theoretical predictions and experimental observations are presented, which show that in static $\mathcal{PT}$ symmetric optical lattices with no disorder, wave transport may suddenly slow down from ballistic to diffusive after a particular transition distance. It is demonstrated that this transition as well as the resulting diffusive transport - which, in the absence of disorder, is impossible in hermitian systems - depends only on a dissipation parameter associated with the system. The analysis carried out in this chapter makes extensive use of the findings of the previous chapter in the sense that sinusoidally bent waveguides represent the dissipative features of the system under consideration.

4.1 THEORY OF NON-HERMITIAN LATTICES

Consider a biatomic lattice, such as the one schematically depicted in fig. 4.1. The two sites within a unit cell couple to each other with

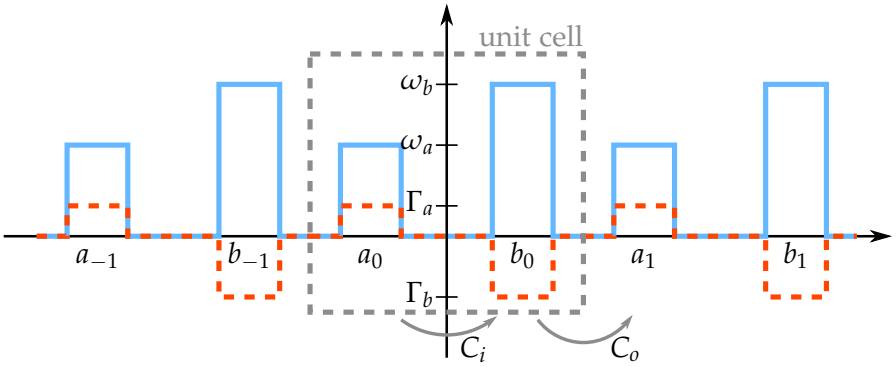

Figure 4.1: Schematic illustration of a biatomic lattice. Each unit cell consists of two sites which couple to each other with a strength of C_i. The inter cell coupling has a strength of C_o. Each lattice site is characterized by an Eigen-frequency ω and a decay rate Γ.

an inner strength C_i whereas sites of neighboring cells couple to each other with an outer coupling strength C_o. Moreover, each lattice site is characterized by a propagation constant ω as well as a decay rate Γ. The evolution of the on site amplitudes $a_n(\zeta)$ and $b_n(\zeta)$ shall be described by a PHE which reads

$$\begin{aligned} i\partial_\zeta a_n &= [\omega_a + i\Gamma_a]\, a_n + C_i b_n + C_o b_{n-1} \\ i\partial_\zeta b_n &= [\omega_b + i\Gamma_b]\, b_n + C_i a_n + C_o a_{n+1}. \end{aligned} \tag{4.1}$$

In order to investigate the dynamics of such a lattice, it is best to study the propagation of the Bloch-modes which are obtained by utilizing

the Ansatz $(a_{n+1}, b_{n+1})^\top = e^{in\varphi}(a_n, b_n)^\top$. With this, one obtains the evolution equation

$$i\partial_\zeta \begin{pmatrix} a \\ b \end{pmatrix} = \begin{pmatrix} \omega_a + i\Gamma_a & C_i + C_o e^{-i\varphi} \\ C_i + C_o e^{i\varphi} & \omega_b + i\Gamma_b \end{pmatrix} \begin{pmatrix} a \\ b \end{pmatrix}$$

that reduces the complexity of the problem to a single unit cell. Then the Eigen-modes evolve in the usual fashion $(a, b)^\top = e^{i\beta\zeta}(a_0, b_0)^\top$ whereas the Eigen-values are given by

$$\beta_\pm = -\bar{\beta} \pm \sqrt{\delta\beta^2 + C_i^2 + C_o^2 + 2C_iC_o\cos(\varphi)}\ . \tag{4.2}$$

Here $\bar{\beta} = \bar{\omega} + i\bar{\Gamma}$ and $\delta\beta = \delta\omega + i\delta\Gamma$ where the mean energy $\bar{\omega} = {}^{(\omega_a+\omega_b)}/_2$, mean decay rate $\bar{\Gamma} = {}^{(\Gamma_a+\Gamma_b)}/_2$, as well as the differences $\delta\omega = {}^{(\omega_a-\omega_b)}/_2$ and $\delta\Gamma = {}^{(\Gamma_a-\Gamma_b)}/_2$ are introduced. The PHE (4.1) represents the most general case of a biatomic lattice considering only next neighbor interaction. From the Eigen-value spectrum, i.e. eq. (4.2), one finds two bands of Eigen-values which are in general complex. Both bands are symmetrically centered around the mean $\bar{\beta}$. Without loss of generality, one can neglect the mean value, or equivalently set $\bar{\beta} = 0$ [$\omega_b = -\omega_a$ and $\Gamma_b = -\Gamma_a$], since it does not play a role in the inter site evolution and only contributes to a global phase and amplitude factor. This argument is analog to the explanations carried out in section 2.4.2. Additionally, let us assume that the waveguides b_n are the more lossy ones, which means that $\Gamma_b < \Gamma_a$ and hence $\delta\Gamma > 0$. With $\bar{\beta} = 0$, one obtains a band structure symmetrically centered around zero, i.e.

$$\beta_\pm = \pm\sqrt{\omega_a^2 + 2i\omega_a\Gamma_a - \Gamma_a^2 + C_i^2 + C_o^2 + 2C_iC_o\cos(\varphi)}\ . \tag{4.3}$$

As one would expect, in the hermitian case, which is obtained for $\Gamma_a = 0$, the spectrum is entirely real, regardless of the specific choice of the parameters ω_a, C_i, or C_o. Equivalently, from fig. 4.1 it can be concluded that only in the case of $\omega_a = 0$ the Hamiltonian is $\mathcal{PT}$ invariant. In this case the band structure reduces to

$$\beta_\pm = \pm\sqrt{-\Gamma_a^2 + C_i^2 + C_o^2 + 2C_iC_o\cos(\varphi)}\ . \tag{4.4}$$

This well studied spectrum exhibits the interesting feature that it can be either entirely real, if $|C_i - C_o| > \Gamma_a$, entirely imaginary, if $C_i + C_o > \Gamma_a$, or exhibit both a real and an imaginary range, as illustrated in fig. 4.2 (a). As it was discussed in sec. 2.4.1, if the spectrum is entirely real, the Hamiltonian of eq. (4.1) and the $\mathcal{PT}$ operator share a common set of Eigen-vectors. On the other hand, if $|C_i - C_o| < \Gamma_a$ the symmetry is broken and the spectrum exhibits a real and an imaginary range.

The dynamics of the lattice governed by eq. (4.1) are well studied in the regime of $\mathcal{PT}$ symmetry and little attention was brought towards

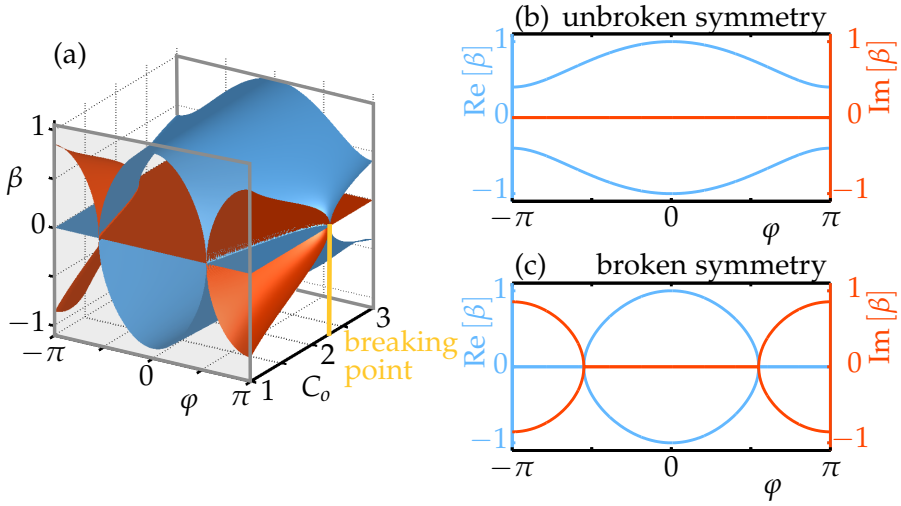

Figure 4.2: (a) Normalized band structure of a $\mathcal{PT}$ invariant Hamiltonian [eq. (4.4)] with $\Gamma_a = 1.3$ and $C_i = 1$ for ranging C_o. The blue surface represents the real part whereas the red surface denotes the imaginary part of the Eigen-value β. $\mathcal{PT}$ symmetry is broken for $C_o < 2.3$. (b) Normalized band structure of a $\mathcal{PT}$ symmetric Hamiltonian. Eigen-values are obtained from (a) for the specific choice of $C_o = 3$. (c) Normalized band structure for a parameter set where $\mathcal{PT}$ symmetry is broken, i.e. $C_o = 1$.

the regime where $\mathcal{PT}$ symmetry is lost. To this end, the subsequent analysis will be carried out in the broken $\mathcal{PT}$ regime. Note that the fact whether $\mathcal{PT}$ symmetry is gained or lost, merely depends on the difference between inner and outer coupling strength relative to the decay rate [fig. 4.2 (a)]. Figure 4.2 (c) exemplarily shows an Eigen-value spectrum with broken symmetry; one can see that the Eigen-values are purely real for $|\varphi| < 0.45\pi$ and purely imaginary for $|\varphi| > 0.45\pi$. For the more general band structure [eq. (4.3)], for which an example is plotted in fig. 4.3, the spectrum looks qualitatively similar if one introduces an energy detuning ω_a which is only small. In this scenario the spectrum looks like a smeared out version of fig. 4.2 (c) - where the imaginary part is zero in fig. 4.2 (c) a small imaginary component is added in fig. 4.3. Also the sharp transition between real and imaginary spectral range is smoothed out. Increasing ω_a would lead to an even "smoother" spectrum.

From fig. 4.3 it is clear that the decay, which each mode experiences, is not constant but rather a function of the transverse momentum φ. Hence, Eigen-modes in different regions of the Brillouin zone experience different losses, depending on the value of the imaginary part of their Eigen-values. As a consequence, in both bands modes in the center of the Brillouin zone (where the lattice momentum $\varphi = 0$) experience an intermediate loss, which is close to the average loss in the system. At the edge of the Brillouin zone (around $\varphi = \pm\pi$) the situation is very different. There, the modes in the lower band suffer from

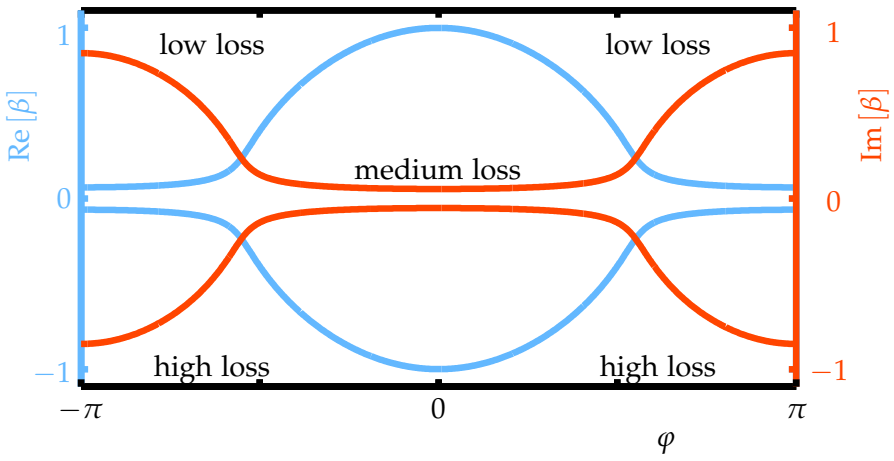

Figure 4.3: Normalized band structure of a general dissipative biatomic lattice. The parameters chosen here are almost equivalent to the broken $\mathcal{PT}$ case shown in fig. 4.2 (c) with $\omega_a = 1.3$ and $C_i = C_o = 1$. In addition here a frequency detuning of $\omega_a = 0.1$ is introduced.

a loss that is much larger than the systems's average loss, whereas in the upper band the modes experience much less loss. Hence, because of this difference, the modes in the lower band at the edge of the Brillouin zone will disappear after a relatively short distance [fig. 4.4 (a)], whereas the modes in the center of the spectrum will disappear somewhat later [fig. 4.4 (a) and (b)]. Only the modes in the upper band around $\varphi = \pm\pi$ will prevail at long propagation distances [fig. 4.4 (b)]. Therefore, the spectrum will considerably be getting narrower during the evolution of the wave packet, and only a part of the spectrum will contribute to transport.

In order the visualize the connection between the spectral behavior, as explained within the last preceding paragraph, and the evolution dynamics in real space, the evolution of a wave packet is plotted in fig. 4.4. As mentioned above, the evolution of the spectrum is plotted in subfigures (a) and (b) whereas the spatial evolution is plotted in subfigure (c). Figure 4.4 shows the special case of a single site excitation; for that reason initially all transverse modes in both bands are excited with the same ampltide. One can clearly observe that as long as all transverse modes possess a finite amplitude, which is the case for $\zeta < 20$ in fig. 4.4, the evolution dynamics in real space [subfigure (c)] exhibits features which are comparable to those of a basic homogeneous lattice [compare fig. 2.4]. To be specific, those features are the strong ballistic side lobes and the amplitude oscillations inside the individual waveguides. On the other hand, for longer propagation distances, that is when the modes around $\varphi = \pm\pi$ are predominant, the evolution dynamics are fundamentally different. In fig. 4.4 one observes that the intensity is mostly confined within the

sub-lattice a_n and central waveguides possess a larger amplitude than outer guides. Also the amplitude beating in individual guides is lost.

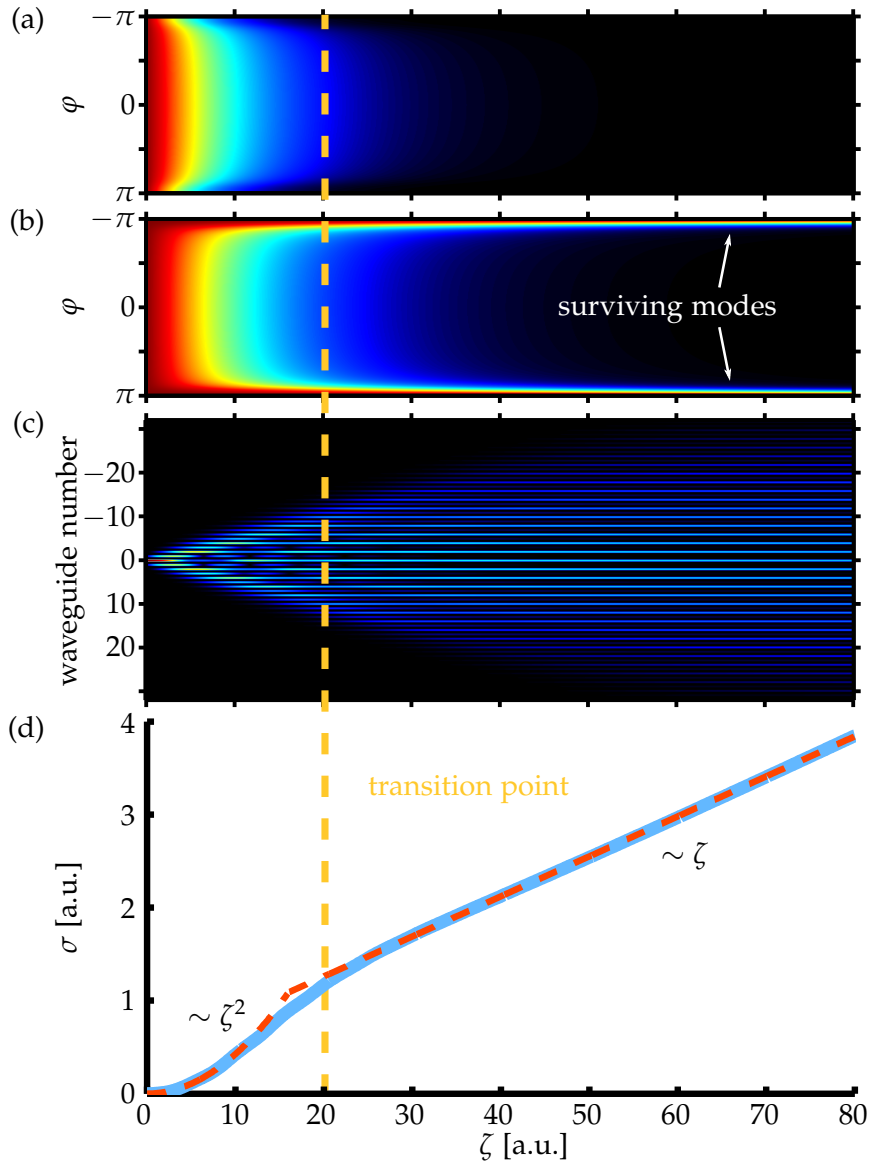

Figure 4.4: Evolution of a wave packet inside a lattice described by eq. (4.1) with the specific parameters $\omega_a = \Gamma_a = 0$, $\omega_b = -0.2$, $\Gamma_b = -0.1$, and $C_i = C_o = 0.3$. Initially only waveguide a_0 is excited with unit amplitude. (a) Evolution of the mode amplitudes in the lower band. (b) Evolution of the mode amplitudes in the upper band. (c) Evolution dynamics in real space. (d) Variance calculated from the evolution shown in (c). The blue solid line represents the actual variance σ^2, whereas the red dashed line is identical to a parabola for $\zeta < 16$ and a straight line for $\zeta > 16$. The transition region is symbolically drawn across all subfigures.

Figure 4.4 (d) poses the connection between the evolution dynamics and the actual transport regime. As the transport regime is charac-

terized by the broadening of the wave packet, from fig. 4.4 (d) one can conclude that there are two distinct regimes for different distances. For small distances the evolution is ballistic, characterized by a quadratic growth of the variance, whereas for longer distances the evolution is diffusive and also remains diffusive. The diffusive transport is characterized by the linear growth of the variance of the wave packet.

In order to prove that the diffusive transport continues indefinitely, a full analytical theory was developed within this thesis. It starts from the evolution of the wave packet represented as a superposition of modes and makes use of the Eigen-vectors

$$\begin{pmatrix} a_0 \\ b_0 \end{pmatrix}_+ = \begin{pmatrix} -C\left(1+e^{i\varphi}\right) \\ \beta_+ + \bar{\beta} + \delta\beta \end{pmatrix} \quad , \quad \begin{pmatrix} a_0 \\ b_0 \end{pmatrix}_- = \begin{pmatrix} \beta_- + \bar{\beta} - \delta\beta \\ -C\left(1+e^{i\varphi}\right) \end{pmatrix}$$

corresponding to eq. (4.2). The subscript of the Eigen-vectors denotes to which Eigen-value they belong. Here additionally $C_i = C_o = C$ was assumed for simplicity; also in this parameter regime $\mathcal{PT}$ symmetry is always broken, which is desired for this analysis. With these vectors, the full formal solution of eq. (4.1) for a single site excitation is given by

$$\begin{pmatrix} a_n \\ b_n \end{pmatrix} = \frac{1}{2\pi} \int_{-\pi}^{\pi} N \left[\alpha_+ \begin{pmatrix} a_0 \\ b_0 \end{pmatrix}_+ e^{-i\beta_+\zeta} + \alpha_- \begin{pmatrix} a_0 \\ b_0 \end{pmatrix}_- e^{-i\beta_-\zeta} \right] e^{in\varphi} \mathrm{d}\varphi \tag{4.5}$$

where the coefficients are

$$\alpha_+ = C\left(1+e^{i\varphi}\right) \quad , \quad \alpha_- = \beta_+ + \bar{\beta} + \delta\beta$$

and normalization is given by

$$N = \frac{-1}{C^2\left(1+e^{i\varphi}\right)^2 + \left(\frac{1}{2}\left(\beta_+ + \beta_-\right) + \delta\beta\right)^2}.$$

Being interested in large propagation distances, it was already argued, that the modes within the lower band decay faster than those in the upper band and can well be neglected for large distances. Moreover, the spectrum contracts around $\varphi = \pm\pi$ and in a small spectral region around these points the band structure can be approximated by the leading terms of its Taylor series, i.e.

$$\beta_+ = -\bar{\beta} + \delta\beta + \frac{C^2\delta\beta^*}{2\left|\delta\beta\right|^2}\left(\varphi - \pi\right)^2. \tag{4.6}$$

If one evaluates the shape of the Eigen-modes in the limit of $\varphi \to \pi$ one finds

$$\frac{\alpha_-}{N}\begin{pmatrix} a_0 \\ b_0 \end{pmatrix}_- \xrightarrow{\varphi\to\pi} \begin{pmatrix} 1 \\ 0 \end{pmatrix}. \tag{4.7}$$

This fact is physically plausible, remembering that the b_n guides were assumed to be lossier than the a_n. As a consequence, if the mode is only confined within the a_n sub-lattice, it only experiences the loss of the a_n guides. Note that this observation is in agreement with fig. 4.4 (c), where it is well visible that after a certain propagation distance only the a_n carry intensity. With the knowledge, that the evolution of the wave packet is only confined to the a_n sub-lattice and the amplitude of the b_n is identical to zero, one can reduce the entire analysis to the a_n. With these refinements eq. (4.5) reduces to

$$a_n = \frac{e^{in\pi}}{2\pi} e^{i\left(\bar{\beta}-\delta\beta\right)\zeta} \int_{-\infty}^{\infty} e^{-iw\varphi'^2\zeta} e^{in\varphi'} \mathrm{d}\varphi' \tag{4.8}$$

where

$$w = \frac{C^2 \delta\beta^*}{2\left|\delta\beta\right|^2}$$

and $\varphi' = \varphi - \pi$ has been applied. Also, the integration limits were extended to infinity. This can be justified by the fact that for large distances the width of the Gaussian Term is much smaller than the initial interval and hence determines the relevant range of integration.

It needs to be emphasized that eq. (4.8) together with the aforementioned approximation arguments is only valid for $\delta\Gamma \neq 0$ that is in the case of a non-vanishing loss detuning between the waveguides a_n and b_n. Clearly, for $\delta\Gamma = 0$, when the lattice is lossless, neither the modes in the upper nor in the lower band decay, hence the modes of the lower band cannot be neglected in eq. (4.5). Also, for a single site excitation the Taylor approximation of β, i.e. eq. (4.6), would not be valid. On the other hand, for every loss detuning $\delta\Gamma > 0$, no matter how small it is, there is a propagation distance ζ_c for which the approximation eq. (4.8) holds. This distance can be calculated by requiring that all modes outside of a certain spectral region ϵ, i.e. $\varphi' > \epsilon$, are damped by a factor δ. Since the damping is due to the Gaussian Term in eq. (4.8) one requires

$$\left|e^{-iw\epsilon^2\zeta}\right| < \delta.$$

A typical condition, which is sufficient for this analysis, is $\delta = e^{-2}$ which leads to

$$\zeta > \zeta_c = \frac{4\left|\delta\beta\right|^2}{\epsilon^2 C^2 \delta\Gamma}.$$

Obviously, the spectral range ϵ cannot be chosen arbitrarily, but has to be chosen such that eqs. (4.6) and (4.7) are ensured. This is the case for

$$\epsilon^2 < \frac{2\left|\delta\beta\right|^2}{C^2}.$$

Inserting this band width criterion into the condition for the propagation distance above, one arrives at the very simple expression

$$\zeta_c = \frac{2}{\delta\Gamma} \tag{4.9}$$

which represents the critical distance after which eq. (4.8) is certainly valid. Interestingly, ζ_c does only depend on the loss detuning between the waveguides and is independent of other system parameters.

To continue the analysis of eq. (4.8), one can easily perform the integration, arriving at

$$a_n = \frac{e^{in\pi}}{2\sqrt{\pi w \zeta}} e^{i\left(\bar{\beta}-\delta\beta\right)\zeta} e^{-\frac{n^2}{4iw\zeta}} \quad . \tag{4.10}$$

This equation completely describes the evolution dynamics on the underlying lattice and represents the closed-form solution for the a_n-sub-lattice for large distances. Remember, that for these distances the amplitude within the b_n-sub-lattice is approximately zero. Equation (4.10) reveals that the wave packet evolves into a Gaussian Shape, whereas neighboring sites have a respective phase difference of π. Moreover, the ζ-dependent phase evolution is identical for all sites.

In order to retrieve the propagation regime of this wave packet, the last step in the evaluation is to compute the variance of a wave packet defined by this equation. Since the lattice is dissipative, the variance is given by the usual variance defined on page 11 normalized to the total energy of the wave packet, i.e.

$$\sigma^2 = \frac{\sum_{n=1}^{\infty} n^2 \left|a_n\right|^2}{\sum_{n=1}^{\infty} \left|a_n\right|^2}. \tag{4.11}$$

Inserting eq. (4.10) into eq. (4.11), for large propagation distances the sums can be approximated as Gaussian Integrals, which can then be evaluated easily. The resulting variance is given by

$$\sigma^2 = \frac{C^2}{2\delta\Gamma}\zeta \tag{4.12}$$

which clearly shows a linear dependence on the propagation distance. As a result, one can conclude that the wave packet spreads diffusively. Again, it is important to note that eq. (4.12) is valid only after a critical distance ζ_c which is determined by eq. (4.9). For distances shorter than ζ_c, the evolution is ballistic, as indicated in fig. 4.4.

The derivation above, reveals that the diffusive spreading of the wave packet is indeed due to the contraction of the spectrum. In fact, the spectrum does not only contract until the diffusive regime sets in, the spectrum keeps contracting around the mode with the least amount of loss, i.e. around $\varphi = \pi$, indefinitely even within the diffusive regime. This understanding leads to the notion that this type of diffusive transport can be found in a more general class of lattices. As a matter of fact, for any arbitrary, dissipative, periodic lattice, for which there exists a transverse momentum φ_s, at which the loss is the smallest, there will be a propagation distance after which only

modes in a small interval surrounding φ_s have a relevant amplitude. Accordingly, if the curvature at this point is quadratic, then also the propagation regime will be diffusive. Moreover, if the curvature at φ_s is not quadratic (but for instance quartic), then a new transport regime in which the wave packet spreads faster than diffusively but slower than ballistically would arise.

4.2 EXPERIMENTAL OBSERVATION OF DIFFUSIVE TRANSPORT

In order to verify the theoretical predictions of the previous section photonic waveguide lattices were utilized. Usually, these waveguide lattices are hermitian, that is lossless, systems. Even though fs-LASER-written waveguides exhibit small intrinsic losses, these can well be neglected in most experimental situations. In contrast, the modeling of eq. (4.1) requires a dissipative system, which is preferably tunable. Specifically, the decay rate of an isolated site needs to be adjustable. It is in this particular sense that the findings of chapter 3 can be applied. One of the important findings of this chapter is that the mode of a single sinusoidally bent waveguide can be approximated to decay exponentially. As a consequence, one can argue that the amplitude of such a mode follows the simple equation $i\partial_\zeta a = [\beta + i\Gamma]\, a$, whereas β is the propagation constant equivalent to that of a straight waveguide and Γ is the decay rate derived in chapter 3. Without giving a rigorous derivation it seems plausible to assume that if such a dissipative waveguide is embedded in an entire lattice, then its evolution is given by an equation such as (4.1). This equation only differs from the usual hermitian case as derived in section 2.2 in the sense that the real propagation constant is replaced by its complex counter part which now incorporates the decay rate as its imaginary part. If this argument is true, then it is perfectly valid to model eq. (4.1) utilizing a biatomic waveguide lattice such as the one schematically depicted in fig. 4.5. In such a lattice every second guide is bent sinusoidally in order to implement intrinsic losses whereas the straight waveguides exhibit no losses [$\Gamma_a = 0$]. The bending plane is perpendicular with respect to the lattice plane in order to prevent light which is radiated away from a lossy waveguide to be reabsorbed by a different lattice guide.

In the specific experimental setup the waveguides are equidistantly separated by a distance of 17 µm which leads to a coupling of $C = 1.1\,\mathrm{cm}^{-1}$. In order for this lattice not to lead to a z-modulated coupling, the amplitude of the sinusoidal modulation needs to be small. For this reason, in the experiments a fixed modulation amplitude of 3 µm was chosen.

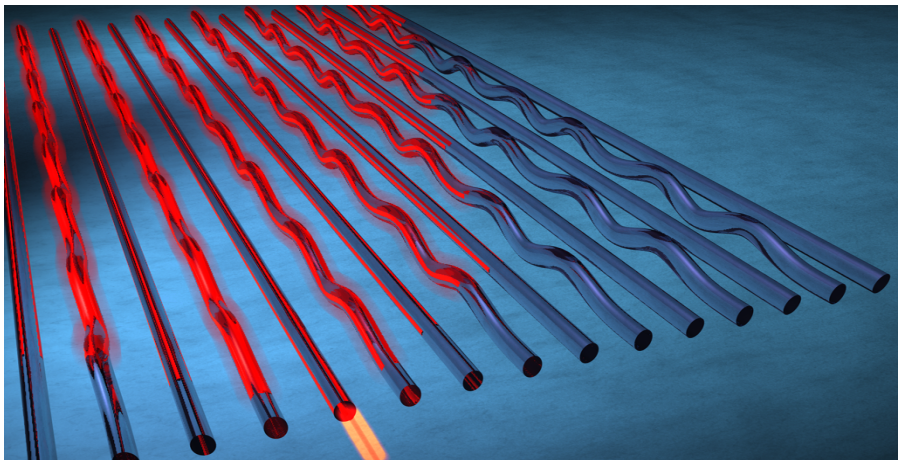

Figure 4.5: Schematic illustration of a biatomic waveguide lattice modeling eq. (4.1). In order to implement tunable losses, every second waveguide is bent sinusoidally, transverse with respect to the lattice plane.

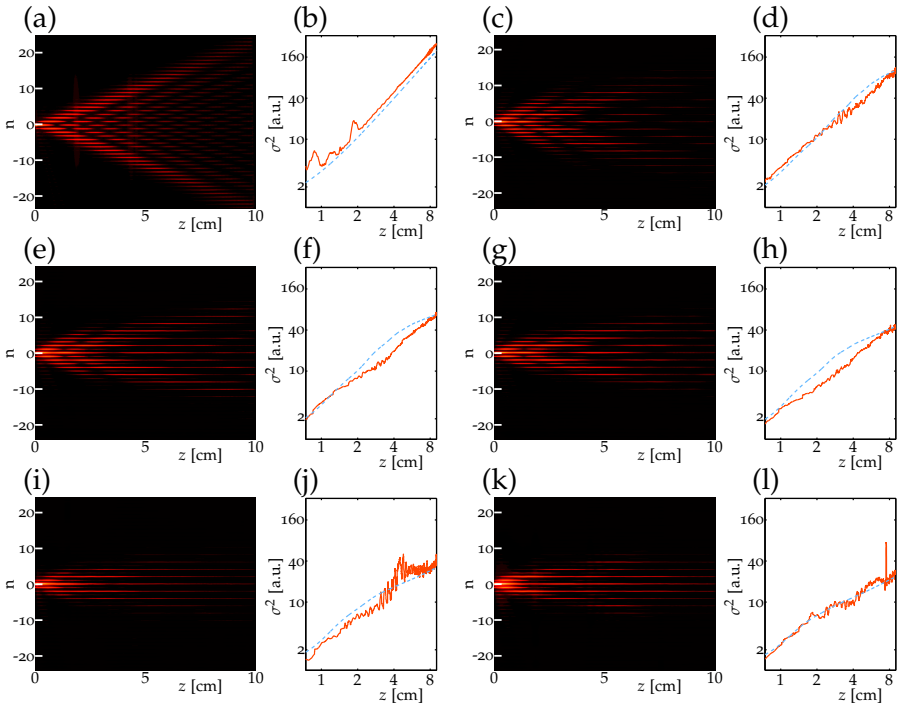

Figure 4.6: Subfigures (a), (c), (e), (g), (i) and (k) show fluorescence microscopy images of the light beams propagating through the lattice. Subfigures (b), (d), (f), (h), (j) and (l) contain the corresponding variance in a double-log plot as a function of the propagation distance z. The experimental data are given by the red line, whereas the blue dotted line depicts the corresponding simulation. (a) and (b) show the purely ballistic case with $\Gamma_b = 0$. In (c) and (d), $\Gamma_b = -0.6\,\mathrm{cm}^{-1}$; (e) and (f), $\Gamma_b = -0.8\,\mathrm{cm}^{-1}$; (g) and (h), $\Gamma_b = -1.1\,\mathrm{cm}^{-1}$; (i) and (j), $\Gamma_b = -1.5\,\mathrm{cm}^{-1}$; (k) and (l), $\Gamma_b = -2.0\,\mathrm{cm}^{-1}$.

To facilitate different intrinsic decay rates the modulation frequency served as the tuning parameter. Figure 4.6 displays the experimental measurements for a range of loss parameters. These range from $\Gamma_b = 0\,\mathrm{cm}^{-1}$ for the ballistic case to a maximum of $\Gamma_b = -2\,\mathrm{cm}^{-1}$ for the lossiest configuration. In addition to the pure fluorescence images which show the intensity evolution of the light, fig. 4.6 also shows the corresponding extracted variance of the wave packet. Moreover, each experimental variance curve is accompanied by its corresponding simulated counter part, where the simulation parameters have been chosen to match the experimental ones. To be precise, for the simulation no fitting parameter was used. The coupling strength C used in the simulation is an experimental value obtained from measurements in a single directional coupler with the aforementioned waveguides separation of 17 µm. Equivalently, the loss parameter Γ_b was extracted from loss measurements in isolated sinusoidally bent waveguides.

From the measurements presented in fig. 4.6, one can conclude that the experiments are in agreement with the theoretical predictions. The fluorescence images show that the ballistic characteristics vanish more and more with increasing loss. In the lossless, ballistic case [fig. 4.6 (a)] the characteristic ballistic side lobes are clearly visible, but already in subfig. (c) they start to vanish, when finally at the largest loss modulation [subfig. (k)] the side lobes are not visible anymore. The same behavior is true for the intensity modulation within individual waveguides - where the Bessel-like modulation is observable in subfig. (a), the central waveguides in subfig. (k) do not show any intensity modulation anymore. Also in subfig. (k) the diffusive propagation is affirmed by the theoretically predicted feature that the guides of the lossy sub-lattice do not carry light anymore.

From all measurements presented in fig. 4.6 the critical distance z_{crit}, around which the transition from ballistic to diffusiv transport happens, was extracted. In order to retrieve z_{crit} from the measurements, a straight line was fitted to the data for $z > z_{\mathrm{crit}}$ and parabola was fitted to $z < z_{\mathrm{crit}}$, whereas z_{crit} was used as a fitting parameter. In fig. 4.7, the critical distances, which were extracted this way, are plotted as a function of Γ_b. Correspondingly, eq. (4.9) is plotted as a blue line in the same figure. It shows that indeed the critical distance at which the transport regime changes is inversely proportional to the loss detuning.

4.3 CHAPTER SUMMARY

In conclusion, it was shown how a mobility transition from ballistic to diffusive transport can occur in static, ordered 1D systems. These findings extend the common perception that the transport in such systems is either ballistic or localized - a notion, which is true in the

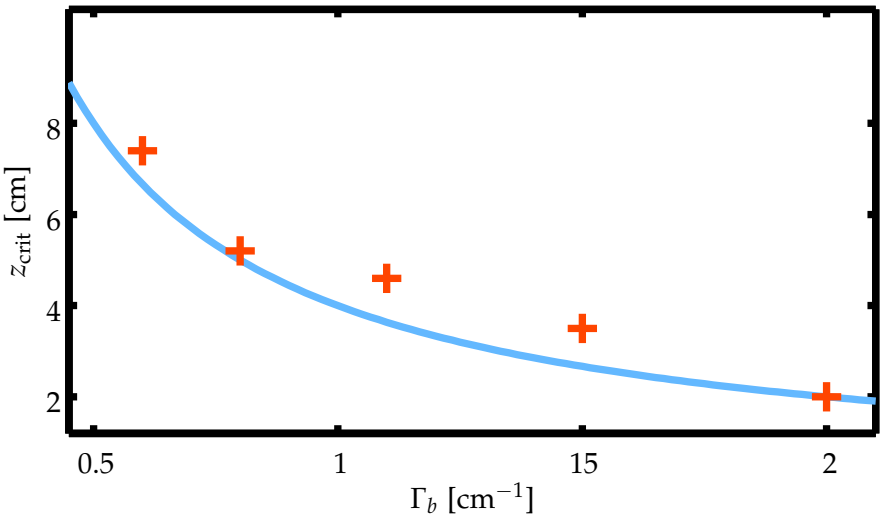

Figure 4.7: The red crosses represent the critical distance z_{crit} extracted from the measurements shown in fig. 4.6. In addition eq. (4.9) is plotted as a solid blue line. For this, Γ_b is also taken from measurements, whereas $\Gamma_a = 0$ is assumed.

case of hermitian system, but false in the case of $\mathcal{PT}$ symmetric or other dissipative systems.

In the particular biatomic lattice, which was considered in this chapter, the mobility transition was induced by the inhomogeneous, i.e. alternating, distribution of dissipation in the system. As a consequence of this particular loss distribution the Eigen-modes of the system decay at different rates and there exists a single mode, that exhibits the least amount of loss. If initially the entire spectrum is excited, for short propagation distances all modes contribute to the characteristic ballistic propagation pattern. However after larger distances only modes with a small decay rate prevail and the spectrum keeps contracting around the mode with the least amount of loss. In accordance, the transport becomes diffusive.

The analytical derivation, carried out in this chapter, revealed that the distance after which the transition from ballistic to diffusive transport takes place is inversely proportional to the loss detuning within the biatomic lattice. This indicates that the transport is still ballistic for a homogeneous loss distribution, for which the band structure would exhibit a constant imaginary part.

The experimental results, presented in this chapter, pose the first demonstration of $\mathcal{PT}$ symmetric dynamics in a fs-LASER-written waveguide array. They verify the existence of a mobility transition as well as the inverse dependence of the transition distance on the loss detuning. As sinusoidally bent waveguides are utilized to introduce the losses, the application of this method was successfully demonstrated in a complex lattice.

5

COUPLED MODE THEORY IN LOSSY MEDIA

As a versatile tool to study the interaction and dynamics in physical systems, coupled mode theory (CMT) is widely applied in many fields of physics. In the early 1950's, it was first heuristically introduced in refs. [76, 61] and later a rigorous theory was formulated [85]. CMT was first discussed within the context of microwave phenomena and introduced to waveguide optics in the 1970's [87, 106, 51]. What the first analyses have in common is the fact that they are all based on lossless single mode waveguides. While in the early days the orthogonality or non-orthogonality of modes of adjacent waveguides was heavily discussed, them being lossless was always postulated. Losses, whether in the context of grating assisted couplers or tapered waveguides, were always considered as an additional perturbation and not as an intrinsic property of the waveguide itself [43]. This approach probably originated from the fact that losses were considered undesirable and were minimized wherever possible.

Even in the study of systems where losses are inherently present, such as plasmonic structures, losses are sometimes neglected when trying to extract meaningful results [77]. However, since then several studies have been addressed at an inherently lossy CMT [6] and interesting properties, such as complex coupling, were found.

In this thesis in chapter 4, it was shown how a mobility transition arises in certain non-hermitian systems, whereas the analysis was also based on CMT. It was argued that if the loss is distributed inhomogeneously on the lattice sites, also the band structure shows a loss modulation and consequently there exists one mode with the least amount of loss. Furthermore, it was proven that due to the contraction of the spectrum an initially ballistic propagation turns into a diffusive one after a critical distance.

While the findings of the previous chapter were directly grounded on coupled mode equations, the influence of loss on these equations was only heuristically incorporated, as argued in section 4.2. The goal of this chapter is to formulate a general CMT for waveguide arrays comprised of lossy media. To this effect, the properties of a bound mode of a lossy waveguide are discussed as a first step. Secondly, a set of general coupled mode equations is derived and applied to the specific case of a homogeneous lattice. In this context, it will

be shown, that even for a homogeneous loss distribution there exists a diffusive transport regime, which is due to a generally complex coupling, that arises in lossy waveguide arrays. Finally, it is discussed how the results of this chapter, which are seemingly contradictory, are in perfect agreement with the findings of chapter 4 and broaden the understanding of light evolution in lossy waveguide lattices.

Experimentally, the theoretical predictions are verified using the technique of sinusoidally modulated waveguides, as established chapter 3. In this context, this chapter serves another purpose, since it verifies that sinusoidally bend waveguides can indeed be viewed as an effective lossy medium, when embedded in a 1D array.

5.1 THEORY OF COUPLED LOSSY WAVEGUIDES

In order to derive a coupled mode theory for lossy media, eq. (2.1) shall serve as a starting point. In this equation the permittivity $\varepsilon = \varepsilon_0 + \varepsilon_\mathrm{m}$ is comprised of a constant background permittivity ε_0 and a variable component ε_m denoting the waveguide modulation. Similar to section 2.1 one can define the wave number as $k^2 = k_0^2\varepsilon_0$ which leads to

$$2ik\partial_z \mathcal{A}(x,z) = -\partial_x^2 \mathcal{A}(x,z) - k_0^2 \varepsilon_\mathrm{m} \mathcal{A}(x,z)\,. \tag{5.1}$$

From the definition of the wave number k, one can then conclude that if ε_0 is complex, then also k is a complex quantity. From this in turn it follows that eq. (5.1) does not have the structure of a SE anymore, but is rather a mixture between SE and heat equation. For simplicity in this section, it shall be assumed that the background medium is absorptionless and hence $\varepsilon_0 \in \mathbb{R}$ - preserving the Schrödinger-like character of eq. (5.1). On the other hand, the modulation permittivity ε_m shall generally be assumed to be complex.

Also in this chapter normalized units are introduced. With $z_0 = {}^2\sqrt{\varepsilon_0}/k_0$ and $x_0^2 = {}^1/k_0^2$ eq. (5.1) reduces to

$$i\partial_\zeta \mathcal{A} = -\partial_\xi^2 \mathcal{A} - \varepsilon_\mathrm{m} \mathcal{A}\,. \tag{5.2}$$

Note that eq. (5.2) is almost equivalent to eq. (2.2) with the difference that it contains the permittivity instead of a refractive index. Even though the use of a refractive index is more common, in the case of dissipative media using the permittivity is more useful, as it allows a less obstructed view on the elementary physical parameters.

Isolated Lossy Waveguide

Before looking at an array of coupled waveguides, consider an isolated lossy waveguide, in order to clarify the fundamental differences and similarities as compared to a lossless waveguide. In the particular case in which the waveguide represents a box-shaped potential,

the Eigen-mode of such a guide can formally be written in the same way as its lossless counterpart, i.e.

$$\Phi(\xi) = \begin{cases} \cos(\kappa_1 w)\, e^{-i\kappa_2(\xi+w)} & ;\ \xi < -w \\ \cos(\kappa_1 \xi) & ;\ |\xi| < w \\ \cos(\kappa_1 w)\, e^{i\kappa_2(\xi-w)} & ;\ \xi > w \end{cases} \tag{5.3}$$

However, deviating from this formal structure is the fact that due to the complex permittivity, also the Eigen-value β, as well as $\kappa_1 = \sqrt{\varepsilon_m + \beta}$ and $\kappa_2 = \sqrt{+\beta}$ are complex[1]. This leads to the phase front of the Eigen-mode being curved, which stands in contrast to the plane phase front of the Eigen-mode of the lossless guide. Figure 5.1 shows the amplitude (blue line) and phase (red line) of the transverse mode profile of an Eigen-mode of a waveguide with a width $w = 2$ and permittivity $\varepsilon_m = 1 + 0.4i$. The corresponding Eigen-value is $\beta_{\text{lossy}} = -0.72 - 0.45i$. For comparison the amplitude of a mode for $\varepsilon_m = 1$ is drawn as a dashed gray line, here the Eigen-value $\beta_{\text{lossless}} = -0.74$. Note that the real part of these two Eigen-values, which fulfill the

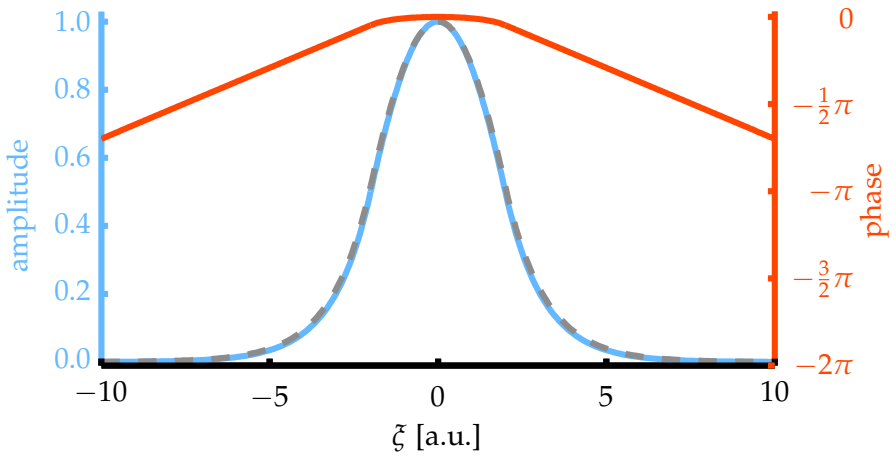

Figure 5.1: Transverse mode profile of an Eigen-mode of a lossy box-shaped waveguide with a width of $w = 2$ and a permittivity of $\varepsilon_m = 1 + 0.4i$. The corresponding Eigen-value is $\beta_{\text{lossy}} = -0.72 - 0.45i$. The solid blue line represents the amplitude, whereas the red line represents the phase of the mode. For comparison the amplitude of a lossless waveguide ($\varepsilon_m = 1$) is plotted as a dashed gray line. For this $\beta_{\text{lossless}} = -0.74$.

complex dispersion relation

$$-\kappa_1 \sin(\kappa_1 w) = i\kappa_2 \cos(\kappa_1 w) \tag{5.4}$$

also deviate only slightly from each other.

1 Note that the complex square root has two leafs. Here, without further reference, $\sqrt{\cdot}$ assumes the principal value of the square root, which has a positive (or zero) imaginary part. This convention ensures that, for instance, $e^{i\kappa_2\xi}$ decays for positive ξ.

It is a non-trivial (mathematical) fact, that the transition from the real dispersion relation eq. (2.7) to its complex counterpart eq. (5.4) preserves the structure of the spectrum, meaning that indeed a unique bound mode can be found. Physically, on the other hand, this statement should be obvious, since no optical system is completely lossless and guided modes can still be found.

To finish the discussion on the isolated lossy box-potential, the normalization of the mode needs to be provided, as the profile in eq. (5.3) is not normalized. In this matter, one has

$$\langle\Phi|\Phi\rangle = \frac{\cos\left(2\kappa_1' w\right)}{2\kappa_2''} + \frac{\sin\left(2\kappa_1' w\right)}{2\kappa_1'} + \frac{\cosh\left(2\kappa_1'' w\right)}{2\kappa_2''} + \frac{\sinh\left(2\kappa_1'' w\right)}{2\kappa_1''} \tag{5.5}$$

where $\kappa_{1/2}'$ denotes the real and $\kappa_{1/2}''$ the imaginary part of the transverse wave number. In the limit of vanishing loss, eq. (5.5) reduces to eq. (3.8).

Homogeneous Dissipative Array

Next, consider an array of well-separated waveguides where the modulation permittivity is given as a discrete superposition, i.e.

$$\varepsilon_{\mathrm{m}} = \sum_j \varepsilon_j$$

and ε_j are non-overlapping, generally complex permittivity modulations. In order to simplify the analysis, the subsequent study will be confined to single mode waveguides, such that each modulation ε_j supports - when isolated - a single bound mode with

$$\mathcal{A}_j = \Phi_j\left(\xi\right) e^{-i\beta_j\zeta} \tag{5.6}$$

where Φ_j is the transverse profile and β_j the possibly complex Eigenvalue. In analogy to section 2.2, inserting the superposition $\mathcal{A} = \sum_j \tilde{a}_j \mathcal{A}_j$ into eq. (5.2) yields

$$i\sum_j e^{-i\beta_{jl}\zeta}\partial_\zeta \tilde{a}_j \left\langle\Phi_m|\Phi_j\right\rangle \quad = \quad -\sum_{j,l\neq j} \tilde{a}_j \left\langle\Phi_m\left|\varepsilon_l\right|\Phi_j\right\rangle e^{-i\beta_{jl}\zeta} \ .$$

For sufficiently far separated waveguides one can assume that $\left\langle\Phi_m|\Phi_j\right\rangle = \delta_{jm}$ as well as $\left\langle\Phi_m\left|\varepsilon_l\right|\Phi_j\right\rangle = \delta_{ml}\left(C_{m+}\delta_{j(m+1)} + C_{m-}\delta_{j(m-1)}\right)$. Together with $a_j = \tilde{a}_j e^{-i\gamma_j\zeta}$ and $\gamma_j = \gamma_{j-1} + \beta_{(j-1)j}$ this leads to the coupled mode equations for dissipative media, i.e.

$$i\partial_\zeta a_j = \gamma_j a_j + C_{j+}a_{j+1} + C_{j-}a_{j-1}. \tag{5.7}$$

Equation (5.7) is almost identical to eq. (2.8), only differing in the fact that the argument relating C_{j+} and $C_{(j+1)-}$ cannot be made, due to the

absence of energy conservation in dissipative systems. Moreover, in this context it was argued that the coupling constants have to be real. For dissipative systems however, the coupling is generally complex. This fact should be clear when looking at the expression $\langle \Phi_{j\pm1} | \varepsilon_j | \Phi_j \rangle$ where all participating quantities are complex functions.

In the particular case of a homogeneous lattice, where indeed all coupling terms are equal [B] and the evolution is determined by the equation

$$i\partial_\zeta a_j = Ca_{j+1} + Ca_{j-1}, \tag{5.8}$$

the interesting situation arises, that the phase of the coupling term depends on the separation between neighboring waveguides. This peculiar behavior is due to the curved phase front of the lossy waveguide mode, which is exemplarily depicted in fig. 5.1. Figure 5.2

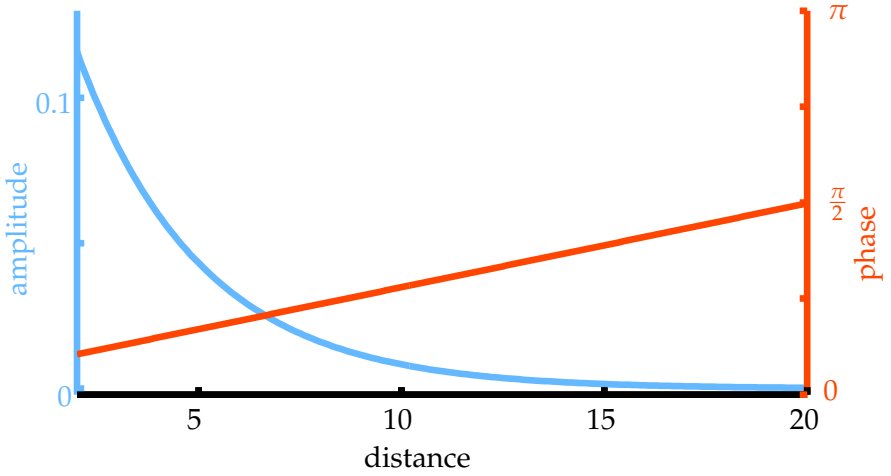

Figure 5.2: Coupling between two waveguides as a function of waveguide separation. The graph shows the amplitude and phase of the normalized coupling coefficient for two adjacent waveguides with a width of $w = 1$ and $\varepsilon = 0.4 + 0.1i$.

shows the separation dependence of the coupling between two neighboring waveguides where each guide has a width of $w = 1$ and a permittivity of $\varepsilon_j = 0.4 + 0.1i$. As expected from the hermitian case, the amplitude of the coupling drops exponentially, whereas the phase grows linearly with the waveguide separation D. An interesting feature of this behavior is, that for any complex permittivity there exists a distance for which the coupling is purely imaginary; in fig. 5.2 this distance is approximately 20. Equivalently, there exists a larger distance at which the coupling is real again, but negative - admittedly the coupling might be quite small. A rigorous calculation of $\langle \Phi_{j\pm1} | \varepsilon_j | \Phi_j \rangle$ using the non-normalized profile in eq. (5.3) yields

$$\langle \Phi_{j\pm1} | \varepsilon_j | \Phi_j \rangle = w\varepsilon_j \cos(\kappa_1^* w) \left[\operatorname{sinc}(\Delta\kappa w) + \operatorname{sinc}(\Sigma\kappa w)\right] e^{i\kappa_2^*(w-D)} \tag{5.9}$$

with $\Delta\kappa = \kappa_1 - \kappa_2^*$ and $\Sigma\kappa = \kappa_1 + \kappa_2^*$. This proofs that indeed

$$C = \frac{\langle \Phi_{i\pm1} | \varepsilon_i | \Phi_i \rangle}{\langle \Phi_i | \Phi_i \rangle} \sim e^{-i\kappa_2^* D} = e^{-\kappa_2'' D} e^{-i\kappa_2' D}. \tag{5.10}$$

It can be concluded that the dissipative nature of a waveguide does not only manifest itself in a pure amplitude decay rate, as it would be the case for an isolated guide, but is also inscribed in the coupling coefficients of an array. In order to investigate the influence of this complex coupling on the propagation dynamics, a basic homogeneous lattice, governed by eq. (5.8), is considered and its evolution illustrated in fig. 5.3. In this figure the coupling is chosen to be $C = 1 + 0.16i$.

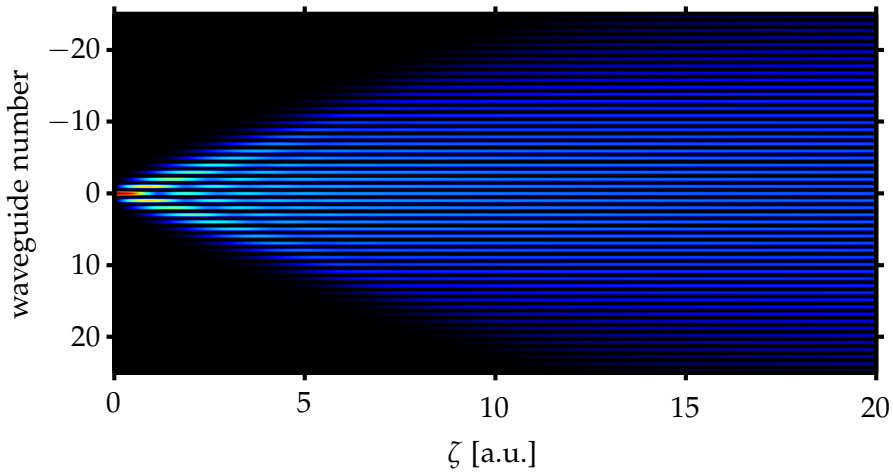

Figure 5.3: Light evolution in a homogeneous lattice with complex coupling coefficients $C = 1 + 0.16i$.

One can observe the characteristic ballistic propagation pattern only at small distances; at larger distances the propagation seems diffusive. In fact, the evolution of light within such a lossy homogeneous lattice is, in complete analogy to its lossless counterpart, formally given by

$$a_j(\zeta) = i^j J_j(2C\zeta) \tag{5.11}$$

only differing in the fact that the Bessel Function is now evaluated at complex arguments. For purely imaginary coupling, that is $C = iC''$, one can rewrite the Bessel Functions $J_j(z)$ in terms of modified Bessel Functions $I_j(z)$, which leads to $a_j(\zeta) = (-1)^j I_j(2C''\zeta)$. At first glance, this seems strange, because the modified Bessel Functions are monotonically increasing and $I_j(z) \to {}^{e^z}/\sqrt{2\pi z}$ for $z \to \infty$. However, this behavior is perfectly valid, recalling the fact, that the true amplitude of the optical field is apodized with an exponential decay which dominates the one induced by the complex coupling [compare eq. (5.6)]. To illustrate the qualitative behavior for an arbitrary complex coupling, fig. 5.4 compares the light evolution within the central waveguide of three different lattices, which are characterized by

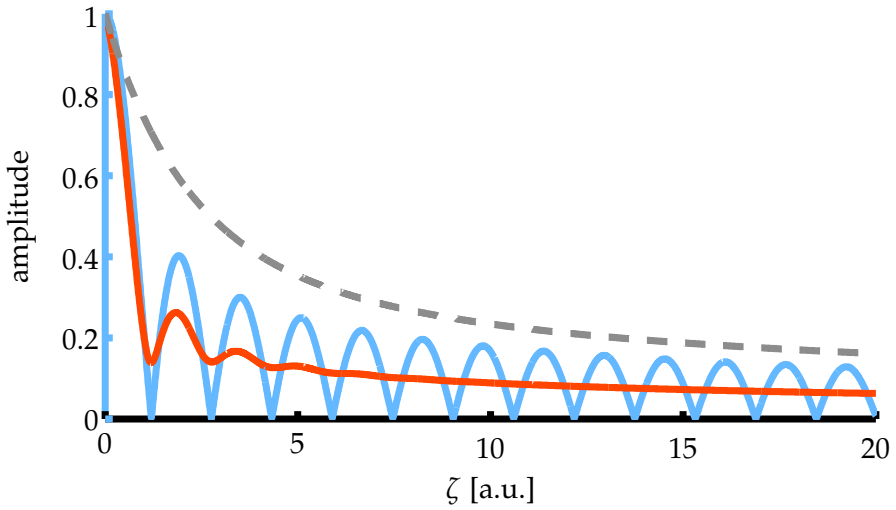

Figure 5.4: Comparison of light evolution in the central waveguide of a homogeneous lattice. The blue line solid represents the lossless array with $C = 1$, the red solid represents the central guide of fig. 5.3 with $C = 1 + 0.16i$ and the gray dashed line shows the evolution for the purely complex coupling case with $C = 0.16i$.

a purely real coupling ($C = 1$; blue solid line), complex coupling ($C = 1 + 0.16i$; red solid line), as well as purely imaginary coupling ($C = 0.16i$; dashed gray line). Here the intermediate regime corresponds to the central guide of fig. 5.4. The comparison in fig. 5.4 shows that the oscillation period of the complex coupling case, visible only at small distances, is equal to the real case. In case of a purely imaginary coupling no oscillations are visible.

The presence or absence of amplitude oscillations can be understood more fundamentally, when considering the evolution of the spectrum. On page 12 it was stated that the evolution of the spectral components $f(\varphi)$ of a homogeneous lattice is given by

$$f(\varphi, \zeta) = f(\varphi)\, e^{-i2C\cos(\varphi)\zeta} = f(\varphi)\, e^{-i2C'\cos(\varphi)\zeta} e^{2C''\cos(\varphi)\zeta} \tag{5.12}$$

whereas the mode amplitudes are related via $a_n = \frac{1}{2\pi} \int_{-\pi}^{\pi} f_0(\varphi)\, e^{-in\varphi} d\varphi$. This relation also holds in the dissipative case considered here. Equation (5.12) states that the real part of the coupling coefficient $C = C' + iC''$ introduces a phase term, which depends on the transverse momentum φ. On the other hand the imaginary part C'' introduces an amplitude increase. Note that this increase is physically valid, since the amplitude of the physical mode is apodized by an additional exponential term, corresponding to the decay of the waveguide mode [eq. (5.6)], which dominates the coupling-induced increase and ensures the decay of energy.

It is well known, that the oscillating propagation pattern of the homogeneous hermitian lattice can be understood in terms of mode beating, meaning that the phases of individual spectral components,

eq. (5.12), evolve at different rates, causing an alternating constructive and destructive interference along the ζ-direction. With the same argument it follows that in the case of purely imaginary coupling, the respective phases of the modes are conserved along the propagation direction and no mode beating occurs. In case of a complex coupling, mode beating occurs for small propagation distances where all modes are present. However, influenced by the imaginary coupling, some modes become predominant after a certain propagation distance, making the phase of all other modes irrelevant. In other words, the phase information of those modes with a negligible amplitude is lost and the mode beating vanishes.

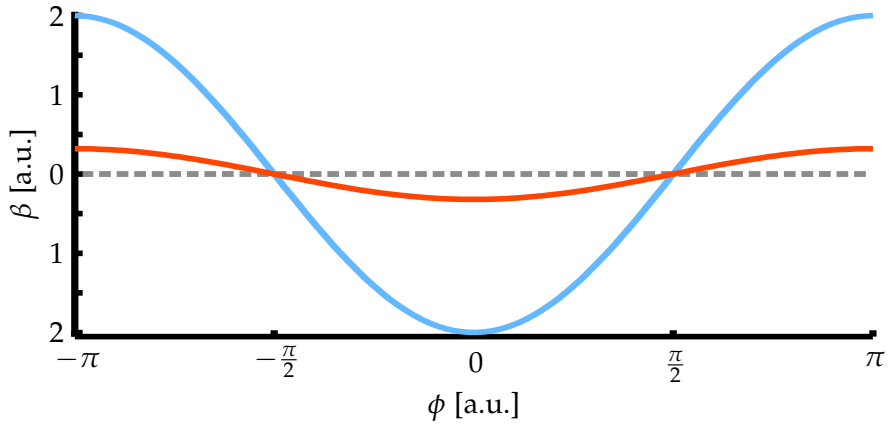

Figure 5.5: Complex Eigen-values for a lattice with complex coupling, i.e. $C = 1 + 0.16i$. The real part of the Eigen-value is denoted by the blue line, whereas the red line represents its imaginary part.

The discussion above, leads to the conclusion that the mode evolution of a homogeneous dissipative lattice is qualitatively similar to the evolution within a biatomic lattice as discussed in the previous chapter. There, it was argued that the complex band structure leads to a contraction of the spectrum and hence a diffusive transport after a certain propagation distance. Indeed, the same dynamics can be observed in the underlying homogeneous lossy lattice. Figure 5.5 shows the Eigen-value spectrum of a lattice with $C = 1 + 0.16i$, where the Eigen-value with the smallest imaginary part can be found at a transverse momentum of $\varphi = 0$. Hence, the spectrum contracts around exactly this momentum. Figure 5.6 contains the variance of the wave packet corresponding to fig. 5.3 in a double-logarithmic plot. For small propagation distances one observes a ballistic spreading (slope of 2) whereas for larger distances the spreading is diffusive (slope of 1). The underlying homogeneous lattice even allows a rigorous analytical calculation of the variance using the spectral decomposition of the amplitudes. With this

$$\Sigma \left|a_n\right|^2 = I_0 \left(4C''\zeta\right)$$

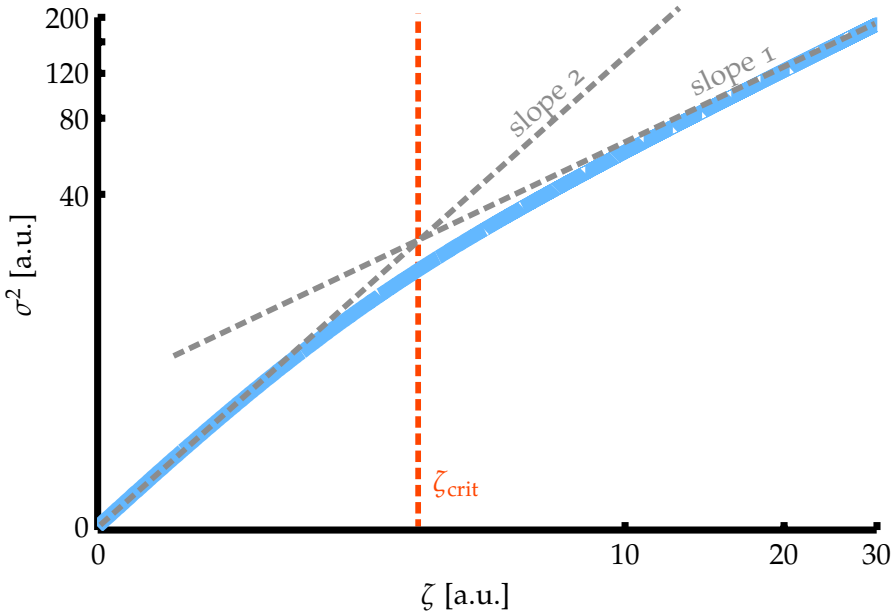

Figure 5.6: Variance of the wave packet corresponding to fig. 5.3.

as well as

$$\Sigma n^2 |a_n|^2 = \frac{|C|^2}{C''} \zeta I_1 \left(4C''\zeta\right).$$

The variance is then given by the ratio

$$\sigma^2(\zeta) = \frac{|C|^2}{C''} \zeta \frac{I_1(4C''\zeta)}{I_0(4C''\zeta)}.$$

With the asymptotic forms $I_n(z) \approx e^z/\sqrt{2\pi z}$ for $z \gg 1$ and $I_n(z) \approx z^n/n!$ for $z \ll 1$, the diffusive spreading for large distances, i.e.

$$\sigma^2(\zeta) \overset{\zeta \gg \zeta_{crit}}{=} \frac{|C|^2}{C''} \zeta$$

and the ballistic spreading for small distances, i.e.

$$\sigma^2(\zeta) \overset{\zeta \ll \zeta_{crit}}{=} 2|C|^2 \zeta^2$$

can be derived, whereas the critical distance that divides both transport regimes is given by the expression

$$\zeta_{crit} = \frac{1}{4C''}. \tag{5.13}$$

Dissipative Biatomic Lattice

In chapter 4 it was claimed that a mobility transition occurs in a biatomic lattice due to an alternating loss distribution within the lattice. Since the starting point of the derivation was eq. (4.1), one could try

to argue that this equation does not take into account complex coupling and hence cannot be valid for optical systems. Furthermore, one could jump to the conclusion that the derivation of chapter 4 is questionable and stands in contradiction to the present chapter. However, this is by no means the case and shall be briefly commented on in this section.

First of all, as it was already mentioned in a previous paragraph, both chapters yield the conclusion that a diffusive transport is due to the curvature of the complex band structure. While the approaches with which these results were obtained differ, both chapters agree in the result.

Secondly, the results of the previous chapter can easily be extended to the case of complex coupling. In the same way, the results of this chapter can be extended to a biatomic lattice. Following either approach leads to the band structure of a biatomic lattice with complex coupling as depicted in fig. 5.7. This graph corresponds to fig. 4.3 of the previous chapter whereas an additional complex coupling appears, such that $C = 1 + 0.16i$. For comparison, the imaginary part of

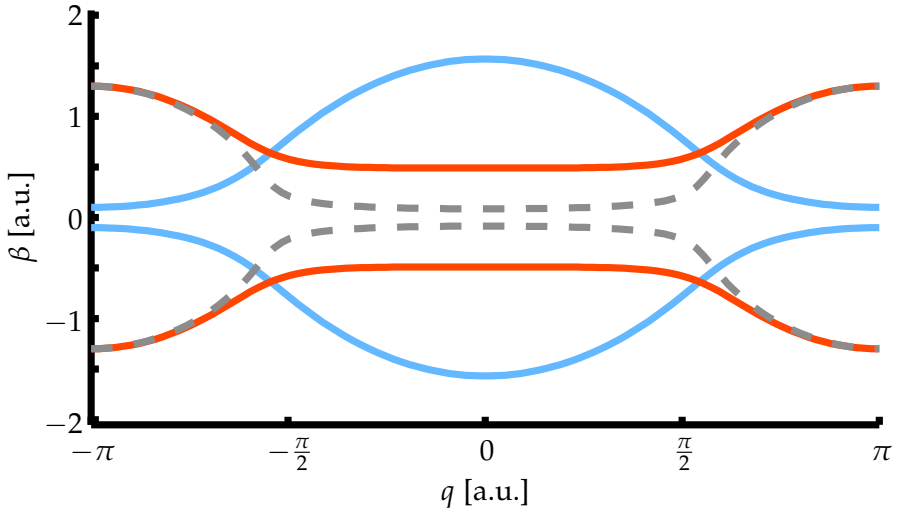

Figure 5.7: Complex band structure of a biatomic lattice with complex coupling. The solid blue lines represent the real part of β while the red lines represent the imaginary part. The values correspond to those of fig. 4.3 whereas an additional complex coupling was introduces, such that $C = 1 + 0.16i$. The gray dotted line corresponds to the exact imaginary part of fig. 4.3.

the Eigen-values for a purely real coupling [$C = 1$] is also included in fig. 5.7. It can be observed, that the spectra clearly deviate in the center of the Brillouin zone, while no deviation is present at the edges. This shows, that the complex coupling only affects the center of the band while the edges are unaffected. Since the array modes with the least amount of loss can still be found at the edge of the band, one can conclude that after a certain propagation distance the

modes of the central part, where the complex coupling plays a role, are negligible and the physics is solely determined by the loss detuning. This claim is experimentally validated as shown in fig. 4.6. The fluorescence images, for which a loss detuning is present, show that the light's intensity alternates and is only present in every second guide. This proves that only modes at the edge of the Brillouin zone are present. On the other hand, a diffusive transport due to complex coupling, leads to an intensity distribution, where neighboring guides have similar amplitude and phase.

In summary, it can be concluded that the findings of chapter 4 are perfectly valid, knowing that complex coupling effects were disregarded.

5.2 EXPERIMENTAL INVESTIGATION OF A HOMOGENEOUS LATTICE

In order to experimentally verify that an optical wave packet spreads diffusively in a homogeneous dissipative lattice, fs-LASER-written waveguide arrays were utilized. In agreement with the experiments presented in the previous chapter, the waveguides are homogeneously spaced with a distance of 17 µm which leads to a coupling of $C = 1.1\,\mathrm{cm}^{-1}$. Also equivalently, losses were introduced by sinusoidally bending the guides with an amplitude of 3 µm. In contrast to the biatomic lattice, where only every second guide is modulated, effects of a z-modulated coupling can be neglected in this setup, since the separation between neighboring guides remains constant at all propagation distances.

Light propagation within a homogeneous array of straight waveguides can be observed in fig. (4.6) (a) and the corresponding variance [fig. (4.6) (b)] clearly shows a ballistic spreading. Even though, also straight waveguides exhibit small intrinsic losses, a transition to a diffusive transport regime cannot be observed. The reason being, that the intrinsic decay rate of the bound mode of an isolated waveguide is in the order of $8.9 \cdot 10^{-3}\,\mathrm{cm}^{-1}$. If this value is taken as a basis for calculating an effective permittivity of the waveguide and retrieving a complex coupling, one finds that the complex coupling coefficient should be in the order of $5 \cdot 10^{-3}\,\mathrm{cm}^{-1}$. With this value, from eq. (5.13) a critical distance of 50 cm would follow. Since the length of the available glass samples is limited to 15 cm only a ballistic spreading can be observed for straight waveguides.

The situation changes, when additional losses are introduced due to a sinusoidal bending of the guides. Figure 5.8 (a) shows the propagation dynamics of light launched in an array where the bending period was 3 mm. It can be observed that initially the evolution shows ballistic characteristics, which then change to diffusive - the initial intensity beating decreases and finally vanishes after some propaga-

tion distance. At large propagation distances [5 – 7 cm] the intensity

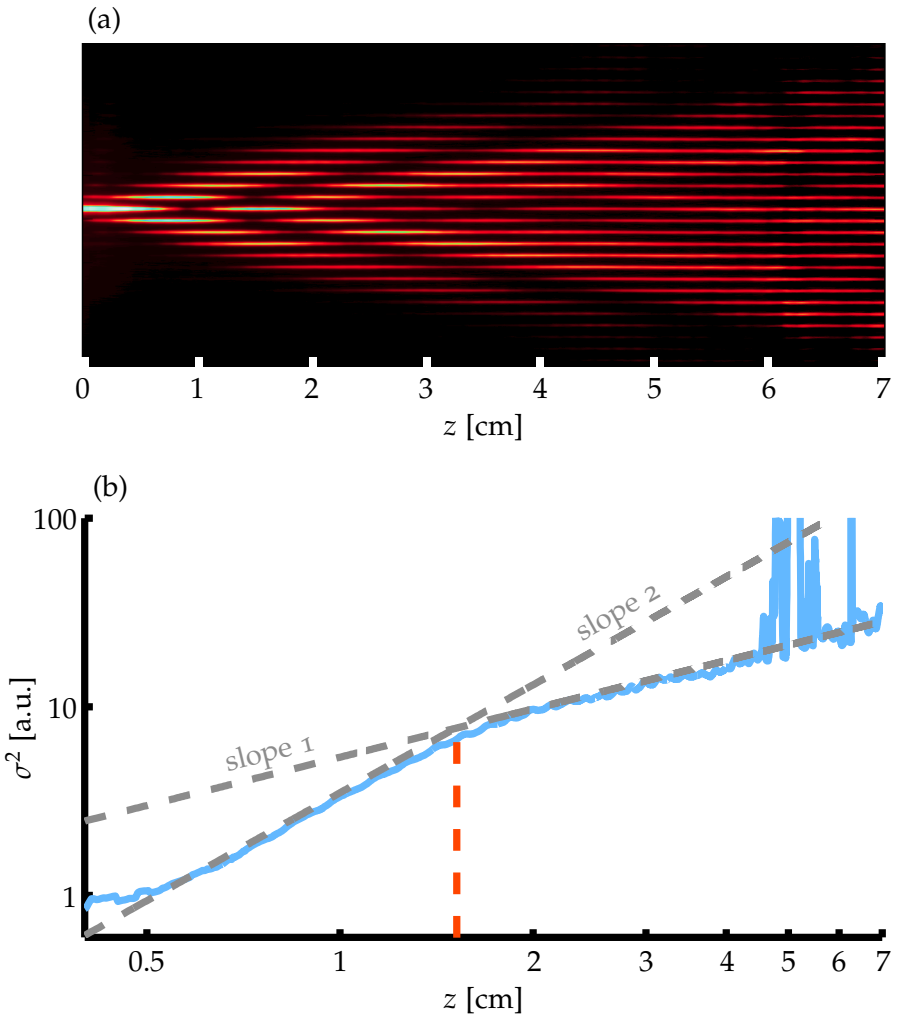

Figure 5.8: (a) Fluorescence image of the light evolution inside a waveguide array where all waveguides are sinusoidally bent with an amplitude of 3 µm and a period of 3 mm. (b) Variance corresponding to fluorescence image (a). The critical distance is visualized by a vertical dashed red line, at $z_{crit} = 1.6\,\text{cm}$.

within the individual guides does not oscillate anymore. Extracting the variance of this wave packet reveals the critical distance, which divides the zones of different transport regimes. This is depicted in fig. 5.8 (b), where the variance is plotted in a double logarithmic plot. For distances smaller than $z_{crit} = 1.6\,\text{cm}$ the slope of the variance is equal to two, whereas for larger distances, the slope is equal to one. The measured critical distance of $z_{crit} = 1.6\,\text{cm}$ also implies a complex coupling coefficient of $C'' = 0.16\,\text{cm}^{-1}$.

Indeed, the conducted measurements proof that the introduction of homogeneous losses manifest in a complex coupling and do not only lead to an exponential decay. Moreover, it needs to be mentioned, that the dissipation in the system was not introduced via a

complex permittivity, but rather a sinusoidal bending of the waveguides. While it was proven in chapter 3 that the sinusoidal bending leads to an exponential decay of the waveguide mode's amplitude, it is not a priori clear that it also acts in the same fashion as a complex refractive index. Intuitively, one would suspect that the coupling of two adjacent bent waveguides is calculated from the overlap between the bound mode and the real refractive index. Hence, no complex coupling should come into play. However, the situation is different, since the experiments clearly show the diffusive transition, which can only be induced by complex coupling. The reason for this behavior can be understood by revisiting fig. 5.1 which shows the tilted wave front of the lossy mode. This tilted phase outside of the dissipative box resembles the physical process of a net energy flux, which transports energy from the exponential tails of the mode, where there is no dissipation, to the dissipative guide, where the energy leaves the system. Relating to the mode of a sinusoidally bent guide this means that if the evolution can be approximated by an exponential decay, the effective mode also has a tilted phase front. In general, such a tilted phase is not unique to the box potential presented above, but a unifying characteristic feature of any Eigen-mode of a dissipative system. Having established this connection, the complex coupling occurring in arrays of homogeneously modulated waveguides can be attributed to the tilted phase front and it's influence on the coupling integral. As it was already stated during the discussion of eq. (5.10), not only the complex permittivity leads to a complex coupling, but also the tilted phase front plays an important role. To express it even more rigorously, the complex permittivity itself can be disregarded, since only the tilted phase front of the Eigen-mode leads to the physically interesting separation dependence of the complex coupling.

In conclusion, the experiments did not merely prove that complex coupling is present in homogeneous dissipative lattices, but also contributed evidence to the claim that sinusoidally bent waveguides are a valid tool for implementing an effective complex refractive index.

5.3 CHAPTER SUMMARY

In this chapter, a general coupled mode theory, which is valid for dissipative waveguide arrays, was derived from the PHE. It was shown that tight binding equations for dissipative systems differ from their hermitian pendants in the sense that the coupling coefficients cannot be written as purely real values, but are generally complex. In this context, one of the most intriguing features is the fact that the phase of the complex coupling coefficients grows linearly with the actual distance between two waveguides, while the amplitude drops exponentially, as expected from the hermitian case.

The reason for this striking behavior can be understood by considering the Eigen-mode profile of a lossy waveguide. While the mode profile has a flat phase front in the case of a lossless waveguide, a lossy waveguide exhibits a tilted wave front [compare fig. 5.1]. Since the coupling coefficient stems from the overlap integral between adjacent modes, the tilted phase front induced the distance dependence of the complex coupling. In this vein, it is interesting to note that even though the complex permitivity of the waveguide is initially responsible for the dissipation, it is only indirectly responsible for the non-trivial complex coupling., which is primarily due to the tilted phase front of the waveguide's Eigen-mode.

It was shown theoretically as well as experimentally that the complex coupling has a substantial influence on the propagation dynamics, already for a homogeneous array. In this case, it was found that the well known ballistic propagation pattern vanishes and is replaced by a diffusive one. In accordance to the previous chapter, the diffusive transport is induced by a non-trivial complex band structure, where modes in different regions of the spectrum experience different amounts of loss.

Similar to chapter 4, a critical distance at which the propagation switches from ballistic to diffusive was derived analytically and verified experimentally. In the particular case of a homogeneous lattice, which was considered in this chapter, the critical distance is inversely proportional to the imaginary part of the complex coupling coefficient.

6

CONCLUSION AND OUTLOOK

The aim of this thesis was to provide a framework which allows one to make the unique properties of $\mathcal{PT}$ symmetry accessible in fs-LASER-written waveguide arrays and hence broaden the versatility of this platform. The ambition was sparked by the desire to investigate novel dynamics in $\mathcal{PT}$ symmetric media. Altogether, this goal was accomplished by providing a thorough theoretical and experimental investigation of sinusoidally bent waveguides as a way to implement well defined losses. In addition, a new coupled mode theory for dissipative waveguides was presented and experimentally verified. With these tools at hand, this thesis contains the first experimental realization of a $\mathcal{PT}$ symmetric structure in fs-LASER-written waveguide arrays.

The cornerstone of this thesis is formed by the investigation of waveguides that were sinusoidally bent transverse with respect to the propagation direction of light. As light is being radiated away from these guides due to the local curvature, the main question of interest was whether this type of modulation leads to an overall exponential decay of the bound mode's amplitude. The fact that this question was positively answered during the theoretical and experimental analysis, made all subsequent experimental investigations even possible in the first place. Beyond that, the investigation of sinusoidally bent waveguides did not only seek a digital answer of yes or no, but was rather concerned with the understanding of the underlying physics, the dependence of the effect on the relevant system parameters and also the limitations which are most important when it comes to experimental applications.

In this respect, it was found that the overall decay rate of light bound to the waveguide strongly depends on bending parameters such as period, since interference effects play a vital role in the propagation dynamics. In order to better grasp the interference effects, occurring in modulated waveguides, the system was compared to blazed diffraction gratings. In such gratings the reflected light of an incident plane wave is being split into several diffraction orders due to an angle-dependent constructive or destructive interference between light reflected from adjacent grating lines. In accordance, the light that is radiated away from neighboring bends of modulated

waveguides also interferes. The difference is that light is predominantly radiated away in one predetermined direction, leading to either an enhancement or suppression of the overall emitted light. This interference effect leads to the beneficial situation that it can be exploited while using the modulation frequency for tuning the exponential decay rate of the guided light.

The importance of exhibiting an exponential decay rate in sinusoidally modulated waveguides stems from the fact that this type of propagation behavior is equivalent to the evolution of light inside of a straight waveguide formed by a dissipative medium. As a consequence, sinusoidally bent waveguides can be utilized to mimic dissipative media and hence enable the implementation of $\mathcal{PT}$ symmetric structures.

Such a $\mathcal{PT}$ symmetric structure was presented in chapter 4, where a biatomic lattice was considered. In this specific biatomic lattice straight and bent waveguides were alternating, which introduces a symmetric refractive index distribution and an anti-symmetric loss modulation - a condition that is necessary for $\mathcal{PT}$ symmetry. Herewith the first experimental realization of a $\mathcal{PT}$ symmetric structure in fs-LASER-written waveguide arrays was presented.

The structure was investigated both theoretically and experimentally primarily in the regime where $\mathcal{PT}$ symmetry is broken, a situation which was implemented experimentally by equally spacing neighboring waveguides. In this regime of broken $\mathcal{PT}$ symmetry the band structure of the system is complex, leading to a non-uniform decay of the Eigen-modes during propagation. When initially the entire spectrum is excited, the modes in the upper band decay first, followed by the modes in the center of the lower band. After a sufficiently long propagation distance only the modes at the edge of the lower prevail, while the spectrum still keeps contracting. In this setup, the resulting propagation dynamics show a diffusive spreading of the wavepacket, characterized by the linear growth of the wavepacket's variance. In contrast, in the ballistic case the variance grows quadratically with the propagation distance. In addition, the analysis revealed that the propagation distance at which the transition from an initially ballistic spreading (when all modes still contribute) to a subsequent diffusive spreading takes place is merely inversely proportional to the loss detuning between the individual guides.

The findings presented in chapter 4 have an enormous impact on the understanding of wave transport in 1D systems. Before, it was naturally assumed that wave transport in a 1D system can either be ballistic or localized, depending on whether the system was subject to disorder. It was understood that any amount of uncorrelated disorder would lead to localization of the otherwise ballistic transport. On the other hand, diffusive transport, was considered to be not observable in 1D quantum systems - especially in ordered systems. Since this

understanding was based on hermitian systems, it cannot simply be transfered to $\mathcal{PT}$ symmetric systems or more generally systems that include dissipative structures. In this matter, the presentation of an ordered 1D lattice that exhibits a diffusive spreading of the wavepacket broadens the view based on hermiticity and suggests a generalization of the notion of wave transport which includes and correctly describes dissipative systems. The strength of the analysis presented here lies in the simplicity of relating the diffusive transport regime to the curvature of the complex band structure.

Another well established notion was questioned in chapter 5, where a new, generalized coupled mode theory for dissipative waveguides was analytically derived and experimentally observed. The elementary finding, which extends the common understanding of hermitian lattices, is the fact that the coupled mode equations for dissipative waveguides exhibit a complex coupling term, which cannot simply be reduced to a real term by means of a transformation.

While the fundamental origin of the complex coupling is formed by the complex permittivity of the individual waveguide, the more interesting and immediate cause of the complex coupling is given by the tilt of the guided mode profile of the dissipative waveguide. Interestingly, it is in this regard that the dissipative waveguides differ most strongly from their lossless counterparts. While for lossless waveguides the transverse mode profile of a guided mode exhibits a flat phase outside of the waveguide region, in the case of a dissipative guide the phase front is tilted in this region. This tilt represents the physical process of energy being constantly transported from the evanescent side lobes into the central region where it dissipates.

As the coupling constant of the coupled mode theory is equated with the overlap-integral between adjacent mode profiles computed inside the waveguide region, it is an interesting finding that the phase tilt of the mode and actual distance between adjacent guides determine the phase of the coupling constant. As an immediate consequence, the investigation in chapter 5 revealed that the distance between adjacent guides can be used to tune the phase of the coupling constant. To be specific, it is interesting to note that regardless of the exact value of the complex permittivity the coupling constant can adopt any phase depending on the distance between adjacent guides. As a matter of fact, there are certain distances at which a purely imaginary or negative coupling can be achieved.

In addition, in chapter 5 the propagation dynamics of a homogeneous, dissipative lattice were investigated. The analysis revealed that due to the complex coupling a non-trivial complex band structure arises which also leads to a diffusive wave transport. As the experimental verification of this effect also utilized sinusoidally bent waveguides more evidence was added to the claim that sinusoidally bent waveguides can mimic dissipative media. The analysis proved

that not only the amplitude of isolated sinusoidally bent waveguides decays exponentially, but also when these waveguides are brought into an array and interact, then propagation dynamics are observed as they would be expected from media exhibiting a complex permittivity.

Judging the impact of this thesis, it is important to note that this work made scientific contributions on three distinct layers. The first and basic layers includes the contributions to field of fundamental physics, especially quantum physics; whereas the second more specific layer denotes the value this thesis provides for the platform of fs-LASER-written waveguides; finally the third layer consists of the ideas one can draw from this thesis regarding specific applications and devices.

Regarding the layer of elementary physics, this thesis made important contributions. Especially the work presented in chapters 3 and 4 bears significance for the field of quantum physics. As it was already stated during the theoretical derivations, the sinusoidally modulated waveguide in paraxial optics is mathematically equivalent to an oscillating potential well in QM. As such it is important in many different fields of physics, such as for instance atto-second science where an electronic wavefunctin inside of an atomic potential is considered. With this in mind, it is rather interesting that even though the stationary potential well is subject to every elementary QM lecture, the analytical description of a wavefunction evolving inside of an oscillating potential well was yet unknown in the literature. With this, one can suspect that the knowledge and ideas gained in this thesis are of value in various research areas and can be applied in fields where similar questions are studied.

As already mentioned in a previous paragraph, the value of chapter 4 for the field of elementary physics lies in the generalization of notions about wave transport beyond the scope of hermiticity. It will be interesting to see, whether in the future one will be able to find a unified theory that generalizes the prediction of a wave transport regime in 1D or 2D structures. Moreover, the analysis has exemplarily shown that the study of $\mathcal{PT}$ symmetry and related topics is important for elementary physics in order to broaden the field of view and loosen the ties of a sometimes overly restrictive thinking - as it was shown in this thesis, new insights into well known topics can be gained. Especially the field of $\mathcal{PT}$ symmetry is a fertile area of research, which needs to be studied intensively. For this matter, it is important that this thesis provided the solid foundation for an experimental platform for $\mathcal{PT}$ symmetry. Already today, work has been published that utilizes the experimental implementation of $\mathcal{PT}$ symmetry, which was established here, in order to study new phenomena in different fields such as quantum optics [36, 100] or topology [107]. Along these lines a lot of insights are still to be gained. It should be expected that the

field of $\mathcal{PT}$ symmetry together with the newly emerging research interest in topology will deliver new perspectives on well established ultimate truths. As there are multiple opportunities to broaden the field of view when studying symmetries in an elementary sense, it is a great advantage to have a versatile experimental platform at hand, as theory and experiment can fruitfully exchange ideas.

In regard to the value this thesis provides for the platform of fs-LASER-written waveguides, one can conclude that it surely poses a significant extension to the toolbox available to this platform. As already stated, the study of topics like $\mathcal{PT}$ symmetry or dissipative systems in general has not been possible before to extend. In this sense, this thesis pointed out that even after decades of extensive use the physics of this platform are not entirely understood. Over the past years the coarser understanding of the basics of light evolution inside of fs-LASER-written waveguide arrays was well sufficient in order to study a number of remarkable phenomena. However, the investigations of this thesis have ignited a new desire to explore the properties of light evolution in waveguide arrays on a much deeper level. For instance, almost all experiments conducted today are confined to and based on the assumption of the tight binding approximation. In this context, quite recently new investigations probed the validity and limitation of this approximation and furthermore provided a suitable extension, which in turn enables the valid prediction of a much wider range of lattices, where for instance waveguides are much closer spaced. In the near future, more advances which extend the available toolbox of fs-LASER-written waveguide arrays are foreseen. An important extension, which directly follows from this work, will be to find a way to implement dissipative waveguides also in 2D lattices, since currently the technique is confined to a single transverse dimension in order to prevent reabsorption of the radiated light.

From an application point of view, this thesis provides a number of promising ideas. The dissipative arrays discussed throughout the chapters might serve as mode filters. Here, in particular the importance of the band structure, which was pointed out in chapter 4, can serve as a guide for fabricating new kinds of structured illumination devices, which in turn can find application in microscopy or telecommunication. The advantage of such structures that rely on dissipation instead of, for instance, interference is the fact that they should be more robust to external conditions, such as temperature, or manufacturing inaccuracies. Today, the platform of fs-LASER-written waveguide arrays shows a great versatility in many aspects, still until now it remains a research platform rather than a platform for manufacturing commercial devices. However, this step will surely be taken in the near future when fs-LASERs, as the main manufacturing device, become more affordable and the fast prototyping is accompanied by

an overall low priced fabrication process. Nevertheless, the true success of this platform regarding applications will only happen, if one is able to actively control the dynamics of the light evolution. Naturally, this obstacle is already tackled by means of different interesting approaches - one of them involves the incorporation of liquid crystals as active switching devices.

In conclusion, as every scientific work should do, this thesis has answered important questions, when it made the unique properties of $\mathcal{PT}$ symmetry accessible in fs-LASER-written waveguide arrays, while at the same time a number of new interesting demands were raised.

BIBLIOGRAPHY

[1] N. V. Alexeeva, I. V. Barashenkov, A. A. Sukhorukov, and Y. S. Kivshar. Optical solitons in PT-symmetric nonlinear couplers with gain and loss. *Phys. Rev. A*, 85:063837, Jun 2012. (Cited on page 22.)

[2] R. Alicki. The Markov Master Equations and the Fermi Golden Rule. *International Journal of Theoretical Physics*, 16(5):351–355, 1977. (Cited on page 38.)

[3] A. Amir, Y. Lahini, and H. B. Perets. Classical diffusion of a quantum particle in a noisy environment. *Phys. Rev. E*, 79: 050105, May 2009. (Cited on page 53.)

[4] P. W. Anderson. Absence of diffusion in certain random lattices. *Phys. Rev.*, 109:1492–1505, Mar 1958. (Cited on pages 11 and 53.)

[5] P. Barthelemy, J. Bertolotti, and D. S. Wiersma. A Levy Flight for light. *Nature*, 453(7194):495–498, May 2008. (Cited on page 53.)

[6] J. Barthes, G. Colas des Francs, A. Bouhelier, and A. Dereux. A coupled lossy local-mode theory description of a plasmonic tip. *New Journal of Physics*, 14(8):083041, 2012. (Cited on page 67.)

[7] C. M. Bender and S. Boettcher. Real spectra in non-hermitian Hamiltonians having PT symmetry. *Phys. Rev. Lett.*, 80:5243–5246, Jun 1998. (Cited on pages 1, 19, 21, 27, and 53.)

[8] C. M. Bender, S. Boettcher, and P. N. Meisinger. PT-symmetric quantum mechanics. *Journal of Mathematical Physics*, 40(5):2201–2229, 1999. (Cited on page 20.)

[9] C. M. Bender, D. C. Brody, and H. F. Jones. Complex extension of quantum mechanics. *Phys. Rev. Lett.*, 89:270401, Dec 2002. (Cited on pages 20 and 21.)

[10] C. M. Bender, P. N. Meisinger, and Q. Wang. Finite-dimensional PT-symmetric Hamiltonians. *Journal of Physics A Mathematical General*, 36:6791–6797, June 2003. (Cited on pages 20 and 21.)

[11] O. Bendix, R. Fleischmann, T. Kottos, and B. Shapiro. Optical structures with local PT-symmetry. *Journal of Physics A: Mathematical and Theoretical*, 43(26):265305, 2010. (Cited on page 22.)

[12] J. Billy, V. Josse, Z. Zuo, A. Bernard, B. Hambrecht, P. Lugan, D. Clement, L. Sanchez-Palencia, P. Bouyer, and A. Aspect. Direct observation of Anderson Localization of matter waves in a

controlled disorder. *Nature*, 453(7197):891–894, Jun 2008. (Cited on page 53.)

[13] J. Burghoff, H. Hartung, S. Nolte, and A. Tünnermann. Structural properties of femtosecond laser-induced modifications in LiNbO3. *Applied Physics A*, 86(2):165–170, 2007. (Cited on page 16.)

[14] J. W. Chan, T. Huser, S. Risbud, and D. M. Krol. Structural changes in fused silica after exposure to focused femtosecond laser pulses. *Opt. Lett.*, 26(21):1726–1728, Nov 2001. (Cited on page 16.)

[15] J. W. Chan, T. R. Huser, S. H. Risbud, and D. M. Krol. Modification of the fused silica glass network associated with waveguide fabrication using femtosecond laser pulses. *Applied Physics A*, 76(3):367–372, 2003. (Cited on page 16.)

[16] D. N. Christodoulides and R. I. Joseph. Discrete self-focusing in nonlinear arrays of coupled waveguides. *Opt. Lett.*, 13(9): 794–796, Sep 1988. (Cited on page 2.)

[17] D. N. Christodoulides, F. Lederer, and Y. Silberberg. Discretizing light behaviour in linear and nonlinear waveguide lattices. *Nature*, 424(6950):817–823, Aug 2003. (Cited on page 2.)

[18] C. Cohen-Tannoudji, B. Diu, and F. Laloe. *Quantum mechanics*. Number Bd. 1 in Quantum Mechanics. Wiley, 1991. ISBN 9780471164333. (Cited on pages 19 and 37.)

[19] M. Combescot. On the generalized golden rule for transition probabilities. *Journal of Physics A: Mathematical and General*, 34 (31):6087, 2001. (Cited on page 38.)

[20] P. B. Corkum and F. Krausz. Attosecond science. *Nat Phys*, 3(6): 381–387, Jun 2007. (Cited on page 37.)

[21] K. M. Davis, K. Miura, N. Sugimoto, and K. Hirao. Writing waveguides in glass with a femtosecond laser. *Opt. Lett.*, 21(21): 1729–1731, Nov 1996. (Cited on pages 2 and 15.)

[22] J.-W. Deng, U. Guenther, and Q.-H. Wang. General PT-symmetric matrices. *ArXiv e-prints*, December 2012. (Cited on page 20.)

[23] S. V. Dmitriev, A. A. Sukhorukov, and Y. S. Kivshar. Binary parity-time-symmetric nonlinear lattices with balanced gain and loss. *Opt. Lett.*, 35(17):2976–2978, Sep 2010. (Cited on page 27.)

[24] P. Dorey, C. Dunning, and R. Tateo. Spectral equivalences, Bethe Ansatz Equations, and reality properties in PT-symmetric quantum mechanics. *Journal of Physics A: Mathematical and General*, 34(28):5679, 2001. (Cited on page 21.)

[25] D. Dragoman. The formulation of Fermi's Golden Rule in phase space. *Physics Letters A*, 274(3-4):93–97, 2000. (Cited on page 38.)

[26] R. Driben and B. A. Malomed. Stability of solitons in parity-time-symmetric couplers. *Opt. Lett.*, 36(22):4323–4325, Nov 2011. (Cited on page 22.)

[27] P. Drude. Zur Elektronentheorie der Metalle. *Annalen der Physik*, 306(3):566–613, 1900. (Cited on page 53.)

[28] O. M. Efimov, L. B. Glebov, K. A. Richardson, E. Van Stryland, T. Cardinal, S. H. Park, M. Couzi, and J. L. Bruneel. Waveguide writing in chalcogenide glasses by a train of femtosecond laser pulses. *Optical Materials*, 17(3):379 – 386, 2001. (Cited on page 16.)

[29] F. Eilenberger, K. Prater, S. Minardi, R. Geiss, U. Röpke, J. Kobelke, K. Schuster, H. Bartelt, S. Nolte, A. Tünnermann, and T. Pertsch. Observation of discrete, vortex light bullets. *Phys. Rev. X*, 3:041031, Dec 2013. (Cited on page 2.)

[30] R. El-Ganainy, K. G. Makris, D. N. Christodoulides, and Z. H. Musslimani. Theory of coupled optical PT-symmetric structures. *Opt. Lett.*, 32(17):2632–2634, Sep 2007. (Cited on pages 1, 22, 27, and 53.)

[31] E. Fermi. Versuch einer Theorie der β-Strahlen. I. *Zeitschrift fur Physik*, 88:161–177, March 1934. (Cited on page 37.)

[32] J. W. Fleischer, M. Segev, N. K. Efremidis, and D. N. Christodoulides. Observation of two-dimensional discrete solitons in optically induced nonlinear photonic lattices. *Nature*, 422(6928): 147–150, Mar 2003. (Cited on page 15.)

[33] L. Fonda, G. C. Ghirardi, and A. Rimini. On the Fermi Golden Rule. *Il Nuovo Cimento A (1965-1970)*, 25(4):537–548, 1975. (Cited on page 38.)

[34] P. Glansdorff and I. Prigogine. *Theory of structure, stability and fluctuations*. John Wiley & Sons Ltd, 1971. ISBN 9780471302803. (Cited on page 53.)

[35] I. S. Gradshteyn and I. M. Ryzhik. *Table of integrals, series, and products*. Elsevier/Academic Press, Amsterdam, seventh edition, 2007. ISBN 978-0-12-373637-6; 0-12-373637-4. (Cited on pages 11 and 111.)

[36] M. Gräfe, R. Heilmann, R. Keil, T. Eichelkraut, M. Heinrich, S. Nolte, and A. Szameit. Correlations of indistinguishable particles in non-hermitian lattices. *New Journal of Physics*, 15(3): 033008, 2013. (Cited on page 86.)

[37] A. Guo, G. J. Salamo, D. Duchesne, R. Morandotti, M. Volatier-Ravat, V. Aimez, G. A. Siviloglou, and D. N. Christodoulides. Observation of PT-symmetry breaking in complex optical potentials. *Phys. Rev. Lett.*, 103:093902, Aug 2009. (Cited on pages 1, 22, 27, and 53.)

[38] N. Hatano and D. R. Nelson. Localization transitions in non-hermitian quantum mechanics. *Phys. Rev. Lett.*, 77:570–573, Jul 1996. (Cited on page 21.)

[39] M. Heinrich, A. Szameit, F. Dreisow, S. Döring, J. Thomas, S. Nolte, A. Tünnermann, and A. Ancona. Evanescent coupling in arrays of type II femtosecond laser-written waveguides in bulk x-cut lithium niobate. *Applied Physics Letters*, 93(10):101111, 2008. (Cited on page 16.)

[40] M. Heinrich, A. Szameit, F. Dreisow, R. Keil, S. Minardi, T. Pertsch, S. Nolte, A. Tünnermann, and F. Lederer. Observation of three-dimensional discrete-continuous *X* waves in photonic lattices. *Phys. Rev. Lett.*, 103:113903, Sep 2009. (Cited on page 16.)

[41] M. Heinrich, F. Eilenberger, R. Keil, F. Dreisow, E. Suran, F. Louradour, A. Tünnermann, T. Pertsch, S. Nolte, and A. Szameit. Optical limiting and spectral stabilization in segmented photonic lattices. *Opt. Express*, 20(24):27299–27310, Nov 2012. (Cited on page 108.)

[42] R. G. Holt, C. C. Clarke, and J. G. McDaniel. An acoustic levitation technique for measuring the rheology of foam near the order-disorder transition. *The Journal of the Acoustical Society of America*, 105(2):1146–1146, 1999. (Cited on page 53.)

[43] W.-P. Huang. Coupled-mode theory for optical waveguides: an overview. *J. Opt. Soc. Am. A*, 11(3):963–983, Mar 1994. (Cited on page 67.)

[44] K. Itoh, W. Watanabe, S. Nolte, and C. B. Schaffer. Ultrafast processes for bulk modification of transparent materials. *MRS Bulletin*, 31:620–625, Jan 2006. (Cited on pages 2 and 15.)

[45] A. L. Jones. Coupling of optical fibers and scattering in fibers. *J. Opt. Soc. Am.*, 55(3):261–271, Mar 1965. (Cited on page 2.)

[46] S. Katayama, M. Horiike, K. Hirao, and N. Tsutsumi. Structures induced by irradiation of femto-second laser pulse in polymeric

materials. *Journal of Polymer Science Part B: Polymer Physics*, 40 (6):537–544, 2002. (Cited on page 16.)

[47] R. Keil, Y. Lahini, Y. Shechtman, M. Heinrich, R. Pugatch, F. Dreisow, A. Tünnermann, S. Nolte, and A. Szameit. Perfect imaging through a disordered waveguide lattice. *Opt. Lett.*, 37 (5):809–811, Mar 2012. (Cited on page 108.)

[48] R. Keil, J. M. Zeuner, F. Dreisow, M. Heinrich, A. Tünnermann, S. Nolte, and A. Szameit. The random mass Dirac Model and long-range correlations on an integrated optical platform. *Nature Communications*, 4:1368 EP –, Jan 2013. Article. (Cited on page 108.)

[49] R. Keil, C. Noh, A. Rai, S. Stützer, S. Nolte, D. G. Angelakis, and A. Szameit. Optical simulation of charge conservation violation and Majorana Dynamics. *Optica*, 2(5):454–459, May 2015. (Cited on page 108.)

[50] C. Kittel and H. Kroemer. *Thermal physics*. WH Freeman, 1980. ISBN 978-0716710882. (Cited on page 53.)

[51] H. Kogelnik. *Theory of dielectric waveguides*, pages 13–81. Springer Berlin Heidelberg, Berlin, Heidelberg, 1975. ISBN 978-3-662-43208-2. (Cited on page 67.)

[52] F. Krausz and M. Ivanov. Attosecond physics. *Rev. Mod. Phys.*, 81:163–234, Feb 2009. (Cited on page 37.)

[53] Y. Lahini, A. Avidan, F. Pozzi, M. Sorel, R. Morandotti, D. N. Christodoulides, and Y. Silberberg. Anderson Localization and nonlinearity in one-dimensional disordered photonic lattices. *Phys. Rev. Lett.*, 100:013906, Jan 2008. (Cited on page 53.)

[54] A. S. Landsman and U. Keller. Attosecond science and the tunnelling time problem. *Physics Reports*, 547:1 – 24, 2015. Attosecond science and the tunneling time problem. (Cited on page 37.)

[55] H. Leblond, B. A. Malomed, and D. Mihalache. Spatiotemporal vortex solitons in hexagonal arrays of waveguides. *Phys. Rev. A*, 83:063825, Jun 2011. (Cited on page 2.)

[56] S. Longhi. Bloch Oscillations in complex crystals with PT symmetry. *Phys. Rev. Lett.*, 103:123601, Sep 2009. (Cited on pages 2, 22, 27, and 53.)

[57] S. Longhi. Spectral singularities in a non-hermitian Friedrichs-Fano-Anderson Model. *Phys. Rev. B*, 80:165125, Oct 2009. (Cited on pages 22 and 27.)

[58] K. G. Makris, R. El-Ganainy, D. N. Christodoulides, and Z. H. Musslimani. Beam dynamics in PT symmetric optical lattices. *Phys. Rev. Lett.*, 100:103904, Mar 2008. (Cited on pages 22, 27, and 53.)

[59] I. Mansour and F. Caccavale. An improved procedure to calculate the refractive index profile from the measured near-field intensity. *Journal of Lightwave Technology*, 14(3):423–428, Mar 1996. (Cited on page 16.)

[60] S. Marksteiner, K. Ellinger, and P. Zoller. Anomalous diffusion and Lévy walks in optical lattices. *Phys. Rev. A*, 53:3409–3430, May 1996. (Cited on page 53.)

[61] S. E. Miller. Coupled wave theory and waveguide applications. *Bell System Technical Journal*, 33(3):661–719, 1954. (Cited on page 67.)

[62] A. Mostafazadeh. A physical realization of the generalized PT-, C-, and CPT-symmetries and the position operator for Klein-Gordon Fields. *International Journal of Modern Physics A*, 21:2553–2572, 2006. (Cited on page 21.)

[63] A. Mostafazadeh and G. Scolarici. Pseudo-hermiticity and electromagnetic wave propagation: The case of anisotropic and lossy media. *Physics Letters A*, 374(24):2401 – 2405, 2010. (Cited on page 21.)

[64] Z. H. Musslimani, K. G. Makris, R. El-Ganainy, and D. N. Christodoulides. Optical solitons in PT periodic potentials. *Phys. Rev. Lett.*, 100:030402, Jan 2008. (Cited on pages 22, 27, and 53.)

[65] U. Naether, J. M. Meyer, S. Stützer, A. Tünnermann, S. Nolte, M. I. Molina, and A. Szameit. Anderson Localization in a periodic photonic lattice with a disordered boundary. *Opt. Lett.*, 37 (4):485–487, Feb 2012. (Cited on pages 2, 11, and 16.)

[66] U. Naether, S. Rojas-Rojas, A. J. Martínez, S. Stützer, A. Tünnermann, S. Nolte, M. I. Molina, R. A. Vicencio, and A. Szameit. Enhanced distribution of a wave-packet in lattices with disorder and nonlinearity. *Opt. Express*, 21(1):927–934, Jan 2013. (Cited on page 2.)

[67] U. Naether, S. Stützer, R. A. Vicencio, M. I. Molina, A. Tünnermann, S. Nolte, T. Kottos, D. N. Christodoulides, and A. Szameit. Experimental observation of superdiffusive transport in random dimer lattices. *New Journal of Physics*, 15(1):013045, 2013. (Cited on page 11.)

[68] A. H. Nejadmalayeri, P. R. Herman, J. Burghoff, M. Will, S. Nolte, and A. Tünnermann. Inscription of optical waveguides in crystalline silicon by mid-infrared femtosecond laser pulses. *Opt. Lett.*, 30(9):964–966, May 2005. (Cited on page 16.)

[69] D. R. Nelson and N. M. Shnerb. Non-hermitian localization and population biology. *ArXiv e-prints*, 58:1383–1403, August 1998. (Cited on page 21.)

[70] S. Nolte, M. Will, J. Burghoff, and A. Tünnermann. Femtosecond waveguide writing: a new avenue to three-dimensional integrated optics. *Applied Physics A*, 77(1):109–111, 2003. (Cited on page 16.)

[71] M. Ornigotti and A. Szameit. Quasi PT-symmetry in passive photonic lattices. *Journal of Optics*, 16(6):065501, 2014. (Cited on page 23.)

[72] J. M. Ottino and S. Wiggins. Introduction: mixing in microfluidics. *Philosophical Transactions of the Royal Society of London A: Mathematical, Physical and Engineering Sciences*, 362(1818):923–935, 2004. (Cited on page 53.)

[73] H. M. Pastawski. Revisiting the Fermi Golden Rule: Quantum dynamical phase transition as a paradigm shift. *Physica B: Condensed Matter*, 398(2):278 – 286, 2007. Proceedings of the Workshop "At the Frontiers of Condensed Matter III" - New Trends in Structural, Electronic and Magnetic Properties of Matter. (Cited on page 38.)

[74] T. Pertsch, U. Peschel, J. Kobelke, K. Schuster, H. Bartelt, S. Nolte, A. Tünnermann, and F. Lederer. Nonlinearity and disorder in fiber arrays. *Phys. Rev. Lett.*, 93:053901, Jul 2004. (Cited on page 15.)

[75] T. Pertsch, U. Peschel, F. Lederer, J. Burghoff, M. Will, S. Nolte, and A. Tünnermann. Discrete diffraction in two-dimensional arrays of coupled waveguides in silica. *Opt. Lett.*, 29(5):468–470, Mar 2004. (Cited on page 2.)

[76] J. R. Pierce. Coupling of modes of propagation. *Journal of Applied Physics*, 25(2):179–183, 1954. (Cited on page 67.)

[77] E. Prodan, C. Radloff, N. J. Halas, and P. Nordlander. A hybridization model for the plasmon response of complex nanostructures. *Science*, 302(5644):419–422, 2003. (Cited on page 67.)

[78] M. C. Rechtsman, J. M. Zeuner, A. Tünnermann, S. Nolte, M. Segev, and A. Szameit. Strain-induced pseudomagnetic field and photonic Landau Levels in dielectric structures. *Nat Photon*, 7(2):153–158, Feb 2013. (Cited on page 2.)

[79] A. Regensburger, C. Bersch, M.-A. Miri, G. Onishchukov, D. N. Christodoulides, and U. Peschel. Parity-time synthetic photonic lattices. *Nature*, 488:167–171, Aug 2012. (Cited on pages 1, 22, 27, and 53.)

[80] A. S. C. Rittner and J. D. Reppy. Disorder and the supersolid state of solid ^{4}He. *Phys. Rev. Lett.*, 98:175302, Apr 2007. (Cited on page 53.)

[81] G. Roati, C. D'Errico, L. Fallani, M. Fattori, C. Fort, M. Zaccanti, G. Modugno, M. Modugno, and M. Inguscio. Anderson Localization of a non-interacting Bose-Einstein Condensate. *Nature*, 453(7197):895–898, Jun 2008. (Cited on page 53.)

[82] C. E. Rüter, K. G. Makris, R. El-Ganainy, D. N. Christodoulides, M. Segev, and D. Kip. Observation of parity-time symmetry in optics. *Nat Phys*, 6:192–195, Mar 2010. (Cited on pages 22, 27, and 53.)

[83] M. Sato, K. Hasebe, K. Esaki, and M. Kohmoto. Time-reversal symmetry in non-hermitian systems. *Progress of Theoretical Physics*, 127:937–974, June 2012. (Cited on page 21.)

[84] C. B. Schaffer, J. F. García, and E. Mazur. Bulk heating of transparent materials using a high-repetition-rate femtosecond laser. *Applied Physics A*, 76(3):351–354, 2003. (Cited on page 16.)

[85] S. A. Schelkunoff. Conversion of Maxwell's Equations into generalized telegraphist's equations. *Bell System Technical Journal*, 34(5):995–1043, 1955. (Cited on page 67.)

[86] T. Schwartz, G. Bartal, S. Fishman, and M. Segev. Transport and Anderson Localization in disordered two-dimensional photonic lattices. *Nature*, 446(7131):52–55, Mar 2007. (Cited on page 53.)

[87] A. W. Snyder. Coupled-mode theory for optical fibers. *J. Opt. Soc. Am.*, 62(11):1267–1277, Nov 1972. (Cited on page 67.)

[88] A. Soffer and M. I. Weinstein. Time dependent resonance theory. *Geometric & Functional Analysis GAFA*, 8(6):1086–1128, 1998. (Cited on page 38.)

[89] S. Somekh, E. Garmire, A. Yariv, H. L. Garvin, and R. G. Hunsperger. Channel optical waveguide directional couplers. *Applied Physics Letters*, 22(1):46–47, 1973. (Cited on page 2.)

[90] S. Somekh, E. Garmire, A. Yariv, H. L. Garvin, and R. G. Hunsperger. Channel optical waveguides and directional couplers in GaAs–imbedded and ridged. *Appl. Opt.*, 13(2):327–330, Feb 1974. (Cited on page 15.)

[91] E. O. Stejskal and J. E. Tanner. Spin diffusion measurements: Spin echoes in the presence of a time-dependent field gradient. *The Journal of Chemical Physics*, 42(1):288–292, 1965. (Cited on page 53.)

[92] S. Stützer, Y. V. Kartashov, V. A. Vysloukh, A. Tünnermann, S. Nolte, M. Lewenstein, L. Torner, and A. Szameit. Anderson Cross-localization. *Opt. Lett.*, 37(10):1715–1717, May 2012. (Cited on pages 2 and 11.)

[93] S. Stützer, Y. V. Kartashov, V. A. Vysloukh, V. V. Konotop, S. Nolte, L. Torner, and A. Szameit. Hybrid Bloch-Anderson Localization of light. *Opt. Lett.*, 38(9):1488–1490, May 2013. (Cited on pages 2 and 11.)

[94] S. Stützer, T. Kottos, A. Tünnermann, S. Nolte, D. N. Christodoulides, and A. Szameit. Superballistic growth of the variance of optical wave packets. *Opt. Lett.*, 38(22):4675–4678, Nov 2013. (Cited on page 11.)

[95] A. Szameit and S. Nolte. Discrete optics in femtosecond-laser-written photonic structures. *Journal of Physics B: Atomic, Molecular and Optical Physics*, 43(16):163001, 2010. (Cited on page 15.)

[96] A. Szameit, F. Dreisow, M. Heinrich, T. Pertsch, S. Nolte, A. Tünnermann, E. Suran, F. Louradour, A. Barthélémy, and S. Longhi. Image reconstruction in segmented femtosecond laser-written waveguide arrays. *Applied Physics Letters*, 93(18):181109, 2008. (Cited on pages 16 and 108.)

[97] A. Szameit, I. L. Garanovich, M. Heinrich, A. A. Sukhorukov, F. Dreisow, T. Pertsch, S. Nolte, A. Tünnermann, S. Longhi, and Y. S. Kivshar. Observation of two-dimensional dynamic localization of light. *Phys. Rev. Lett.*, 104:223903, Jun 2010. (Cited on page 16.)

[98] A. Szameit, M. C. Rechtsman, O. Bahat-Treidel, and M. Segev. PT-symmetry in honeycomb photonic lattices. *Phys. Rev. A*, 84: 021806, Aug 2011. (Cited on pages 22 and 27.)

[99] D. Taj, R. C. Iotti, and F. Rossi. Dissipation and decoherence in nanodevices: A generalized Fermi's Golden Rule. *Semiconductor Science and Technology*, 24(6):065004, 2009. (Cited on page 38.)

[100] M. H. Teimourpour, R. El-Ganainy, A. Eisfeld, A. Szameit, and D. N. Christodoulides. Light transport in PT-invariant photonic structures with hidden symmetries. *Phys. Rev. A*, 90:053817, Nov 2014. (Cited on page 86.)

[101] J. Thomas, M. Heinrich, J. Burghoff, S. Nolte, A. Ancona, and A. Tünnermann. Femtosecond laser-written quasi-phase-matched waveguides in lithium niobate. *Applied Physics Letters*, 91(15):151108, 2007. (Cited on page 16.)

[102] P. D. Townsend. Ion implantation and integrated optics. *Journal of Physics E: Scientific Instruments*, 10(3):197, 1977. (Cited on page 15.)

[103] S. K. Turitsyn, A. M. Rubenchik, M. P. Fedoruk, and E. Tkachenko. Coherent propagation and energy transfer in low-dimension nonlinear arrays. *Phys. Rev. A*, 86:031804, Sep 2012. (Cited on page 2.)

[104] X. Wang, A. Bezryadina, Z. Chen, K. G. Makris, D. N. Christodoulides, and G. I. Stegeman. Observation of two-dimensional surface solitons. *Phys. Rev. Lett.*, 98:123903, Mar 2007. (Cited on page 15.)

[105] Z. Wang, K. Sugioka, and K. Midorikawa. Three-dimensional integration of microoptical components buried inside photosensitive glass by femtosecond laser direct writing. *Applied Physics A*, 89(4):951–955, 2007. (Cited on page 16.)

[106] A. Yariv. Coupled-mode theory for guided-wave optics. *IEEE Journal of Quantum Electronics*, 9(9):919–933, Sep 1973. (Cited on page 67.)

[107] J. M. Zeuner, M. C. Rechtsman, Y. Plotnik, Y. Lumer, S. Nolte, M. S. Rudner, M. Segev, and A. Szameit. Observation of a topological transition in the bulk of a non-hermitian system. *Phys. Rev. Lett.*, 115:040402, Jul 2015. (Cited on page 86.)

[108] J. M. Zhang and Y. Liu. Fermi's Golden Rule: Its derivation and breakdown by an ideal model. *European Journal of Physics*, 37(6): 065406, 2016. (Cited on page 38.)

[109] M. C. Zheng, D. N. Christodoulides, R. Fleischmann, and T. Kottos. PT optical lattices and universality in beam dynamics. *Phys. Rev. A*, 82:010103, Jul 2010. (Cited on page 27.)

DECLARATION

Ich erkläre hiermit ehrenwörtlich, dass ich die vorliegende Arbeit selbständig, ohne unzulässige Hilfe Dritter und ohne Benutzung anderer als der angegebenen Hilfsmittel und Literatur angefertigt habe. Die aus anderen Quellen direkt oder indirekt übernommenen Daten und Konzepte sind unter Angabe der Quellen gekennzeichnet.

Bei der Auswahl und Auswertung des folgenden Materials haben mir die nachstehend aufgeführten Personen in der jeweils beschriebenen Weise unentgeltlich geholfen:

Die für die Experimente verwendeten Glasproben wurden von Christiane Otto vorbereitet, das heißt geschnitten und poliert.

Die experimentellen Daten, welche Abb. 3.16 und Abb. 5.8 zugrunde liegen, wurden von Steffen Weimann aufgenommen.

Weitere Personen waren an der inhaltlich-materiellen Erstellung der vorliegenden Arbeit nicht beteiligt. Insbesondere habe ich hierfür nicht die entgeltliche Hilfe von Vermittlungs- bzw. Beratungsdiensten (Promotionsberater oder anderen Personen) in Anspruch genommen. Niemand hat von mir unmittelbar oder mittelbar geldwerte Leistungen für Arbeiten erhalten, die im Zusammenhang mit dem Inhalt der vorgelegten Dissertation stehen.

Teile dieser Arbeit wurden aus Prioritätsgründen bereits veröffentlicht oder zur Veröffentlichung eingereicht.

Die Arbeit wurde bisher weder im In- noch im Ausland in gleicher oder ähnlicher Form einer anderen Prüfungsbehörde vorgelegt.

Die geltende Promotionsordnung der Mathematisch - Naturwissenschaftlichen Fakultät ist mir bekannt.

Ich versichere ehrenwörtlich, dass ich nach bestem Wissen die reine Wahrheit gesagt und nichts verschwiegen habe.

Jena, June 12, 2019

Toni Eichelkraut

ACKNOWLEDGMENTS

First of all, I would like to thank my family, especially my parents and my wife, who always supported me both mentally and physically and gave me strength to proceed my path.

Also, I would like to express my gratitude to my supervisor Dr. Alexander Szameit for his guidance and support throughout the entire time of my research activity. Especially, I would like to thank him for always giving me the freedom and encouragement to pursuit and investigate my areas of interest. I will always remember the time with our research group as a time during which fruitful discussions were possible and encouraged. It was mainly the achievement of Alex to provide such a creative environment.

Furthermore I wish to thank my former supervisors Dr. Carsten Rockstuhl and Dr. Demetrios N. Christodoulides. With their knowledge and experience they helped me take the step from a student to a researcher and greatly provided me with all the tools necessary for successfully conducting my PhD research.

Many thanks I owe to all the people involved in organizing the MILMI program, as it played a big in role in my scientific develoepement. The commitment of Mrs. Szilvia Mammel, Mrs. Rachel Franzetta, Mrs. Leslie Bilger, Dr. Stefan Nolte, and Dr. Martin Richardson went far beyond just doing their job and allowed me and others to have such a memorable experience.

When it comes to the content of this thesis in particular, I must admit that it would not have reached this theoretical depth if it wasn't for Mr. Steffen Weimann. Long after we had already published the contents of chapters 4 and 5, the main theoretical basis of chapter 3 remained unknown and unclear for us. For quite a long time we were not able to get a grip on the theoretical description of the exponential decay. Even though the principal idea was already clear in our mind, we were not able to write it down analytically in a closed form. Honestly, if it was not for Steffen, I probably would have given up. Thanks to him and his numerous encouragements, I started working on this topic again after it had lingered in my drawer for a long time. For this encouragement and the endless fruitful and essential discussions I am very thankful. With his physical intuition, his sense of completeness and accuracy, he always challenged intermediate results and flaws in the derivation. Overall, I am very grateful for his presence during my PhD time. Moreover and most importantly, I am grateful for his friendship.

Special thanks I would also like to give to Dr. Marco Ornigotti for the final proofs of this thesis.

Last, but truly not least, I need to express my deep thanks to two people without whom this thesis would not have come into existence. Probably, without the likes of Mr. Bodo Martin the entire Institute of Applied Physics would not function. I would like to thank him, because he was always there with quick and uncomplicated support, when you needed it. It is needless to say that without Mrs. Christiane Otto none of the waveguide-based experiments of our research group would have been conducted. I really appreciate the fact, that we always had our glass samples readily prepared to such a high degree of perfection. Moreover, Mrs. Otto was always there to support us with any type of pre- or post-processing.

A

APPENDIX TO CHAPTER 3

This part of the appendix serves as supplement to chapter 3. It contains additional information to some other attempts to control loss in waveguides, as well as some lengthy calculations for the analytical derivation.

A.1 ATTEMPTS TO CONTROL LOSS

In the course of this thesis mainly three approaches to establish a well defined amount of loss inside Laser written waveguides have been examined. It turned out that only periodically bending the waveguides in a sinusoidal fashion was suitable for further use. In this section the drawbacks of less advantageous methods shall be discussed briefly.

Defect Scattering

One attempt to introduce loss in Laser written waveguides was to generate scattering centers inside the waveguide by operating the Laser during the FLDW process close to the damage threshold. The idea behind this approach is that above the so-called damage threshold the FLDW technique does not yield guiding glass modifications anymore but the glass rather burns in the focal region resulting in non-guiding modifications that strongly scatter light. Due to several effects such as a slightly fluctuating Laser power, roughness of the glass surface, or inhomogeneity of the bulk material one can operate the writing Laser at a threshold level at which the resulting glass modifications are guiding waveguides laced with several spot-like scattering centers at which the waveguide is burned. These scatterers are distributed randomly along the longitudinal waveguide dimension. Schematically the scattering loss in waveguides is depicted in fig. A.1. When light that is usually bound hits the scattering centers parts are being scattered away from the waveguide region and only a fraction continues propagating in the bound state.

What makes this approach unfeasible for further practical use is the fact that the occurrence of scattering centers is randomly distributed with a very high variance, that is the distribution of the spacing between two consecutive scattering centers along the waveguide has a

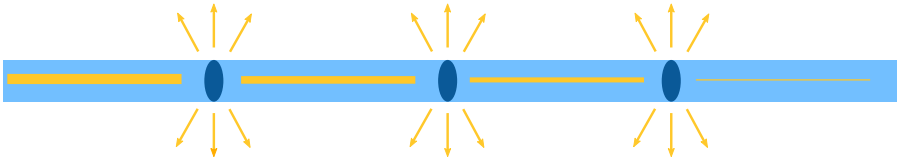

Figure A.1: Illustrating scattering losses. The waveguide contains spot-like scattering centers which correspond to the waveguide being burned. When light that is usually bound hits the scattering centers parts are being scattered and only a fraction continues propagating in the bound state.

very high variance. As a result, one could write two waveguides using the same writing parameters and one waveguide would lack any scattering centers whereas the other waveguide would contain several scatterers. Consequentially, this process is not reproducible enough for practical application. Even though one could envision modifying the approach to a scenario in which the scattering centers are implanted in a determined fashion, this would still leave the scheme impractical as also the strength of the scatterers varies broadly.

Segmentation

The segmentation of Laser written waveguides has already been applied in many studies [96, 47, 41, 48, 49]. However, in all of these cases the purpose of segmenting waveguides was to introduce pure phase shifts. This can be achieved by periodically interrupting the waveguide along its transverse dimension. In those segments where the waveguide is omitted light propagates freely without being bound. If the gap between two consecutive waveguide segments is large the light spreads during this free space propagation and when entering a section where the waveguide is present only a fraction of the field is coupled back into the bound mode, as schematically depicted in fig. A.2 (a). However, the fact that this segmentation technique can be utilized to introduce a phase shift without significant loss in the segmentation region is due to the large Rayleigh length compared the interruption length. For a quick back-of-the-envelope calculation lets assume the mode exiting the waveguide to approximately of Gaussian shape with a width of $w = 5$ µm, the typical wavelength is $\lambda = 633$ nm and the bulk refractive index is $n = 1.45$. With these parameters one finds a Rayleigh length of $z_R = \pi w^2 n/\lambda = 180\,\mu\text{m}$. From this rough estimate it is clear that in segments where the interruption length is in the order of 20 µm the loss is negligibly small. Also globally the loss can be neglected regarding the fact that the number of such interruptions is not larger than 50 in typical designs of such phase shifting regions [47]. Nevertheless, if one increases the interruption length significantly to be in the order of the Rayleigh length one is able to introduce well pronounced amounts of loss.

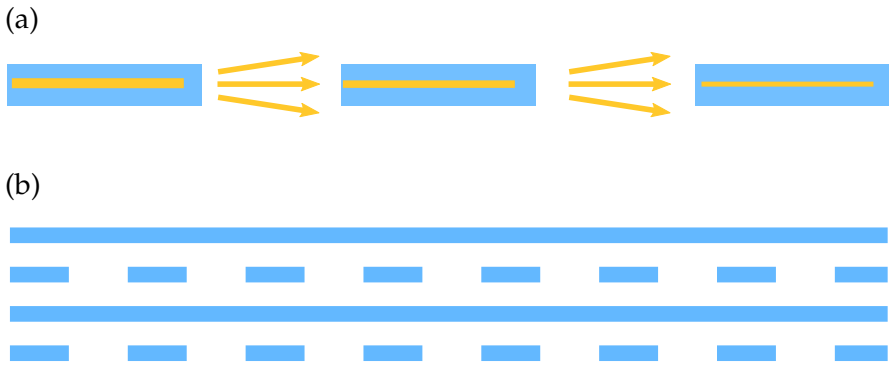

Figure A.2: (a) Illustrating loss due to segmentation. Light exiting one waveguide segment spreads during free space propagation. When entering the next waveguide segment only a fraction is coupled into the bound mode. (b) Scheme of four waveguides where two waveguides are segmented (second and fourth) while two guides are continuous (first and third).

The drawback of this technique one encounters when implementing waveguide lattices that include segmented as well as non-segmented waveguides. For instance if one considers a setup such as the one illustrated in fig. A.2 (b) one would not be able to describe this setup by the coupled mode equation (2.8) derived in section 2.2. The reason for that is that in section 2.2 it was argued that next-nearest neighbor coupling can be neglected, however in the setup shown in fig. A.2 (b) this is not the case. It is evident that in those regions where waveguides two and four are interrupted the coupling between them and their nearest neighbors is zero, hence the coupling between guides one and three must be taken into account in these regions. It can only be neglected in those regions where waveguides two and four are present since the coupling strength decreases exponentially increasing distance between waveguides.

Even though increasing the impact of next-nearest neighbor coupling might be desirable in some applications segmented waveguides were regarded as unfeasible for experiments tied to this thesis and hence dropped from further investigations.

Sinusoidal Bending

It is well known that optical waveguides exhibit losses when being bent. For Instance for optical fibers this fact is important if one is interested in how much a fiber can be curled up. Also in integrated photonic devices bending losses are one of the limiting factors for miniaturization. With this knowledge it seems somewhat natural to utilize bending losses when trying to implement well-defined losses in photonic waveguides. To this effect, the approach which was investigated within this thesis was to let the waveguide oscillate in a

sinusoidal fashion transverse to the propagation direction in order to introduce losses along the propagation direction. The nature of this

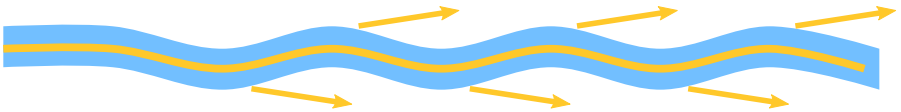

Figure A.3: Illustrating losses due to sinusoidal bending. As the bound mode of the waveguide is only weakly guided it can not "follow" the waveguide in the regions of strong curvature. In these regions light is radiated away from the waveguide resulting in a loss of the bound modes amplitude.

loss mechanism, as schematically depicted in fig. A.3, will be discussed in more detail in the following sections of this chapter. It will be shown that this approach is well suitable for implementation in $\mathcal{PT}$ symmetric structures provided that the oscillation amplitude is small and the frequency of oscillation is large. Moreover, even though bending loss has been studied for many decades the nature of this geometry was little understood and could not be analytically predicted before.

A.2 MATHEMATICAL PREPARATION

In order to derive the correct normalization for the radiation modes it is necessary to consider the integral

$$I = \int_0^\infty \int_0^\infty e^{i\Delta k x} \mathrm{d}x \, f(\omega) \, \mathrm{d}\omega \tag{A.1}$$

first. It's value will be essential for subsequent calculations. In this expression $\Delta k = k_0 - k$ and $k = \sqrt{\omega}$. For eq. (A.1) it is hard to carry out the x-integration. This will be easier when considering the equivalent expression

$$I = \lim_{\epsilon \to 0^+} \int_0^\infty \int_0^\infty e^{[i\Delta k - \epsilon]x} \mathrm{d}x \, f(\omega) \, \mathrm{d}\omega.$$

This way the x-integration can be carried out and the integral reads

$$I = i \lim_{\epsilon \to 0^+} \int_0^\infty \frac{f(\omega)}{\Delta k + i\epsilon} \mathrm{d}\omega \ .$$

Splitting the real and imaginary part, one obtains

$$I = \lim_{\epsilon \to 0^+} \int_0^\infty \frac{\epsilon}{\Delta k^2 + \epsilon^2} f(\omega) \, \mathrm{d}\omega + i \lim_{\epsilon \to 0^+} \int_0^\infty \frac{\Delta k}{\Delta k^2 + \epsilon^2} f(\omega) \, \mathrm{d}\omega \ .$$

The real part can be transformed in the following way

$$\begin{aligned} I_1 &= \lim_{\epsilon \to 0^+} \int_0^\infty \frac{\epsilon}{\Delta k^2 + \epsilon^2} f(\omega)\, \mathrm{d}\omega \\ &= 2\pi \lim_{\epsilon \to 0^+} \int_{-k_0}^\infty \frac{1}{\pi} \frac{\epsilon}{\kappa^2 + \epsilon^2} (\kappa + k_0) f(\omega(\kappa + k_0))\, \mathrm{d}\kappa \end{aligned}$$

regarding the fact that

$$\int_{-\infty}^{\infty} \frac{p}{p^2 + x^2} \mathrm{d}x = \pi \tag{A.2}$$

which was taken from ref. [35]. This way the limit $\lim_{\epsilon \to 0^+} \ldots \frac{1}{\pi} \frac{\epsilon}{\kappa^2 + \epsilon^2}$ acts as a Dirac-δ-function, extracting the value of the integral at $\kappa = 0$. Hence the integral can be evaluated as

$$I_1 = 2\pi k_0 f(\omega(k_0)).$$

In a similar fashion, one can transform the imaginary part to

$$\begin{aligned} I_2 &= i \lim_{\epsilon \to 0^+} \int_0^\infty \frac{\Delta k}{\Delta k^2 + \epsilon^2} f(\omega)\, \mathrm{d}\omega \\ &= -2i \lim_{\epsilon \to 0^+} \int_{-k_0}^\infty \frac{\kappa^2}{\kappa^2 + \epsilon^2} \left(1 + \frac{k_0}{\kappa}\right) f(\omega(\kappa + k_0))\, \mathrm{d}\kappa. \end{aligned}$$

In this expression, the term $\frac{\kappa^2}{\kappa^2 + \epsilon^2}$ approaches 1 for $|\kappa| \gg \epsilon$ and it approaches o for $|\kappa| \ll \epsilon$ and is exactly symmetric about $\kappa = 0$. Therefore, the limit of the above integral is the Chauchy Principal Value Integral. At this point, this integral cannot be evaluated further without knowledge about the function $f(\omega)$, however the common notation of the Chauchy Principal Value can be adopted and the integral can be written as

$$I_2 = -2i\, PV \int_0^\infty \frac{k}{k - k_0} f(\omega(k))\, \mathrm{d}k$$

or equivalently

$$I_2 = -i\, PV \int_0^\infty \frac{f(\omega)}{k - k_0} \mathrm{d}\omega$$

in terms of ω-integration. Using the results of this short excursus, one can choose to write

$$\int_0^\infty e^{i\Delta k x} \mathrm{d}x = 2\pi k_0\, \delta(\omega - \omega_0) - i \frac{PV}{k - k_0}$$

where $\delta(\omega)$ denotes the Dirac-δ-function, $\omega_0 = \omega(k_0)$, and PV shall be used as a short hand notation for the Chauchy Principal Value Integration, that means whenever one integrates over a term including PV the Chauchy Principal Value shall be applied.

A.3 CALCULATIONS FOR SECTION 3.2

In order to derive the results of section 3.2 a few calculations are necessary.

It is easy to verify the orthogonality relation between the modes. Since the bound mode and the radiation modes are Eigen-modes with different Eigen-values it simply follows that they are mutually orthogonal, i.e.

$$\int_{-\infty}^{\infty} \Phi_b^* (\xi, \beta_b) \, \Phi_s (\xi, \beta_s) \, \mathrm{d}\xi = \int_{-\infty}^{\infty} \Phi_b^* (\xi, \beta_b) \, \Phi_a (\xi, \beta_a) \, \mathrm{d}\xi = 0.$$

The fact that symmetric and antisymmetric modes are mutually orthogonal simply follows from their symmetry, hence also

$$\int_{-\infty}^{\infty} \Phi_s^* (\xi, \beta_s) \, \Phi_a (\xi, \beta_a) \, \mathrm{d}\xi = 0.$$

It is important to note, that neither the bound mode given by eq. (5.3) nor the radiation modes above are normalized. Since normalization is import when using these modes as a basis, it needs to be calculated for all modes. The norm of the bound mode is rather simple to retrieve, since this mode profile poses a square integrable function. When it comes to the subject of the radiation modes, which are not square integrable, more effort is necessary.

Normalization of Modes

From mode profile provided in eq. (5.3), the norm of the bound mode is rather straight forward to calculate; it equates to

$$\int_{-\infty}^{\infty} |\Phi_b|^2 \, \mathrm{d}\xi = \frac{\cos(\kappa_1 w)}{\kappa_1 \kappa_2} \left[\kappa_1 \cos(\kappa_1 w) + \kappa_2 \sin(k_1 w)\right] + w. \tag{A.3}$$

In order to calculate the norm of the radiation modes [eqs. (3.4) and (3.5)], the integral needs to be evaluated separately in all three regions, that is the left and right region outside of the waveguide as well as the inside of the waveguide, i.e. for the symmetric modes one has

$$\begin{aligned} \int_{-\infty}^{\infty} \Phi_s^* (\xi, \beta) \, \Phi_s (\xi, \beta') \, \mathrm{d}\xi \quad = \quad & \int_{-\infty}^{-w} \Phi_s^* (\xi, \beta) \, \Phi_s (\xi, \beta') \, \mathrm{d}\xi \\ + \quad & \int_{-w}^{w} \Phi_s^* (\xi, \beta) \, \Phi_s (\xi, \beta') \, \mathrm{d}\xi \\ + \quad & \int_{w}^{\infty} \Phi_s^* (\xi, \beta) \, \Phi_s (\xi, \beta') \, \mathrm{d}\xi. \end{aligned} \tag{A.4}$$

The finite part of this integral, which corresponds to the inside of the potential, is equal to

$$\int_{-w}^{w} \Phi_s^* (\xi, \beta)\, \Phi_s (\xi, \beta')\, \mathrm{d}\xi = \frac{\sin((k_1' + k_1)\, w)}{k_1' + k_1} + \frac{\sin((k_1' - k_1)\, w)}{k_1' - k_1},$$

where the short hand notation $k_1' = k_1(\beta')$ is used. Equivalently, $k_2' = k_2(\beta')$ and $A_s' = A_s(\beta')$ will be used subsequently. Moreover, since the Φ_s are symmetric, that is $\Phi_s(\xi, \beta) = \Phi_s(-\xi, \beta)$, the integrals over left and right half space are equal to each other. Utilizing the mathematical preparation above one finds

$$\begin{aligned} \int_{w}^{\infty} \Phi_s^* (\xi, \beta)\, \Phi_s (\xi, \beta')\, \mathrm{d}\xi &= \int_{-\infty}^{-w} \Phi_s^* (\xi, \beta)\, \Phi_s (\xi, \beta')\, \mathrm{d}\xi \\ &= \pi k_2 |A_s|^2\, \delta(\beta - \beta') \\ &\quad - \tfrac{1}{2} PV \left\{ \tfrac{\mathrm{Im}[A_s' A_s]}{k_2' + k_2} + \tfrac{\mathrm{Im}[A_s' A_s^*]}{k_2' - k_2} \right\}, \end{aligned}$$

where one is left with two terms. One of these terms is proportional to a δ-function while the other one includes a principal value integration. After some calculations using basic trigonometric identities of finds

$$\mathrm{Im}[A_s' A_s] = \tfrac{k_1'}{k_2'} \sin(k_1' w) \cos(k_1 w) + \tfrac{k_1}{k_2} \cos(k_1' w) \sin(k_1 w)$$

and

$$\mathrm{Im}[A_s' A_s^*] = \tfrac{k_1'}{k_2'} \sin(k_1' w) \cos(k_1 w) - \tfrac{k_1}{k_2} \cos(k_1' w) \sin(k_1 w)\ .$$

Using the relationship $k_1'^2 - k_1^2 = k_2'^2 - k_2^2$, it can be shown that the principal value part can be rewritten as

$$\frac{\mathrm{Im}[A_s' A_s]}{k_2' + k_2} + \frac{\mathrm{Im}[A_s' A_s^*]}{k_2' - k_2} = \frac{\sin((k_1' + k_1)\, w)}{(k_1' + k_1)} + \frac{\sin((k_1' - k_1)\, w)}{(k_1' - k_1)}.$$

Inserting all individual parts into eq. (A.4) one finds that the terms including the Chauchy Principal Value cancel with the integral over the potential region and only the terms proportional to the Dirac-δ remain, i.e.

$$\int_{-\infty}^{\infty} \Phi_s^* (\xi, \beta)\, \Phi_s (\xi, \beta')\, \mathrm{d}\xi = 2\pi k_2 |A_s|^2\, \delta(\beta - \beta').$$

Little surprising, this calculation shows that indeed the symmetric radiation modes for different propagation constants are orthogonal. More importantly, the above calculation yields the correct normalization of the symmetric radiation modes. In analogy to that the normalization of the antisymmetric modes can be found, it reads

$$\int_{-\infty}^{\infty} \Phi_a^* (\xi, \beta)\, \Phi_a (\xi, \beta')\, \mathrm{d}\xi = 2\pi k_2 |A_a|^2\, \delta(\beta - \beta').$$

Derivation of Equation 3.15

In order to derive eq. (3.15), one needs to evaluate the overlap integral, which represents a matrix element of the perturbation operator,

$$\begin{aligned}\left\langle \Phi_b \left| \partial_\xi \right| \Phi_a(\beta) \right\rangle &= \int_{-\infty}^{\infty} \Phi_b^*(\xi)\, \partial_\xi \Phi_a(\xi,\beta)\, \mathrm{d}\xi \\ &= \int_{-\infty}^{-a} \Phi_b^*(\xi)\, \partial_\xi \Phi_a(\xi,\beta)\, \mathrm{d}\xi \\ &+ \int_{-a}^{a} \Phi_b^*(\xi)\, \partial_\xi \Phi_a(\xi,\beta)\, \mathrm{d}\xi \\ &+ \int_{a}^{\infty} \Phi_b^*(\xi)\, \partial_\xi \Phi_a(\xi,\beta)\, \mathrm{d}\xi .\end{aligned} \tag{A.5}$$

The evaluation of the individual regions yields

$$\int_{w}^{\infty} \Phi_b^* \partial_x \Phi_a \mathrm{d}x = \frac{\cos(\kappa_1 w)}{k_2^2+\kappa_2^2}\left[\kappa_2 k_1 \cos(k_1 w) - k_2^2 \sin(k_1 w)\right]$$

as well as

$$\int_{-w}^{w} \Phi_b^* \partial_x \Phi_a \mathrm{d}x = \frac{2k_1 \cos(\kappa_1 w)}{\kappa_1^2-k_1^2}\left[\kappa_2 \cos(k_1 w) - k_1 \sin(k_1 w)\right] .$$

With this

$$\begin{aligned}\left\langle \Phi_b \left| \partial_\xi \right| \Phi_a(\beta) \right\rangle &= \frac{2\cos(\kappa_1 w)}{k_2^2+\kappa_2^2}\left[\kappa_2 k_1 \cos(k_1 w) - k_2^2 \sin(k_1 w)\right] \\ &+ \frac{2k_1 \cos(\kappa_1 w)}{\kappa_1^2-k_1^2}\left[\kappa_2 \cos(k_1 w) - k_1 \sin(k_1 w)\right] .\end{aligned} \tag{A.6}$$

With these expressions, after some lengthy but straight forward calculations one finds eq. (3.15).

Validity of Approximation

The derivation carried out in sec. 3.2 heavily relies on the condition (3.13). This section shall provide the experimental bounds for its validity. In order to do so, (3.13) needs to be carried over to physical units. Recall that in chapter 2 dimensionless units were introduced, where $x = x_0\xi$ and $z = z_0\zeta$ with $z_0 = 1/k_0$ and $x_0 = 1/k_0\sqrt{2n_0}$. With this (3.13) can be rewritten as

$$\frac{1}{2\pi\sqrt{2n_0}} > \frac{d_{ph}}{p_{ph}}$$

where d_{ph} is the amplitude in physical units and p_{ph} is the oscillation period in physical units. With a refractive index of $n_0 = 1.45$, the left hand side of the expression above $1/2\pi\sqrt{2n_0} \approx 10$. Hence in physical units condition (3.13) becomes

$$\frac{p_{ph}}{d_{ph}} > 10 .$$

In all experiments the modulation amplitude was kept constant at $d_{ph} = 1.45\,\mu m$ and the smallest period under consideration was $p_{ph} = 100\,\mu m$. From this $p_{ph}/d_{ph} \approx 69$ and one can conclude that condition (3.13) is fulfilled in all experiments.

Integral in Equation 3.18

The integral in eq. (3.18) evaluates to

$$\begin{aligned}\int_0^\infty \sin\left(\nu\left(\zeta-\tau\right)\right) e^{i\beta_{ba}\tau}\mathrm{d}\tau \quad = \quad & \frac{\pi}{2i} e^{i\nu\zeta}\delta\left(\beta_b-\beta_a+\nu\right) \\ - \quad & \frac{\pi}{2i} e^{-i\nu\zeta}\delta\left(\beta_b-\beta_a-\nu\right) \\ + \quad & \cos\left(\nu\zeta\right) PV\frac{\nu}{\left(\beta_a-\beta_b\right)^2-\nu^2} \\ - \quad & i\sin\left(\nu\zeta\right) PV\frac{\beta_a-\beta_b}{\left(\beta_a-\beta_b\right)^2-\nu^2}\end{aligned} \tag{A.7}$$

B

APPENDIX TO CHAPTER 5

B.1 DERIVATION OF EQUATION 5.9

In this section eq. (5.9) will be derived. Explicitely, it is of interest that left and right neighbor coupling are equal. Using eq. (5.3) one finds

$$\left\langle \Phi_{j\pm1} \left| \varepsilon_j \right| \Phi_j \right\rangle = \int_{-w}^{w} \left(\cos\left(\kappa_1 w\right) e^{\mp i\kappa_2(\xi \mp D \pm w)} \right)^* \varepsilon_j \cos\left(\kappa_1 \xi\right) \mathrm{d}\xi$$

The constant terms can be pulled out of the integral and the exponential can be simplified. With this, one has

$$\left\langle \Phi_{j\pm1} \left| \varepsilon_j \right| \Phi_j \right\rangle = \varepsilon_j \cos\left(\kappa_1^* w\right) e^{i\kappa_2^*(w-D)} \int_{-w}^{w} \cos\left(\kappa_1 \xi\right) e^{\pm i\kappa_2^* \xi} \mathrm{d}\xi$$

Finally, the integration yields

$$\begin{aligned}
\left\langle \Phi_{j\pm1} \left| \varepsilon_j \right| \Phi_j \right\rangle &= \varepsilon_j \cos\left(\kappa_1^* w\right) e^{i\kappa_2^*(w-D)} \int_{-w}^{w} \frac{1}{2} \left[e^{i\kappa_1 \xi} + e^{-i\kappa_1 \xi} \right] e^{\pm i\kappa_2^* \xi} \mathrm{d}\xi \\
&= \varepsilon_j \cos\left(\kappa_1^* w\right) e^{i\kappa_2^*(w-D)} \int_{-w}^{w} \frac{1}{2} \left[e^{i(\kappa_1 \pm \kappa_2^*)\xi} + e^{-i(\kappa_1 \mp \kappa_2^*)\xi} \right] \mathrm{d}\xi \\
&= \varepsilon_j \cos\left(\kappa_1^* w\right) e^{i\kappa_2^*(w-D)} \frac{1}{2} \times \\
&\quad \left[\frac{1}{i\left(\kappa_1 \pm \kappa_2^*\right)} \left(e^{i(\kappa_1 \pm \kappa_2^*)w} - e^{-i(\kappa_1 \pm \kappa_2^*)w} \right) \right. \\
&\quad \left. + \frac{1}{-i\left(\kappa_1 \mp \kappa_2^*\right)} \left(e^{-i(\kappa_1 \mp \kappa_2^*)w} - e^{i(\kappa_1 \mp \kappa_2^*)w} \right) \right] \\
&= \varepsilon_j w \cos\left(\kappa_1^* w\right) e^{i\kappa_2^*(w-D)} \times \\
&\quad \left[\frac{1}{2i\left(\kappa_1 \pm \kappa_2^*\right)w} \left(e^{i(\kappa_1 \pm \kappa_2^*)w} - e^{-i(\kappa_1 \pm \kappa_2^*)w} \right) \right. \\
&\quad \left. + \frac{1}{2i\left(\kappa_1 \mp \kappa_2^*\right)w} \left(e^{i(\kappa_1 \mp \kappa_2^*)w} - e^{-i(\kappa_1 \mp \kappa_2^*)w} \right) \right] \\
&= \varepsilon_j w \cos\left(\kappa_1^* w\right) e^{i\kappa_2^*(w-D)} \times \\
&\quad \left[\operatorname{sinc}\left[\left(\kappa_1 \pm \kappa_2^*\right) w \right] + \operatorname{sinc}\left[\left(\kappa_1 \mp \kappa_2^*\right) w \right] \right] \\
&= \varepsilon_j w \cos\left(\kappa_1^* w\right) e^{i\kappa_2^*(w-D)} \left[\operatorname{sinc}\left[\Delta\kappa w\right] + \operatorname{sinc}\left[\Sigma\kappa w\right] \right]
\end{aligned}$$

This proves eq. (5.9) and the fact that left and right neighbor coupling are equal.